THE FUTURE OF THE AMAZON POST 2005 AND 2010 DROUGHTS: AN INTER-COMPARATIVE MODEL STUDY

A Thesis

Presented to the Faculty of the Graduate School

of Cornell University

In Partial Fulfillment of the Requirements for the Degree of

Master of Science

by

Yun Zheng

August 2013

ABSTRACT

The Amazon Rainforest is a dynamically intricate hotspot region with high biodiversity and importance to the global hydrological and carbon cycles. Over the last decade, the frequency of extreme events in the Amazon has increased due to climate change. This study presents a brief background overview of the causes and impacts of the Amazon droughts of 2005 and 2010 based on past and current studies in literature. This study also reports the analysis of the performance of 34 fully coupled global climate models from the Coupled Model Intercomparison Project Phase 5 (CMIP5) and a Community Land Model 4 (CLM4) run to simulate current seasonal cycles of precipitation, temperature, leaf area index (LAI), surface runoff, and aboveground biomass stock against observational datasets. The land and atmospheric model variables of interest include precipitation, temperature, leaf area index, carbon storage in vegetation, net primary production, total runoff, total surface runoff, and total soil moisture content. The present day climatology obtained from CMIP5 historical runs is 1980-2005, and future climatology from 4 representative concentration pathway scenarios (RCPs 2.6, 4.5, 6.0, and 8.5) is 2075-2100. All model outputs are monthly means from the r1i1p1 ensemble. The seasonal and interannual means extracted from the variables are analyzed to compare against observational data to evaluate model performance. Model variability index (MVI) was calculated to compare each model's variability in the North and South Amazon grid boxes to assess the standard deviation difference between model and observed datasets to identify biases in each model. MVI values differ among variables and location of the Amazon. Results also show that models were able to reproduce seasonal and annual cycles of precipitation in the

Amazon better than other observed data. Two types of skill scores were used to rank models to provide comparison to the seasonal and interannual variability in observed data. The root mean square error (RMSE) statistical approach is used to check the model's ability to reproduce both the phase and amplitude of the observations during the climatology period and account for the errors in the spatial pattern and annual cycle. The probability density function (PDF) approach compares the common area under the PDF curves based on Epanechnikov kernel smoothing to evaluate the ability of the model to reproduce both the mean state and interannual variability of a variable. Poor model simulations are close to 0, and perfect model simulations are close to 1. The metrics in this study found no significant correlation between current skill scores and future projections of climate variables. However, correlation studies between variables suggest good relationship between temperature, precipitation, and LAI in models. Future changes in RCP 8.5 show overall decreases in precipitation and increases in temperature, surface runoff, soil moisture, and carbon stock, although uncertainty remains to the exact fate of the Amazon towards the end of the century.

BIOGRAPHICAL SKETCH

Yun Zheng grew up in Brooklyn, NY and earned her Bachelor of Science degree in Earth and Environmental Engineering from Columbia University's Fu Foundation School of Engineering and Applied Science in 2010. She worked extensively on several field projects with Dr. Wade McGillis during her undergraduate career, including the Lamont Atmospheric Carbon Observation Project (LACOP) and Gulf Oil Spill Air-Sea Exchange Experiment (GOSASEE). Since 2010, Yun has been pursuing her Master of Science degree in the field of Environmental Fluid Mechanics and Hydrology at Cornell University while working with Dr. Natalie Mahowald on understanding climate implications of drought in the Amazon region.

ACKNOWLEDGMENTS

I would like to thank my advisor Natalie Mahowald for her encouragement, support, and patience throughout my thesis work. This thesis project would not have been accomplished without her motivation and engagement in all our meetings and discussions.

I would also like to thank Peter Hess for challenging my research and all the feedbacks he suggested to improve my work.

I would also like to thank friends and colleagues from the entire Mahowald and Hess research meeting group. Special thanks to Dan Ward and Nick Heavens who first introduced me to climate modeling with their tutorials and tremendous help in modeling issues, and Wenxiu (Tracy) Sun, Flora Min, and Rachel Scanza for their company and encouragement throughout my graduate life at Cornell University.

Last but not least, I am thankful to the National Science Foundation for funding my graduate study through these projects: 1) NSF project: Mineral Aerosol Variability in the Anthropocene, 2) NSF Collaborative Research: Improved Regional and Decadal Predictions of the Carbon Cycle, and 3) NSF IGERT Traineeship Program in Cross-Scale Biogeochemistry and Climate.

TABLE OF CONTENTS

1 INTRODUCTION

The Amazon is a dynamic region of high-diversity ecosystems that play a key role in global carbon and water budgets. It contains many old growth forests with diverse ecosystems, and holds about 30% of the world's species (*Malhi et al., 2008*). The Amazon receives, on average, 2000 mm of rain each year and although the Amazon basin is only the world's second longest river, it has the highest discharge rate and largest drainage area in the world. Extreme events, such as droughts, in the Amazon rainforest have been previously known to occur "once-in-a-century" and in the Amazon River basin to occur, "once-in-a-decade", as suggested by river records (*Marengo et al., 2011*).

Over the last decade however, two major droughts occurred in 2005 and 2010, alarming scientists and garnering public attention worldwide. The droughts impose stress on the Amazon ecosystem, exacerbating the growing conditions for vegetation and altering the natural cycles of important greenhouse gases, such as carbon dioxide and methane (*Phillips et al., 2009*). While many climate models have predicted a warmer climate associated with an increased frequency of extreme events in the future, uncertainties remain as to the magnitude of change in important variables such as precipitation and leaf area index in Amazon's future climate (*IPCC AR4*).

Old growth forests in the Amazon store about 120 Pg (1.2×10^{17} g) of carbon and recycles about 18 Pg C annually (*Phillips et al., 2009*). The Amazon also accounts for about 15% of global terrestrial photosynthesis (*Field et al., 1998*). Droughts can increase tree mortality, fire frequency, and suppress tree growth (*van der Molen et al., 2011*). A drier forest could also mean a decrease in the carbon uptake capacity of the Amazon and potentially reverses its role as a carbon sink to a major carbon source (*Cox et al., 2000*). Land use changes also puts the Amazon at risk by releasing carbon dioxide into the atmosphere through clearing of the land for

agricultural needs. *Galford et al. (2011)* estimates that within the last century, land conversions have led to a cumulative release of 4.8 Pg C and residual undisturbed ecosystems accumulated 0.3 Pg C in response to CO_2 fertilization. *Houghton et al. (2000)* reported that the net flux of carbon from land use changes accounted for 12.5% of the anthropogenic carbon emissions within the last two decades.

The hydrological cycle in the Amazon is heavily influenced by greenhouse gas emissions. *Huntington (2006)* reports a 7% change in specific humidity per 1 degree C of warming based on the Clausius-Clapeyron equation, suggesting an intensification of the global water cycle. Observational studies (ie. *Allan and Soden, 2008*; *Robock et al., 2000; Zeng et al., 2008*) and model studies (ie. *Trenberth et al., 2003, John et al., 2009*) have argued that enhanced climate warming contributes to an increase in extreme events, and that wet areas will become wetter and dry areas will become drier. This could also mean amplification of future seasonal cycles and shift of ecosystem feedback. The possibility of an Amazon "dieback", leading to concern for the future of the Amazon, is an important issue to investigate (ie. *Cox et al., 2008*).

Many field and model studies (ie. *Cox et al., 2004; Li et al., 2006; Meir et al., 2008; Pouter et al., 2010, Tomasella et al., 2010; and many more*) have looked at several major climatic variables (ie. precipitation, temperature, etc.) in the Amazon to predict vulnerability and impact of droughts in this region. *Cox et al. (2004)* looked at the phenomenon of the Amazonian rainforest dieback under elevated carbon dioxide levels in the Hadley Centre climate-carbon cycle model. *Li et al. (2006)* looked at rainfall variability and seasonality in the Amazon using eleven models supporting the IPCC AR4. *Poulter et al. (2010)* looked at 8 general circulation models combined with a dynamic global vegetation model to compare simulations of carbon stocks and aboveground biomass in the Amazon with observed data. A recent study by *Anav et*

al. (2013) used 18 models from CMIP5 (Coupled Model Intercomparison Project Phase 5) to assess the land and ocean carbon cycles for the present climate globally.

This study is unique in that it analyzes 34 major global climate models from the Comparative Model Inter-comparative Project Phase 5 (CMIP5) to evaluate each model's capability in reproducing the seasonal cycle and interannual variability in the Amazon region specifically, which has not been done before. The purpose of this study is to understand the skill of global climate models in matching current climatology from observed data and to determine the future projected change in the Amazon. The questions this study seeks to answer are: 1) How skillful are climate models in simulated current climate conditions? 2) Are the models capturing the frequency and strength of droughts in the Amazon? and 3) What is the likely future of the Amazon as predicted by models? The performance metrics defined in this study evaluate models that can answer those questions by examining and comparing present day observations and model outputs, in hopes of understanding what the future of carbon and water budgets in the Amazon holds.

1.1 Background and Theory

The atmospheric circulation of moisture transport over the Amazon region is though to be influenced by the neighboring two major bodies of water. The Amazon River basin is surrounded by the Pacific Ocean and the Atlantic Ocean. Precipitation plays an important role in rainforests as it supports the large carbon storage and recycling in the region. In addition, it is responsible for the washout of atmospheric pollutants via wet deposition and the cycling of important nutrients throughout the ecosystem. It is also one of the main drivers that process the exchange of gas elements between the biosphere, ocean, and atmosphere reservoirs. In the past, rainfall variability and moisture transport into the Amazon has been linked more exclusively to the

better-understood Pacific El Niño Southern Oscillation (ENSO) phenomenon (ie. *Kousky et al.,1984; Figueroa and Nobre, 1990; Fu et al., 2001;* and many more). ENSO is a climate pattern that occurs on a cycle of every 5 years across the tropical Pacific Ocean. It refers to the variations of sea surface temperature (SST) in the tropical eastern Pacific and of air surface pressures in the tropical western Pacific. For El Niño years, the pattern is generally warming SST in the eastern Pacific and high air pressures in the western Pacific. For La Niña years, the pattern is cooling SST in the eastern Pacific and low air pressures in the western Pacific. The low phase of the Southern Oscillation, known as El Niño years, is thus associated with reduced Amazon rainfall while opposite anomalies are associated with the high phase, known as La Niña years. More recently, there has been more studies (ie. *Marengo, 1992* and *Rao et al., 2006*) that suggests the influence of Atlantic SSTs on rainfall variability in the Amazon as well.

The location of the Amazon plays a major role in its moisture transport regime. The Amazon is located just south of the equator near the Intertropical Convergence Zone (ITCZ), which is where surface convergence and high altitude divergence of air occurs, consistent with rising motion. The Hadley Cell is the circulation of warm air towards the mid-latitudes and cool air towards the equator. The Amazon is located in the realm of trade winds, which is a belt of easterly winds that circle the globe near the tropics. The winds bring moist air from the tropical Atlantic Ocean over the continent, where northern or southerly winds then determine where the moisture will end up in the Amazon. Between January and July, the prevailing winds over the Amazon flips from Northerly to Southerly, which shifts the rainy season back and forth between the areas of where the moisture is deposited – either north or south of the equator. The cause for this shift in wind patterns is primarily due to the shift in the latitude of the maximum solar radiance and local sources of moisture enhance the water cycle. It is evident that the vegetation

of the Amazon rainforest has a strong influence to the moisture budget in the atmosphere, and the seasonal swings in the forest's leaf area is not just a response to the seasonal rainfall cycles, but may also be a cause for them as well (*Myneni et al., 2007*). This has strong implications on how the onset period of the wet season may be altered, under drought stresses that can increase tree mortality and plant livelihood.

As we discuss later, some studies suggest droughts during 2005 and 2010. Here we discuss the mechanisms proposed in the literature for these droughts. Contrary to the widely accepted view that precipitation in the Amazon is predominately controlled by ENSO, the El Niño impact was actually quite neutral in 2005 with small rainfall anomalies. According to *Zeng et al. (2008),* the Amazon drought in 2005 was caused by a combination of warm Atlantic SSTs and an intensified 2002-2003 ENSO phenomenon with lingering effects due to warm Pacific SSTs. They reported an abnormal warming of the northern tropical Atlantic of about 2 degrees warmer than average and suggested that the sequential occurrence of the warming Pacific and Atlantic SSTs were the cause of the 2005 drought. The study further reported that the atmospheric convection responses to warmer SSTs produce above-normal rainfall over the warmer tropical North Atlantic Ocean which generates subsidence in the south of the South Atlantic Ocean and the Amazon. This produces a "see-saw" like effect to the southern region of the Hadley Circulation and a northward shift of the ITCZ. According to climatology, Atlantic moisture flux into the Amazon would normally flow westward up the Amazon River and then turn southward along the Andes but this "see-saw" effect results in enhanced rainfall north of the ITCZ and reduced rainfall in the southern and western parts of the Amazon.

The 2010 drought was more intense than the 2005 drought in terms of spatial impact of aboveground biomass and maximum water deficit, possibly due to an already drought-weakened

forest. Contrary to the cause of the 2005 drought, the drought in 2010 experienced simultaneous warming of North Atlantic SST and Pacific SST, which indicate that severe droughts are likely to occur in the Amazon when warm spells in the eastern Pacific and North Atlantic occur near-simultaneously or sequentially (*Yoon and Zeng, 2010*). The authors also noted that whenever there is a major ENSO event, Amazon rainfall variability is dominated by the Pacific Ocean influence. However, during the period when ENSO is weak and NATL is warm, Atlantic SST has a larger impact on Amazon rainfall than Pacific SSTs.

The impacts of the two droughts varied spatially. In a study by *Lewis et al. (2011)*, they saw 1.6 Pg C change in carbon storage in 2005 with a 1.9 million km^2 spatial impact versus 2.2 Pg C in carbon storage change and 3 million km^2 spatial impact in 2010. There was one epicenter heavily impacted by the drought in the southwest region in 2005 compared to three epicenters along the southern parts of the Amazon Basin in 2010. The southern and western parts of the Amazon basin was affected the most where river and lake water levels were at the lowest in many years. In addition, rainfall reductions were the largest during Amazon's dry season (July to October) when subtropical North Atlantic SST was at its warmest. This perhaps coincidental occurrence of warm Atlantic SST and the dry season of the Amazon resulted in the intensification of extremely low water levels in many water bodies.

Several studies drew connections of droughts with tree mortality and forest responses. A study by *Phillips et al. (2009)* used records from multiple long-term monitoring plots of land across the Amazon to assess the forest response to drought. The RAINFOR network they used consisted of 136 permanent plots across 44 sites. They determined that total biomass and rates of biomass change (gain as growth and loss as mortality) at each point in time using tree diameter, wood density, and allometric models. They reported that the 2005 drought had a total biomass

carbon impact of 1.2-1.6 Pg C and about 5.3 Mg of aboveground biomass carbon relative to pre-2005 drought conditions were estimated for an average forest hectare subjected to a 100 mm maximum water deficit loss. Their study supports the claim that forests were drought sensitive and also identified the trees that died. Fast growing, light-wooded trees may be especially vulnerable to drought by cavitation or carbon starvation. The trees dying during the 2005 period were found to have lower densities than those dying before. They conclude that Amazon droughts kill selectively and therefore may alter species composition, indicating potential consequences of biodiversity and shift in tree types in the Amazon region.

Another study by *Saleska et al. (2007)* used satellites data to determine whether an Amazon drought has reduced the greenness of the Amazon rainforest. The enhanced vegetation index (EVI) measures canopy greenness and the measurements were from the Moderate Resolution Imaging Spectroradiometer (MODIS) onboard NASA's Terra satellite. They found that intact Amazon forest affected by drought (indicated by anomalously low precipitation) had higher photosynthetic activity, as indicated by EVI and concluded that the Amazon was more drought resistant than previously thought.

The complexity in observed data interpretation drew dispute over the issue of whether or not the Amazon had "greened up" during the 2005 drought. While *Saleska et al. (2007)* found higher photosynthetic productivity after the drought, *Samanta et al. (2010)* suggested that the higher EVI values observed in the previous study was due to a flaw in inclusion of atmosphere-corrupted data in those results, associated with aerosol loadings. They used an improved version of the previous EVI dataset and showed that during the 2005 drought, 11-12% of affected forest displayed greening, 28-29% shows browning or no change, and the rest lacked sufficient data to conclude any changes. They were unable to find any significant relationships between drought

severity and greenness changes. To clear up matters, a site specific study by *Brando et al. (2010)* determined that monthly EVI was relatively insensitive to LAI but had positive correlation with leaf flushing and photosynthetically active radiation (PAR), which suggests that the production of new leaves could play as an important role in interannual EVI variability in the Amazon. They concluded that droughts *could* increase EVI by leaf flushing which has effects on leaf bud development. Overall, forest response to droughts is difficult to assess due to lack of understanding in vegetation adaptations to a drier climate. For example, results from two partial throughfall exclusion experiments in the Amazon only saw a reduction in forest productivity under mild drought conditions with increasing tree mortality rates after 2-3 years of drought simulation (*Meir et al., 2009*).

While it is difficult to understand the implications of droughts on Amazon's current climate, we can turn to climate models to simulate potential responses in forest and hydrological variables to explore all possibilities of Amazon ecosystem feedback in the future to understand Amazon's carbon role towards the end of the century.

2 METHODS

2.1 Observation Datasets

The observational datasets used in this study is listed in Table 1 and represent monthly averages for each variable over the entire time period it was recorded. Precipitation data is obtained from the Global Precipitation Climatology Project and covers from 1979 to 2010.

Temperature data was constructed by the Climate Research Unit (CRU) from the British Atmospheric Data Center (BADC) using statistical interpolations of all station observations. Previous model-observation data comparison studies use ERA40, which is an reanalysis of

global atmospheric and surface conditions over the last 45 years from 1957 to 2002 by the European Centre for Medium-Range Weather Forecasts (ECMWF) or other reanalysis approaches based on physical principles, that incorporates a combination of weather model output and assimilated different observational datasets. The CRU dataset however, is statistics based and therefore provides a longer time frame of data during the 20th century. *Scherrer (2011)* reported that the comparison of ERA40 dataset and CRU temperature dataset shows good agreement for most regions and that differences are relatively small compared to model differences.

Most land variables are limited in long-term datasets, including soil moisture and soil carbon and nitrogen content. However, the leaf area index dataset, LAI3g, was available from satellite data that was combined from two satellite missions – the Advanced Very High Resolution Radiometer (AHVRR) and Moderate Resolution Imaging Spectroradiometer (MODIS). This dataset is generated using an Artificial Neural Network (ANN) from the latest version of the Global Inventory Modeling and Mapping Studies (GIMMS), which is a dataset for normalized difference vegetation index (NDVI) data for the period of July 1981 to end of 2011 at a frequency of 15-days. The satellite image files were converted using the method by *Zhu et al. (2013)* to monthly mean averages.

The Global Runoff Data Centre (GRDC) provides river discharge data of nearly 9000 gauging stations from 157 countries. Long-term river discharge data from five stations located along the main stem of the Amazon River were analyzed for current day climatology, namely Sao Paulo de Olivenca (1973-2010), Santo Antonio Do Ica (1972-2010), Manacapuru (1972-2010), Jatuarana (1977-2010), and Obidos-Linigrafo (1968-2008). Table 2 shows more

information of each station site. Runoff data was then calculated by dividing the annual river discharge rate by the catchment size of each station site and converted to mm/day units.

Lastly, the Amazon basin aboveground live biomass dataset is downloaded from project LBA-ECO LC-15 at the Oak Ridge National Laboratory (ORNL) Distributed Active Archive Center for Biogeochemical Dynamics (DAAC). The dataset is a single raster image generated using a land cover map, remote sensing metrics, and more than 500 forest plots in the Amazon by *Saatchi et al. (2007)*. Both remote sensing and ground data from 1990-2000 were used to represent the average aboveground biomass distribution across the Amazon basin in the form of a classification map of 11 biomass classes with an accuracy of 88% (*Saatchi et al., 2009*). Only the average value of aboveground live biomass was used due to lack of long term monthly data for seasonal and annual cycles.

2.2 Amazon

In order to distinguish Amazon's diverse climate, I dissected my analysis into North and South Amazon using the definition of the Amazon region found in other studies (ie. *Marengo et al., 2011; Samanta et al., 2012; Cox et al., 2004*). Table 3 details the latitude and longitude boundaries of the Amazon grid box definition explored in this study. The onset of the dry and wet season in the Amazon is different for the North and South due to the influence of moisture transport from the Pacific and Atlantic Oceans (explained in Background and Theory section). The wet season is FMAM for the North and DJFM for the South Amazon, while the dry season is JASO for the North and JJAS for the South Amazon. The seasonal cycle varies depending on the definition of the Amazon coordinates (Figure 1) Using the *Marengo et al. (2011)* grid box best captures the distinct wet and dry seasons in the North and South Amazon using the GPCP precipitation dataset.

2.3 Model Simulations

Precipitation, temperature, and LAI outputs were analyzed from using model outputs from a Community Land Model version 4.0 run, the land component of the Community Climate System Model (CCSM). The simulation was performed by forcing the model with CRUNCEP atmospheric reanalysis dataset for the period of 1940-2010 in order to set the meteorology as close as possible to real conditions. Model runs were performed at resolutions of 1.9 x 2.5 degrees. A total of 8 variables (see Table 4) were analyzed from r1i1p1 ensemble runs of 34 global coupled-climate models, which are part of the Coupled Model Intercomparison Project phase-5 (CMIP5) retrieved from http://pcmdi9.llnl.gov/. Table 5 lists the models used along with their institution and modeling group. Models that do not include RCP 6.0 only are BNU-ESM, CanESM2, CNRM-CM5, FGOALS-g2, MPI-ESM-LR, and MPI-ESM-MR. Models that do not include both RCP 2.6 and RCP 6.0 runs are ACCESS1-0, ACCESS1-3, CMCC-CM, CMCC-CMS, HadGEM2-CC, and IPSL-CM5B-LR. Models lacking dynamic vegetation components (therefore no output for LAI, cVeg, and NPP) include all CMCC models, CSIRO-Mk3-6-0, FGOALS-g2, all GISS models, HadGEM2-AO, and MRI-CGCM3. All flux variables (ie. precipitation and runoff, etc.) are converted to mm/day for comparison consistency with observed data.

2.4 Model Performance Assessments

Standard measures of model mean variability suffer problems with regions with too large or too small interannual variability and may give a too optimistic picture of model performance (*Gleckler et al., 2008* and *Scherrer, 2011)*. The two studies introduced a different performance index to cancel these effects. The Model Variability Index (MVI) is used to assess model performance by comparing differences between model and observed data standard deviations to

identify consistent biases in the standard deviations of each model. The MVI values are computed as:

$$MVI^{M}_{N,S}=\left(\frac{sd^{M}_{N,S}}{sd^{O}_{N,S}}-\frac{sd^{O}_{N,S}}{sd^{M}_{N,S}}\right)^{2} \quad \text{[Equation 1]}$$

where sd^{M} and sd^{O} are standard deviations of annual time series of model and observation datasets for each variable at North and South Amazon regions. A perfect model-observation agreement would have a MVI value of 0 to indicate perfect representation of interannual variability, whereas good model-observation agreements are chosen as any value below the 0.5 threshold, adopted from *Scherrer (2011)*. A recent study by *Anav et al. (2013)* confirmed that although a 20-year window is not long enough to capture the long time-scale variance of the model by comparing MVI over the period of 1901-2005 to MVI for the period of 1986-2005, they still decided to analyze MVI over the period of 20 years (1986-2005) to be consistent with physical and biological variable available. In this study, the time period will also be kept consistent between all variables from 1980-2005 under the limitations of observed data.

In order to rank the models' ability to reproduce the mean annual cycle of the North and South Amazon, two skill scores were computed for comparison (*Anav et al., 2013*). The first skill score is the root-mean square error (RMSE) statistical approach, which checks the model's ability to reproduce the phase and amplitude of the mean annual cycle in observational data. The equation is as follows:

$$E^{M^2}_{N,S}=\frac{1}{N}\sum_{1}^{N=12}\left[\left(M_t^{N,S}-\bar{M}^{N,S}\right)-\left(O_t^{N,S}-\bar{O}^{N,S}\right)\right]^2 \quad \text{[Equation 2]}$$

where t is the temporal dimension (1980-2005), N is the number of months in the annual cycle (12), and $\overline{M}^{N,S}$ and $\overline{O}^{N,S}$ is the climatological annual mean of the model and observational data at

North and South Amazon. The error is then normalized between 0 and 1 by dividing it by the maximum error from all the models, as shown:

$$RMSE_{N,S}^{M} = 1 - \frac{E_{N,S}^{M^2}}{\max\left(E_{N,S}^{2}\right)} \quad \text{[Equation 3]}$$

Therefore, the model with the maximum error receives a skill score of 0, which indicates poor performance, and the models that perform well achieve a skill score close to 1.

The second skill score is based on the Epanechnikov kernel smoothing probability density function, which assesses both the mean state and the interannual variability of a variable by calculating the common overlapped area under the model and observation PDFs (ie. *Maxino et al., 2008; Errasti et al., 2011*). Using yearly data available from observed variables within the period of 1980-2005, the common area $C_{N,S}$ under the observed and model PDF is calculated as follows:

$$C_{N,S} = \min\left(PDF_{N,S}^{O}, PDF_{N,S}^{M}\right) \quad \text{[Equation 4]}$$

where the minimum area overlapped between the observed and model PDFs yield can be further integrated to calculate the skill score:

$$s_{N,S} = \int_{1}^{N} C_{N,S} \quad \text{[Equation 5]}$$

where N=100 is the number of bins use to discretize the PDF via the Epanechnikov kernel method. Similar to the RMSE based skill score, a model that perfectly reproduces the interannual variability and mean state of the observed variable achieves a PDF based skill score close to 1, whereas a model that does so poorly has a PDF based skill score close to 0.

2.5 Composite High and Low Models

Top 5 largest and top 5 lowest model outputs for all variables were determined for each variable during current climate conditions to see if models that tend to underestimate or

overestimate a variable is sensitive to change in future climate. This classification of high and low models helps to show whether models that underestimate in the current climate will show larger (or smaller) impacts of change in variables compared to models that overestimates.

3 RESULTS AND DISCUSSION

3.1 Current Climate in Observed Data

Precipitation in North Amazon shows an increasing trend in the annual data while in the South Amazon, precipitation shows a slightly decreasing trend (Figure 2a). LAI has remained relatively steady throughout the last two decades for both North and South Amazon, but temperature has been steadily increasing over the last century, and more so over the last two decades. Observed surface runoff show an increasing trend over the last few decades (see Figure 3), ranging between 3 to 5 mm/day. The mean seasonal cycle of surface runoff show 2-3 months lag from average precipitation in the Amazon and peaks during AMJ months and dips during SON months. No annual or seasonal cycle is analyzed for aboveground live biomass due to data limitation.

The annual mean cycle of observed precipitation indicate a slightly wetter (average about 1 mm/day difference) North Amazon than South Amazon. Climatology reveals that the wet season for the Amazon is FMAM and DJFM for north and south respectively, consistent with *Marengo et al. (2011).* The dry season for the Amazon however, is ASON and MJJA for the north and south respectively. Mean precipitation for North Amazon is 7.0 mm/day, receiving on average 9.2 mm/day during the wet season and 5.1 mm/day during the dry season. South Amazon, on the other hand, receives on average 5.2 mm/day annually and 9.7 mm/day during the wet season and 1.8 mm/day during the dry season.

Average temperatures are 26.1^{o}C and 26.0^{o}C for North and South Amazon, and temperature trend over the last century show consistent warming with climate change (Figure 2b). Wet and dry season temperatures in North Amazon are 26.2^{o}C and 26.3^{o}C respectively. There is a larger temperature difference in the South Amazon with wet and dry season temperatures at 25.6^{o}C and 26.0^{o}C respectively. Temperature anomalies over the Amazon are overall positive within the last decade with relatively high positive anomalies compared to the beginning of the century. Relationship between temperature and precipitation anomalies shows peaks of positive temperature anomalies associated with peaks of negative precipitation anomalies.

North Amazon receives more precipitation and has a higher LAI than South Amazon. The average LAI is 4.2 and 3.1 in the North and South Amazon respectively. Dry season LAI is higher than wet season LAI due to an increase in near-infrared reflectance (NIR) during the dry season because of enhanced photosynthetic activity, which contributed to leaf area changes from new leaves, and change in leaf optical properties of new leaves compared to old leaves (ie. *Myneni et al., 2007; Brando et al., 2010*). North Amazon has a dry season LAI of 4.6 compared to its wet season LAI of 3.8, and South Amazon has a dry season LAI of 3.3 compared to a wet season LAI of 2.9. The average aboveground biomass in the Amazon is about 22.5 kg/m^2, calculated by taking the average of estimated biomass density for 6 areas covered by terra firme and floodplain forest from the biomass distribution map (*Saatchi et al., 2007*).

A closer dissection of the dry season anomalies within the last decade reveals an overall negative precipitation anomaly with positive temperature anomaly in the dry seasons, indicating the dry spell associated with the Amazon droughts in 2005 and 2010 (Figure 4a and 4b). Particularly for South Amazon's dry season, 2005 and 2010 were the driest years within the last

decade. However, looking further back there were larger negative precipitation anomalies within the last 3 decades, an indication of this region's vulnerability to drier conditions. A comparison with CLM4-CRU run (Figure 4b) shows that model did not capture the similar precipitation anomalies as observed data showed. Particularly for the South Amazon dry season, the model was not able to reproduce the amplitudes of the normalized anomalies in observed data within the last few decades.

3.2 Current Climate in Model

The models were able to reproduce the seasonal variability in precipitation well in both North and South Amazon but most models underestimate rainfall intensity especially that in the North Amazon region (Figure 6). There is not a lot of variability in temperature and leaf area index, as expected from a tropical, evergreen region. However, it is evident that most models show more variability in temperature and leaf area index than what is observed. The observed runoff peaks at JMJ and dips at SON, while most models precede the observed data by peaking at JFM and dipping at JJA. Also, aboveground biomass is much higher in observed than predicted.

Models such as the bcc group showed a much smaller inter-quantile range compared to observed precipitation, and some models have skewed distributions in precipitations (ie. HadGEM2 models) (Figure 7a). Models were able to capture the width of rainfall distribution better in the South Amazon than the North Amazon. Temperature variability was exaggerated in model simulations while LAI variability was lacking in many of the models (Figures 7b and 7c). Models such as the inmcm4 and CanESM2 show a significantly low and exaggerated seasonal cycle in temperature compared to other models. Most models that underestimate Amazon temperature are the NorESM1 models, inmcm4, and CCSM/CESM models. The seasonal cycle

signal is the weakest in LAI model outputs, with most models showing little variability of LAI in the Amazon, especially in the North Amazon. A closer look at the distribution (Figure 7c) shows more seasonal cycle variability in the South Amazon than the North. The CanESM2 model is an outlier for its extremely low LAI values while the BNU-ESM model is an outlier for its extremely large LAI values. Most models underestimate surface runoff and a few fail to capture the seasonal variability at all.

Few models (ie. CCSM4, CESM1-BGC, GFDL models, and inmcm4) show good model-observation agreement based on MVI values (Table 6), showing small biases in the standard deviations of model and observed data. There are more biases across models for temperature, LAI, and runoff than precipitation. The models show large biases in temperature and LAI predictions. Models show less bias with LAI in South Amazon as compared to North Amazon. Most models do mediocre in reproducing the mean annual seasonal cycle of runoff in the Amazon but all models underestimate the runoff values by 1-2 mm/day. A few models (ie. ACCESS1-0, CanESM2, CSIRO, IPSL models, and MRI-CGCM3) were unable to capture the runoff seasonal variability while others that do, show a lag from observed runoff data.

A closer look at the average of the largest 5 and lowest 5 of the models (as described in Section 2.5) show that the largest climatological mean from the largest 5 models in precipitation is agreeable to the observed climatological mean than the mean from the lowest 5 models (Figure 8). This is consistent with the previous result that most tend to underestimate rainfall intensity in the Amazon, especially in the North (Figure 7a). While the climatological mean for observed temperature is similar in the North and South Amazon, the models show a smaller temperature mean for the South than the North (Figure 8). This shows that models underestimated temperatures in the South. The climatological mean for LAI on the other hand, show that most

models overestimate the LAI mean compared to the observed value. Other variables such as NPP, total runoff, and soil moisture show that observed mean in that variable leans more toward the high 5 models than the low 5 models. For cVeg, all models underestimate the observed mean in the South Amazon. For surface runoff, all models also underestimate the observed mean, but in both North and South Amazon.

Models such as GFDL-ESM2M and CLM4-CRU show high correlation coefficients, while models such as bcc-csm1-1-m and IPSL-CM5B-LR show negative correlations in precipitation. In South Amazon, the RMS error is smaller overall than the North and most models show high correlations with observed precipitation (Figure 9). Almost all modeled temperature data falls outside the statistical range of the observed due to high seasonal variability predicted by the models not seen in observed data (Figure 9). The bcc-csm1-1-m model is the only one that falls within 2 mm/day standard deviation and 2 mm/day RMS error for both the North and South. The CLM4-CRU agrees well with North Amazon temperature, but represented South Amazon seasonal temperature poorly. The LAI climatology in model outputs show about 7 highly correlated model output (falling between 0.8-0.9) with almost no variability in the seasonal cycles. These results (Figure 9), combined with MVI values in Table 6 and RMSE values in Table 7 show significant bias in the models for temperature, LAI, and runoff.

To evaluate interannual variability, we use the area under the overlapping PDF curves. Most models perform poor because the models tend to either overestimate or underestimate the variables, especially in the case of LAI (Table 8). Most models indicate better performance in the North than the South Amazon (ie. CLM4-CRU, ACCESS models, GISS models, and HadGEM2 models) (Table 8). A closer look at the historical probability density curves for observed precipitation, temperature, leaf area index, and runoff show that most models capture the

frequency distribution of precipitation well with a few underestimated models (Figure 10a). Temperature and LAI show that most models do not capture the frequency distribution with many showing a wider spread and tendency to fall out of the observed range (Figures 10b-c). In addition, all models significantly underestimate surface runoff in the Amazon (Figure 10d).

3.3 Future Climate predicted by Models: RCP 2.6,RCP 4.5, RCP 6.0, and RCP 8.5

Representative Concentration Pathways (RCP) are greenhouse concentration trajectories (not emissions) adopted by the IPCC AR5. For example, RCP 4.5 and RCP 8.5 refer to 4.5 and 8.5 W/m^2 change in radiative forcing. There is no significant shift in the PDF curve for precipitation, but the CanESM2 model shows shift toward low precipitation and some models show shift toward wetter conditions for South Amazon (Figure 10a). All models show shifts in PDF curves toward warmer temperature in future climate scenarios (Figure 10b). For LAI, there was no significant shift in PDF curves overall, but models such as BNU-ESM show shift towards a greener Amazon while CanESM2 show shift towards an Amazon dieback (Figure 10c). No significant shifts were present for average surface runoff in the Amazon (Figure 10d).

The time series of different variables show that for precipitation significant drifts are not seen in many models, similar to what is seen in the PDFs (Figures 11-12). More change is seen in temperature, NPP, and LAI while runoff remains relatively constant (Figure 12a-h). A better understanding of the changes in the variables in the future climate is presented in Table 9.

Figures 15-16 show the range of the percent increase in variables among all the models. Here, the CanESM2 model stands out again as the model showing the highest decrease in all its variable outputs. On the other hand, the IPSL-CM5A-MR model shows large positive increases in carbon in vegetation, runoff, surface runoff, and precipitation. A closer look at the future projections of the CMIP5 models show extremely high positive increases in NPP (GFDL, GISS,

and IPSL models show 50-150% increase) for North Amazon while extremely high positive increases in surface runoff is noted in CSIRO and MRI-CGCM3 models for South Amazon (Figures 18a,b and 19a,b). The CanESM2 model is a major outlier from the rest of the models as it shows an overall decrease in all its projected variables. Future changes in RCP 8.5 show overall decreases in precipitation and increases in temperature, surface runoff, soil moisture, and carbon stock, although uncertainty remains to the exact fate of the Amazon towards the end of the century.

In order to better understand the changes projected from the models, the changes across different variables are compared. There is relatively high positive correlation for model predictions of precipitation and temperature in both North and South Amazon as compared to precipitation and LAI or temperature and LAI (Figures 14a-c). Higher temperatures yield lower precipitation, indicating a drier Amazon with less rainfall in a warming climate. Temperature and precipitation changes are correlated with changes in LAI on R^2 values. Higher temperatures changes yield less green forests, suggesting an inhibiting environment for forest growth also due to decrease in rainfall.

Overall, low models predict a positive change in precipitation while high models predict a more negative change (Figure 20). For temperature, low models for South Amazon predict more change than the average and the high models. Low models also predict more negative change for LAI, indicative of the sensitivity of these low models to an inhibiting warmer climate. Net primary productivity (NPP) and carbon in aboveground vegetation (cVeg) show an overall positive change from models but low models suggest a significant decrease in both for South Amazon. High 5 models in cVeg show a significant negative change for North Amazon as well.

Total runoff, surface runoff, and soil moisture saw the largest change from low models, with total runoff decreasing and surface runoff increasing in future climate.

Many studies would like to reduce the large uncertainty in future projections by focusing on the models which perform the best, but often there is not reduction in uncertainty in focusing on skill because there is not correlation between skill and projections (ie. *Cook, 2007*). The skill score rankings based on RMSE and common PDF yield no significant correlation between the projected changes in precipitation, temperature, LAI, runoff, and biomass carbon (Figures 22-22). No significant results and conclusions can be made regarding the relationship among variables in models.

4 CONCLUSIONS

The two recent droughts are key demonstrations of how the Amazon rainforest can alter the biogeochemistry of the rainforest. Ground assessments of the impact of the drought show that while few trees died per hectare, there has been significant change in carbon balance. It shifts the Amazon from the role of being a carbon sink, buffering the increase in atmospheric carbon dioxide, to a carbon source. A significant amount of uncertainty still remains, primarily due to lack of field measurements of the rainforest as well as a poor understanding of the theoretical response to drought. With a warmer climate, the likelihood of extreme events like droughts increases, leading to higher tree mortality rates and fire frequencies, which could eliminate major carbon sinks and decrease rainfall. Droughts in the Amazon will most likely occur more frequently in our century, therefore more research is motivated to observe and quantify current impacts in order to better assess future adaptation plans to our changing climate.

The understanding, quantification, and prediction of drought occurrences, intensity, and impacts are great challenges limited by modeling capability and observational datasets.

Numerical climate models are improving but quantifying out-of-the-norm extreme events such as droughts in the Amazon is highly uncertain. The difficulty of determining the impact of droughts in the Amazon forest drought lies within the design of each climate model. *Toomey et al., 2011* determined that daytime thermal anomalies explained 38.6% ($p<0.01$) of the variability in the reduction of aboveground living biomass in impacted sites. Their results suggest that heat stress also plays an important role in the two droughts and that models should incorporate both heat and moisture stress to predict drought effects on tropical forests better. Here, this paper showed that temperature anomalies during the 2005 and 2010 droughts were larger than the precipitation anomalies, suggesting that temperature could be playing a strong role.

The metrics used in this study to assess model performance show no significant correlation between current skill scores and future projections. However, correlation plots between variables do show significant influence of temperature and precipitation on leaf area index. The skill scores based on overlapping PDFs, and the centered root mean square error vary across variables for the models. Models perform better for precipitation than other observed variables. Observational data are limited in space and time, and are lacking in the range of variables of interest. This study also does not account for any uncertainties in observed data, which can have their own error during data extraction and interpretation. Accurate and recent datasets are needed to conduct more model studies to compare the bias of model predictions against observations to improve model prediction accuracy. The lack of useful data, soil moisture data in the tropics for example, would be useful for us to understand the effects of temperature and hydrological changes on plant photosynthesis and respiration. In addition, since interannual and interdecadal variations in biological productivity are very sensitive to variations of hydrology and temperature, the timing and degree of the destabilization in the terrestrial carbon

sink as a result of droughts is still uncertain.

APPENDIX: TABLES AND FIGURES

VARIABLE	DATA SOURCE	TIME PERIOD	Units
Precipitation, pr	Global Precipitation Climatology Project (GPCP), NASA, USA	1979/01-2010/12	[mm/s]
Temperature, ts	British Atmospheric Center (BADC), UK	1901/01-2011/12	[°C]
Leaf Area Index, lai	Advanced Very High Resolution Radiometer (AVHRR) and Moderate Resolution Imaging Spectroradiometer (MODIS), NASA, USA	1981/07-2011/12	[--]
Runoff, mrros	Global Runoff Data Centre, World Meteorological Organisation (WMO), hosted by the German Federal Institute of Hydrology (Bundesanstalt für Gewässerkunde or BfG)	Varies*	[mm/yr]
Aboveground Live Biomass, AGLB	LBA-ECO LC-15, Distributed Active Archive Center for Biogeochemical Dynamics, Oak Ridge National Laboratory. USA	1990-2000	Mg/ha

Table 1. Observational datasets of long-term variables.
* See Table 3 for more description

Station	Lat	Long	Catchment Area (km^2)	Year Start	Year End	Mean Annual Discharge (m^3/s)	Mean Annual Volume (km^3)	Mean Annual Depth (mm)
Jatuarana	-3.06	-59.65	2854286	1977	2010	125531.00	3958.75	1387
Santo Antonio do Ica	-3.10	-67.94	1134540	1972	2010	55807.44	1759.94	1551
Manacapurú	-3.31	-60.61	2147736	1972	2010	103233.66	3255.58	1516
Sâo Paulo de Olivenca	-3.45	-68.75	990781	1973	2010	46652.97	1471.25	1485
Óbidos Linígrafo	-1.92	-55.51	4680000	1968	2008	178451.19	5627.64	1202

Table 2. GRDC stations used to analyze runoff data.

Region	Marengo et al., 2011	Samanta et al., 2012	Cox et al., 2004	My Box
North	50W-75W 5N-7.5S	40W-80W 0-10S	50W-70W 0-7.5S	50W-70W 2-9S
South	50W-75W 5S-15S	40W-80W 10S-20S	50W-70W 7.5S-15S	50W-70W 9-20S

Table 3. Amazon grid box definition corresponding to rainfall patterns in the North/South Amazon regions.

VARIABLE	COMMENTS	UNITS	REALM
Precipitation, pr	at surface, includes both liquid and solid phases from all types of clouds	kg/m2/s	atmos
Temperature, ts	"skin temperature"	K	atmos
Leaf Area Index, lai	ratio of total upper leaf surface area of vegetation and horizontal surface area of the land on which it grows	[--]	land
Net Primary productivity, npp	carbon mass flux out of atmosphere due to net primary production on land	kg/m2/s	land
Carbon Mass in Vegetation, cVeg	aboveground vegetation carbon content	kg/m2	land
Total Runoff, mrro	runoff flux including drainage through base of soil model, leaving the land portion of grid cell	kg/m2/s	land
Surface Runoff, mrros	surface runoff flux leaving land portion of grid cell	kg/m2/s	land
Total Soil Moisture Content, mrso	mass per unit area (summed over all layers) of water in all phases	kg/m2	land

Table 4. Variables from CMIP5 model outputs.

#	MODEL NAME	INSTITUTE/GROUP
My Run	**CLM4 CRUNCEP**	National Center for Atmospheric Research, USA
1	**ACCESS1-0**	The Centre for Australian Weather and Climate Research, Australia
2	**ACCESS1-3**	The Centre for Australian Weather and Climate Research, Australia
3	**bcc-csm1-1**	Beijing Climate Center, China Metereological Administration, China
4	**bcc-csm1-1-m**	Beijing Climate Center, China Metereological Administration, China
5	**BNU-ESM**	Beijing Normal University, China
6	**CanESM2**	Canadian Centre for Climate Modelling and Analysis, Canada
7	**CCSM4**	National Center for Atmospheric Research, USA
8	**CESM1-BGC**	National Center for Atmospheric Research, USA
9	**CESM1-CAM5**	National Center for Atmospheric Research, USA
10	**CMCC-CM**	Centro Euro-Mediterraneo per I Cambiamenti Climatici, Italy
11	**CMCC-CMS**	Centro Euro-Mediterraneo per I Cambiamenti Climatici, Italy
12	**CNRM-CM5**	Centre National de Recherches Meterologiques/Centre Europeen de Recherche et Formation Avancees en Calcul Scientifique
13	**CSIRO-Mk3-6-0**	Commonwealth Scientific and Industrial Research Organization/Queensland Climate change Centre of Excellence, Australia
14	**FGOALS-g2**	LASG, Institute of Atmospheric Physics, Chinese Academy of Sciences, China
15	**GFDL-CM3**	Geophysical Fluid Dynamics Laboratory, USA
16	**GFDL-ESM2G**	Geophysical Fluid Dynamics Laboratory, USA
17	**GFDL-ESM2M**	Geophysical Fluid Dynamics Laboratory, USA
18	**GISS-E2-H**	NASA Goddard Institute for Space Studies, USA
19	**GISS-E2-R**	NASA Goddard Institute for Space Studies, USA
20	**HadGEM2-AO**	Met Office Hadley Centre, UK
21	**HadGEM2-CC**	Met Office Hadley Centre, UK
22	**HadGEM2-ES**	Met Office Hadley Centre, UK
23	**inmcm4**	Institute for Numerical Mathematics, Russia
24	**IPSL-CM5A-LR**	Institut Pierre Simon Laplace, France
25	**IPSL-CM5A-MR**	Institut Pierre Simon Laplace, France
26	**IPSL-CM5B-LR**	Institut Pierre Simon Laplace, France
27	**MIROC-ESM**	Japan Agency for Marine-Earth Science and Technology, Atmosphere and Ocean Research Institute, and National Institute for Environmental Sciences, Japan
28	**MIROC-ESM-CHEM**	Japan Agency for Marine-Earth Science and Technology, Atmosphere and Ocean Research Institute, and National Institute for Environmental Sciences, Japan
29	**MIROC5**	Atmosphere and Ocean Research Institute, National Institute for Environmental Studies, and Japan Agency for Marine-Earth Science and Technology, Japan
30	**MPI-ESM-LR**	Max Planck Institute for Metereology, Germany
31	**MPI-ESM-MR**	Max Planck Institute for Metereology, Germany
32	**MRI-CGCM3**	Metereological Research Institute, Japan
33	**NorESM1-M**	Norwegian Climate Centre, Norway
34	**NorESM1-ME**	Norwegian Climate Centre, Norway

Table 5. List of all models and their institutions.

MVI values Table		Precipitation		Temperature		Leaf Area Index		Runoff
#	MODEL NAME	North	South	North	South	North	South	Average
	CLM4-CRU	0.004	0.002	0.003	0.587	>5	0.034	NA
1	ACCESS1-0	0.489	0.001	1.798	3.275	>5	>5	3.737
2	ACCESS1-3	0.185	0.242	>5	>5	0.928	0.009	>5
3	bcc-csm1-1	0.834	0.121	1.892	3.093	>5	1.026	1.120
4	bcc-csm1-1-m	1.400	0.869	>5	>5	1.386	1.658	0.241
5	BNU-ESM	0.058	0.002	3.201	3.732	1.453	0.238	>5
6	CanESM2	0.115	0.001	>5	>5	3.864	0.091	>5
7	CCSM4	0.012	0.009	0.817	4.481	>5	0.796	0.023
8	CESM1-BGC	0.010	0.006	0.497	3.755	>5	0.966	0.033
9	CESM1-CAM5	0.001	0.099	0.716	3.190	>5	0.425	0.438
10	CMCC-CM	0.255	0.040	4.897	>5	NA	NA	NA
11	CMCC-CMS	0.195	0.023	>5	>5	NA	NA	NA
12	CNRM-CM5	0.601	0.075	>5	>5	NA	NA	2.185
13	CSIRO-Mk3-6-0	0.004	0.180	>5	>5	NA	NA	>5
14	FGOALS-g2	0.008	0.296	>5	>5	NA	NA	1.352
15	GFDL-CM3	0.000	0.008	>5	>5	3.074	0.043	0.006
16	GFDL-ESM2G	0.574	0.136	>5	>5	2.941	0.072	0.218
17	GFDL-ESM2M	0.601	0.091	>5	>5	1.005	0.005	0.293
18	GISS-E2-H	0.019	0.195	0.420	3.953	NA	NA	NA
19	GISS-E2-R	0.162	0.292	2.750	>5	NA	NA	0.926
20	HadGEM2-AO	0.516	0.000	2.266	>5	NA	NA	2.208
21	HadGEM2-CC	0.492	0.005	1.813	>5	>5	>5	NA
22	HadGEM2-ES	0.883	0.017	2.364	>5	>5	>5	NA
23	inmcm4	0.958	0.013	0.185	>5	>5	2.639	0.052
24	IPSL-CM5A-LR	0.025	0.334	2.580	>5	>5	0.086	>5
25	IPSL-CM5A-MR	0.022	0.141	2.857	>5	1.214	0.002	>5
26	IPSL-CM5B-LR	0.601	0.020	4.530	>5	0.424	0.072	>5
27	MIROC-ESM	0.382	0.002	3.538	>5	4.113	0.013	0.198
28	MIROC-ESM-CHEM	0.432	0.004	3.105	>5	>5	0.004	0.410
29	MIROC5	0.032	0.373	3.412	>5	0.562	0.007	2.392
30	MPI-ESM-LR	0.002	0.032	>5	>5	0.015	4.717	3.838
31	MPI-ESM-MR	0.053	0.112	>5	>5	0.004	4.753	5.483
32	MRI-CGCM3	0.005	0.102	0.028	1.679	NA	NA	>5
33	NorESM1-M	0.240	0.000	0.570	4.554	>5	0.998	0.255
34	NorESM1-ME	0.231	0.004	0.597	4.475	4.912	1.114	0.306

Note: Large values due to model std << obs std

Legend	
0.0	Perfect
0.5	
1.0	Poor

Table 6. The model variability index is an assessment of biases in the standard deviations of the models against the observed data. A threshold of ≤0.5 for "good" model-observation agreement is adopted from *Scherrer, 2011*.

RMSE Table		Precipitation		Temperature		Leaf Area Index		Runoff
#	MODEL NAME	North	South	North	South	North	South	Average
0	CLM4-CRU	0.97	0.98	0.90	0.88	0.73	0.71	NA
1	ACCESS1-0	0.82	0.87	0.94	0.86	0.83	0.94	0.47
2	ACCESS1-3	0.60	0.72	0.82	0.54	0.96	0.97	0.51
3	bcc-csm1-1	0.30	0.72	0.97	0.97	0.72	0.50	0.00
4	bcc-csm1-1-m	0.03	0.00	0.87	0.94	0.70	0.47	0.01
5	BNU-ESM	0.71	0.89	0.86	0.88	0.43	0.89	0.50
6	CanESM2	0.72	0.72	0.49	0.58	0.81	0.81	0.50
7	CCSM4	0.70	0.94	0.98	0.85	0.70	0.53	0.47
8	CESM1-BGC	0.55	0.93	0.98	0.85	0.69	0.53	0.46
9	CESM1-CAM5	0.79	0.92	0.96	0.88	0.72	0.59	0.53
10	CMCC-CM	0.42	0.94	0.79	0.61	NA	NA	NA
11	CMCC-CMS	0.42	0.94	0.69	0.52	NA	NA	NA
12	CNRM-CM5	0.31	0.86	0.86	0.60	NA	NA	0.44
13	CSIRO-Mk3-6-0	0.75	0.59	0.62	0.69	NA	NA	0.49
14	FGOALS-g2	0.50	0.78	0.39	0.69	NA	NA	0.08
15	GFDL-CM3	0.65	0.67	0.48	0.30	0.78	0.81	0.52
16	GFDL-ESM2G	0.74	0.22	0.00	0.00	0.80	0.82	0.56
17	GFDL-ESM2M	0.78	0.41	0.11	0.07	0.79	0.82	0.56
18	GISS-E2-H	0.60	0.86	0.95	0.89	NA	NA	NA
19	GISS-E2-R	0.63	0.80	0.85	0.85	NA	NA	0.55
20	HadGEM2-AO	0.69	0.98	0.94	0.76	NA	NA	0.47
21	HadGEM2-CC	0.77	0.96	0.95	0.79	0.73	0.91	NA
22	HadGEM2-ES	0.71	0.95	0.93	0.73	0.73	0.91	NA
23	inmcm4	0.75	0.91	0.98	0.48	0.59	0.21	0.73
24	IPSL-CM5A-LR	0.88	0.13	0.94	0.62	0.83	0.82	0.52
25	IPSL-CM5A-MR	0.86	0.35	0.91	0.62	0.83	0.82	0.52
26	IPSL-CM5B-LR	0.00	0.84	0.84	0.80	0.72	0.85	0.49
27	MIROC-ESM	0.62	0.81	0.85	0.79	0.75	0.82	0.12
28	MIROC-ESM-CHEM	0.68	0.85	0.86	0.77	0.75	0.82	0.11
29	MIROC5	0.82	0.55	0.90	0.83	0.92	0.97	0.13
30	MPI-ESM-LR	0.58	0.91	0.64	0.52	0.06	0.00	0.18
31	MPI-ESM-MR	0.59	0.79	0.60	0.49	0.00	0.00	0.06
32	MRI-CGCM3	0.42	0.72	0.98	0.89	NA	NA	0.52
33	NorESM1-M	0.66	0.78	0.98	0.83	0.69	0.47	0.40
34	NorESM1-ME	0.72	0.79	0.98	0.83	0.69	0.46	0.41

Legend	
0	Poor
0.5	
1	Perfect

Table 7. The relative root mean square error based skill score of all model predictions against observational datasets is a measure of each model's ability to reproduce the mean annual/seasonal cycle of observed data.

Common PDF Area		Precipitation		Temperature		Leaf Area Index		Runoff
#	MODEL NAME	North	South	North	South	North	South	Average
0	CLM4-CRU	0.76	0.62	0.92	0.14	0.00	0.00	NA
1	ACCESS1-0	0.62	0.42	0.48	0.14	0.00	0.00	0
2	ACCESS1-3	0.92	0.09	0.00	0.66	0.00	0.00	0
3	bcc-csm1-1	0.00	0.00	0.18	0.81	0.69	0.00	0
4	bcc-csm1-1-m	0.00	0.00	0.00	0.00	0.19	0.05	0
5	BNU-ESM	0.08	0.13	0.64	0.08	0.11	0.00	0
6	CanESM2	0.08	0.00	0.00	0.21	0.00	0.00	0
7	CCSM4	0.29	0.22	0.15	0.09	0.00	0.00	0
8	CESM1-BGC	0.32	0.34	0.10	0.01	0.00	0.00	0
9	CESM1-CAM5	0.05	0.00	0.00	0.00	0.00	0.00	0
10	CMCC-CM	0.01	0.31	0.78	0.07	NA	NA	NA
11	CMCC-CMS	0.00	0.19	0.52	0.23	NA	NA	NA
12	CNRM-CM5	0.00	0.03	0.79	0.00	NA	NA	0
13	CSIRO-Mk3-6-0	0.00	0.00	0.00	0.24	NA	NA	0
14	FGOALS-g2	0.00	0.00	0.41	0.05	NA	NA	0
15	GFDL-CM3	0.00	0.10	0.54	0.09	0.74	0.00	0
16	GFDL-ESM2G	0.00	0.00	0.20	0.64	0.40	0.03	0
17	GFDL-ESM2M	0.00	0.08	0.22	0.46	0.37	0.16	0
18	GISS-E2-H	0.49	0.00	0.47	0.11	NA	NA	NA
19	GISS-E2-R	0.72	0.00	0.22	0.03	NA	NA	0
20	HadGEM2-AO	0.62	0.39	0.82	0.10	NA	NA	0
21	HadGEM2-CC	0.59	0.24	0.35	0.00	0.00	0.00	NA
22	HadGEM2-ES	0.61	0.26	0.58	0.00	0.00	0.00	NA
23	inmcm4	0.48	0.23	0.00	0.00	0.00	0.00	0
24	IPSL-CM5A-LR	0.00	0.06	0.46	0.02	0.73	0.00	0
25	IPSL-CM5A-MR	0.00	0.01	0.00	0.78	0.49	0.00	0
26	IPSL-CM5B-LR	0.00	0.18	0.16	0.02	0.07	0.00	0
27	MIROC-ESM	0.00	0.00	0.35	0.03	0.50	0.04	0
28	MIROC-ESM-CHEM	0.00	0.00	0.34	0.00	0.44	0.00	0
29	MIROC5	0.26	0.64	0.74	0.16	0.00	0.00	0
30	MPI-ESM-LR	0.00	0.16	0.37	0.17	0.76	0.00	0
31	MPI-ESM-MR	0.00	0.34	0.27	0.12	0.68	0.00	0
32	MRI-CGCM3	0.71	0.45	0.00	0.00	NA	NA	0
33	NorESM1-M	0.09	0.01	0.00	0.00	0.00	0.00	0
34	NorESM1-ME	0.10	0.00	0.00	0.00	0.00	0.00	0

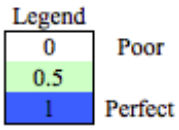

Table 8. The common PDF area based skill score is a measure of the model's ability to capture the mean state and interannual variability in observed data.

#	% Change MODEL NAME	Precipitation North RCP 2.6	RCP 4.5	RCP 6.0	RCP 8.5	Precipitation South RCP 2.6	RCP 4.5	RCP 6.0	RCP 8.5	Temperature North RCP 2.6	RCP 4.5	RCP 6.0	RCP 8.5	Temperature South RCP 2.6	RCP 4.5	RCP 6.0	RCP 8.5
1	ACCESS1-0	NA	-8.01	NA	-18.03	NA	-3.82	NA	-5.85	NA	12.54	NA	23.44	NA	13.22	NA	24.30
2	ACCESS1-3	NA	-10.28	NA	-15.81	NA	-3.65	NA	-5.54	NA	11.32	NA	20.36	NA	11.85	NA	21.15
3	bcc-csm1-1	4.13	0.22	0.06	0.45	0.04	1.97	-1.24	0.40	3.88	7.93	9.82	15.63	0.04	8.40	10.47	16.81
4	bcc-csm1-1-m	-0.08	-2.92	-5.37	-9.69	-0.01	-2.43	-3.25	-3.67	4.41	7.40	9.58	15.43	0.05	7.87	10.31	16.43
5	BNU-ESM	-3.11	-0.49	NA	4.34	-0.02	0.77	NA	4.65	4.61	7.77	NA	14.82	0.06	9.41	NA	17.81
6	CanESM2	-67.89	-72.75	NA	-76.49	-0.40	-43.37	NA	-47.86	8.88	14.08	NA	23.10	0.12	17.00	NA	27.92
7	CCSM4	-0.03	-0.45	1.65	-1.40	0.01	1.68	3.88	4.00	3.99	7.52	9.22	16.29	0.04	8.01	9.70	17.30
8	CESM1-BGC	NA	0.65	NA	-3.09	NA	1.64	NA	3.09	NA	7.26	NA	16.08	NA	7.85	NA	16.91
9	CESM1-CAM5	0.70	-1.88	-5.08	-8.89	0.03	3.04	1.45	1.06	6.65	10.48	12.74	19.69	0.08	11.74	13.77	21.79
10	CMCC-CM	NA	3.32	NA	-2.19	NA	4.66	NA	4.61	NA	10.34	NA	19.45	NA	11.94	NA	21.81
11	CMCC-CMS	NA	2.03	NA	-2.65	NA	1.60	NA	0.85	NA	10.51	NA	20.36	NA	11.91	NA	23.04
12	CNRM-CM5	1.92	-2.49	NA	-6.85	0.04	3.46	NA	4.44	4.13	8.52	NA	16.54	0.05	9.61	NA	17.50
13	CSIRO-Mk3-6-0	9.18	1.34	2.60	4.96	0.03	-1.89	-3.87	1.53	7.66	11.87	11.81	18.78	0.10	14.31	14.43	23.01
14	FGOALS-g2	4.37	8.43	NA	17.62	0.06	6.91	NA	15.06	1.04	3.60	NA	8.01	0.02	4.59	NA	10.39
15	GFDL-CM3	-8.50	-6.73	-5.98	-10.09	-0.11	-9.90	-11.55	-15.82	11.15	14.87	16.11	23.94	0.13	17.25	18.88	28.13
16	GFDL-ESM2G	-0.17	1.75	6.36	12.71	-0.04	-1.94	-0.58	0.02	2.83	5.83	7.05	11.86	0.04	6.92	8.52	14.66
17	GFDL-ESM2M	0.11	4.23	8.65	9.94	0.00	1.77	3.98	1.51	3.80	5.64	6.76	12.14	0.04	6.95	7.99	14.19
18	GISS-E2-H	1.32	1.72	2.42	2.25	0.00	-1.33	-0.68	-5.60	3.08	6.29	7.49	11.86	0.04	7.36	8.72	13.52
19	GISS-E2-R	-0.86	-3.73	-1.66	-3.02	-0.03	-5.16	-4.72	-7.97	2.81	6.43	7.62	11.37	0.03	7.17	8.54	12.55
20	HadGEM2-AO	-5.86	-2.76	-6.64	-14.75	-0.08	1.42	0.39	-5.53	4.53	11.64	12.17	21.47	0.06	12.58	12.95	23.15
21	HadGEM2-CC	NA	-5.26	NA	-11.89	NA	-2.89	NA	-6.45	NA	NA	NA	NA	NA	NA	NA	NA
22	HadGEM2-ES	NA	NA	NA	-14.76	NA	NA	NA	-6.49	NA	NA	NA	NA	NA	NA	NA	NA
23	inmcm4	NA	1.49	NA	0.46	NA	-1.07	NA	-1.31	NA	4.44	NA	9.96	NA	6.47	NA	13.86
24	IPSL-CM5A-LR	-1.15	6.90	5.94	9.95	-0.01	5.76	5.17	7.44	6.01	10.04	11.56	20.66	0.07	11.90	13.58	24.52
25	IPSL-CM5A-MR	10.03	14.83	18.78	17.62	0.04	6.30	7.48	6.98	3.89	9.30	10.42	18.95	0.05	11.30	12.57	22.65
26	IPSL-CM5B-LR	NA	-4.16	NA	-12.89	NA	-2.62	NA	-8.63	NA	7.85	NA	16.20	NA	8.95	NA	18.62
27	MIROC-ESM	-2.31	-0.18	1.08	4.48	-0.05	-6.33	-5.79	-9.22	8.05	11.55	12.76	19.92	0.11	14.47	16.17	27.47
28	MIROC-ESM-CHEM	0.59	-0.05	2.16	3.36	-0.06	-6.32	-7.14	-11.77	7.46	11.70	12.53	21.90	0.12	15.16	16.84	29.22
29	MIROC5	0.41	1.47	3.61	0.65	0.01	2.99	1.79	2.16	5.58	7.75	8.95	15.27	0.08	9.87	11.61	18.78
30	MPI-ESM-LR	-2.54	-5.46	NA	-17.29	-0.03	-1.12	NA	-12.03	5.24	9.57	NA	21.24	0.05	9.74	NA	22.78
31	MPI-ESM-MR	-4.32	-1.96	NA	-17.16	-0.01	0.75	NA	-11.78	5.00	9.54	NA	20.73	0.05	10.07	NA	22.66
32	MRI-CGCM3	-2.00	-1.93	-2.14	-4.50	0.02	4.76	2.23	3.36	3.99	6.58	7.48	13.01	0.05	7.21	8.55	14.52
33	NorESM1-M	2.14	0.40	2.46	2.11	0.01	-1.12	0.08	-0.64	4.41	8.35	9.48	16.40	0.05	8.88	9.80	17.59
34	NorESM1-ME	-0.16	2.23	1.06	-1.26	0.02	3.26	-0.58	0.67	4.21	8.14	9.48	16.57	0.04	8.09	9.82	17.20

Table 9a. Future percent changes in precipitation and temperature.

#	% Change MODEL NAME	Leaf Area Index North RCP 2.6	RCP 4.5	RCP 6.0	RCP 8.5	Leaf Area Index South RCP 2.6	RCP 4.5	RCP 6.0	RCP 8.5	Carbon Storage in Vegetation North RCP 2.6	RCP 4.5	RCP 6.0	RCP 8.5	Carbon Storage in Vegetation South RCP 2.6	RCP 4.5	RCP 6.0	RCP 8.5
1	ACCESS1-0	NA	0.00	NA	0.00	NA	0.00	NA	0.00	NA	NA	NA	NA	NA	NA	NA	NA
2	ACCESS1-3	NA	0.00	NA	0.00	NA	0.00	NA	0.00	NA	NA	NA	NA	NA	NA	NA	NA
3	bcc-csm1-1	-1.58	-0.78	-0.35	1.44	0.00	1.38	1.98	3.24	-0.53	22.18	28.96	37.19	0.13	24.20	30.57	40.42
4	bcc-csm1-1-m	-1.01	-0.37	0.60	0.64	0.01	2.14	2.83	3.71	-0.67	17.28	20.01	24.57	0.08	19.46	23.42	29.51
5	BNU-ESM	3.54	11.73	NA	21.65	0.02	8.31	NA	12.03	-0.22	8.26	NA	12.57	-0.01	1.21	NA	2.73
6	CanESM2	-47.19	-62.57	NA	-66.89	-0.37	-41.42	NA	-45.84	-1.42	-70.71	NA	-74.15	-0.42	-43.06	NA	-47.41
7	CCSM4	3.47	7.40	11.30	13.91	0.03	8.59	12.56	18.48	-0.17	2.07	-0.24	-9.39	-0.01	5.79	5.25	-5.63
8	CESM1-BGC	NA	9.10	NA	14.45	NA	9.35	NA	20.63	-0.16	1.11	NA	-6.67	NA	3.79	NA	-1.85
9	CESM1-CAM5	NA	NA	NA	9.10	NA	NA	NA	10.99	-0.17	NA	NA	-15.03	NA	NA	NA	-13.38
10	CMCC-CM	NA	NA	NA	NA	NA	NA	NA	NA	NA	NA	NA	NA	NA	NA	NA	NA
11	CMCC-CMS	NA	NA	NA	NA	NA	NA	NA	NA	NA	NA	NA	NA	NA	NA	NA	NA
12	CNRM-CM5	NA	NA	NA	NA	NA	NA	NA	NA	NA	NA	NA	NA	NA	NA	NA	NA
13	CSIRO-Mk3-6-0	NA	NA	NA	NA	NA	NA	NA	NA	NA	NA	NA	NA	NA	NA	NA	NA
14	FGOALS-g2	NA	NA	NA	NA	NA	NA	NA	NA	NA	NA	NA	NA	NA	NA	NA	NA
15	GFDL-CM3	-10.51	0.00	5.94	5.70	-0.09	2.21	4.58	3.28	NA	NA	NA	NA	NA	NA	NA	NA
16	GFDL-ESM2G	9.24	19.63	28.13	42.45	0.05	17.53	23.62	28.46	-0.50	21.41	27.46	24.63	0.03	19.91	20.08	7.84
17	GFDL-ESM2M	NA	27.94	37.08	45.26	NA	21.76	29.67	35.78	-0.47	31.60	33.13	28.41	NA	22.90	22.36	11.55
18	GISS-E2-H	NA	NA	NA	NA	NA	NA	NA	NA	NA	NA	NA	NA	NA	NA	NA	NA
19	GISS-E2-R	NA	NA	NA	NA	NA	NA	NA	NA	NA	NA	NA	NA	NA	NA	NA	NA
20	HadGEM2-AO	NA	NA	NA	NA	NA	NA	NA	NA	NA	NA	NA	NA	NA	NA	NA	NA
21	HadGEM2-CC	NA	NA	NA	NA	NA	NA	NA	NA	-0.31	NA	NA	NA	NA	NA	NA	NA
22	HadGEM2-ES	NA	NA	NA	NA	NA	NA	NA	NA	-0.32	NA	NA	NA	NA	NA	NA	NA
23	inmcm4	NA	-0.35	NA	-0.92	NA	-1.73	NA	-2.30	-0.48	21.86	NA	29.68	NA	19.44	NA	30.02
24	IPSL-CM5A-LR	-2.07	4.68	4.93	2.91	-0.06	0.36	-0.29	-6.67	-0.45	NA	49.07	NA	0.10	NA	41.23	NA
25	IPSL-CM5A-MR	7.36	10.21	12.08	8.69	-0.01	3.27	3.42	-2.39	-0.50	60.76	70.28	79.73	0.21	45.73	54.07	54.49
26	IPSL-CM5B-LR	NA	4.87	NA	0.00	NA	2.28	NA	-5.82	-0.90	58.76	NA	64.89	NA	41.65	NA	35.44
27	MIROC-ESM	-4.40	2.47	1.09	1.15	-0.12	0.09	-2.50	-14.52	-0.40	4.65	3.94	9.86	-0.06	6.09	4.98	-11.08
28	MIROC-ESM-CHEM	-2.91	0.56	0.40	-5.20	-0.17	-3.35	-8.38	-17.61	-0.50	5.23	8.08	-5.95	-0.23	-5.47	-13.83	-26.62
29	MIROC5	-0.36	0.10	-1.50	-2.61	-0.03	0.19	-3.14	-4.76	NA	NA	NA	NA	NA	NA	NA	NA
30	MPI-ESM-LR	-6.23	-6.72	NA	-18.63	-0.04	-3.76	NA	-12.65	-0.56	14.39	NA	-11.25	-0.01	16.94	NA	-8.71
31	MPI-ESM-MR	-5.80	-6.24	NA	-17.54	-0.04	-4.34	NA	-13.52	-0.51	12.94	NA	-9.57	0.00	16.84	NA	-8.31
32	MRI-CGCM3	NA	NA	NA	NA	NA	NA	NA	NA	NA	NA	NA	NA	NA	NA	NA	NA
33	NorESM1-M	3.07	3.31	5.46	10.97	0.02	2.54	5.85	10.45	-0.19	-0.78	-6.15	-14.68	-0.04	3.12	-2.86	-12.63
34	NorESM1-ME	1.95	5.56	6.88	10.01	0.05	8.13	9.44	16.28	-0.18	-0.08	-5.98	-15.50	-0.04	4.01	-3.96	-12.44

Table 9b. Future percent change in leaf area index and carbon in vegetation.

% Change		Net Primary Production								Total Runoff							
#	MODEL NAME	North				South				North				South			
		RCP 2.6	RCP 4.5	RCP 6.0	RCP 8.5	RCP 2.6	RCP 4.5	RCP 6.0	RCP 8.5	RCP 2.6	RCP 4.5	RCP 6.0	RCP 8.5	RCP 2.6	RCP 4.5	RCP 6.0	RCP 8.5
1	ACCESS1-0	NA	NA	NA	NA	NA	NA	NA	NA	NA	NA	NA	NA	NA	NA	NA	NA
2	ACCESS1-3	NA	NA	NA	NA	NA	NA	NA	NA	NA	NA	NA	NA	NA	NA	NA	NA
3	bcc-csm1-1	↑ 2.11	↑ 5.36	↑ 13.68	↑ 14.98	— 0.04	↑ 7.97	↑ 14.76	↑ 16.30	↑ 8.96	↑ 4.17	↑ 5.45	↑ 8.62	— 0.08	↑ 4.10	— 0.15	↑ 4.43
4	bcc-csm1-1-m	↑ 5.62	↑ 15.63	↑ 12.41	↑ 3.83	— 0.03	↑ 9.96	↑ 10.54	— 0.57	— 0.78	— -0.36	↓ -100.00	↓ -14.20	— 0.01	— 0.00	↓ -100.00	↑ 2.18
5	BNU-ESM	↑ 2.21	↑ 13.33	NA	↑ 24.96	— 0.03	↑ 12.68	NA	↑ 17.24	↓ -11.12	↓ -9.63	NA	↓ -1.14	— -0.03	— 0.46	NA	↑ 8.61
6	CanESM2	↓ -42.22	↓ -59.70	NA	↓ -57.42	— -0.31	↓ -38.82	NA	↓ -35.92	↓ -2.27	↓ -48.97	NA	↓ -64.97	— -0.21	↓ -26.56	NA	↓ -41.21
7	CCSM4	↑ 2.22	↑ 6.69	↑ 9.71	↑ 13.11	— 0.04	↑ 9.04	↑ 13.30	↑ 21.00	— 0.72	— -0.08	↑ 4.05	↓ -1.36	— 0.04	↑ 8.68	↑ 12.81	↑ 15.86
8	CESM1-BGC	NA	↑ 7.36	NA	↑ 12.20	NA	↑ 8.94	NA	↑ 19.59	NA	— 0.23	NA	↓ -8.86	NA	↑ 3.86	NA	↑ 7.47
9	CESM1-CAM5	NA	NA	NA	NA	NA	NA	NA	NA	NA	NA	NA	↓ -26.93	NA	NA	NA	↑ 9.87
10	CMCC-CM	NA	NA	NA	NA	NA	NA	NA	NA	NA	↑ 3.11	NA	↓ -11.12	NA	↑ 4.86	NA	↑ 2.41
11	CMCC-CMS	NA	NA	NA	NA	NA	NA	NA	NA	NA	↑ 6.27	NA	↓ -12.36	NA	↑ 2.08	NA	↓ -3.96
12	CNRM-CM5	NA	NA	NA	NA	NA	NA	NA	NA	↑ 9.49	↓ -3.67	NA	↓ -12.54	— 0.06	↑ 7.71	NA	↑ 9.59
13	CSIRO-Mk3-6-0	NA	NA	NA	NA	NA	NA	NA	NA	↑ 18.30	↑ 10.62	↑ 6.22	↑ 10.01	— 0.11	↑ 2.40	↑ 2.02	↑ 9.12
14	FGOALS-g2	NA	NA	NA	NA	NA	NA	NA	NA	↑ 9.30	↑ 18.15	NA	↑ 33.95	— 0.17	↑ 17.15	NA	↑ 34.67
15	GFDL-CM3	NA	NA	NA	NA	NA	NA	NA	NA	↓ -4.29	— 0.75	↑ 6.28	— 0.09	— -0.17	↓ -18.72	↓ -18.68	↓ -27.32
16	GFDL-ESM2G	↑ 13.54	↑ 23.49	↑ 37.62	↑ 59.58	— 0.09	↑ 18.99	↑ 32.97	↑ 44.36	↑ 5.12	↑ 4.72	↑ 14.11	↑ 28.96	— -0.05	↓ -2.31	↓ -2.85	↑ 2.37
17	GFDL-ESM2M	↑ 16.23	↑ 42.20	↑ 61.87	↑ 71.14	— 0.11	↑ 23.78	↑ 42.05	↑ 53.43	NA	↑ 7.73	↑ 17.15	↑ 17.91	NA	↑ 5.57	↑ 15.27	↑ 4.85
18	GISS-E2-H	↑ 22.15	↑ 43.95	↑ 81.37	↑ 114.86	— -0.58	↑ 4.51	↓ -232.68	↓ -358.30	NA	NA	NA	NA	NA	NA	NA	NA
19	GISS-E2-R	NA	↑ 42.91	↑ 109.03	↑ 162.09	NA	↑ 63.08	↑ 5.37	↓ -43.44	↓ -1.51	↓ -9.74	↓ -5.22	↓ -7.02	— -0.08	↓ -18.09	↓ -15.70	↓ -19.55
20	HadGEM2-AO	NA	NA	NA	NA	NA	NA	NA	NA	NA	NA	NA	NA	NA	NA	NA	NA
21	HadGEM2-CC	NA	NA	NA	NA	NA	NA	NA	NA	NA	NA	NA	NA	NA	NA	NA	NA
22	HadGEM2-ES	NA	NA	NA	NA	NA	NA	NA	NA	NA	NA	NA	NA	NA	NA	NA	NA
23	inmcm4	NA	NA	NA	NA	NA	NA	NA	NA	NA	↑ 1.43	NA	↓ -3.07	NA	↓ -8.24	NA	↓ -11.76
24	IPSL-CM5A-LR	↑ 10.66	↑ 29.72	↑ 44.56	↑ 59.20	— 0.11	↑ 22.33	↑ 34.05	↑ 43.69	↓ -2.95	↑ 17.97	↑ 14.53	↑ 27.23	— 0.01	↑ 17.93	↑ 20.20	↑ 25.81
25	IPSL-CM5A-MR	↑ 26.98	↑ 41.02	↑ 63.32	↑ 74.35	— 0.18	↑ 26.37	↑ 42.42	↑ 51.11	↑ 30.99	↑ 48.69	↑ 60.78	↑ 55.32	— 0.14	↑ 15.95	↑ 19.26	↑ 20.45
26	IPSL-CM5B-LR	NA	↑ 22.34	NA	↑ 41.80	NA	↑ 20.93	NA	↑ 39.92	NA	↓ -9.18	NA	↓ -19.73	NA	↓ -8.78	NA	↓ -9.81
27	MIROC-ESM	— -0.61	↑ 10.10	↑ 15.07	↑ 15.61	— -0.12	↑ 3.63	↑ 3.39	— 0.74	↓ -4.67	↓ -1.50	↓ -2.08	↑ 1.01	— -0.07	↓ -10.43	↓ -13.38	↓ -16.67
28	MIROC-ESM-CHEM	↑ 1.03	↑ 10.34	↑ 14.88	↑ 15.70	— -0.07	↑ 7.79	↑ 9.84	↑ 11.11	↑ 2.48	— 0.04	↑ 3.61	↑ 5.40	— -0.06	↓ -10.30	↓ -10.78	↓ -19.02
29	MIROC5	NA	NA	NA	NA	NA	NA	NA	NA	↑ 1.65	— -0.34	↑ 7.94	↑ 5.98	— 0.02	↑ 5.65	↑ 7.49	↑ 11.73
30	MPI-ESM-LR	↑ 7.70	↑ 17.46	NA	↑ 17.44	— 0.10	↑ 22.29	NA	↑ 27.58	↓ -2.43	↓ -5.58	NA	↓ -23.41	— -0.08	↓ -2.65	NA	↓ -21.44
31	MPI-ESM-MR	↑ 6.47	↑ 17.25	NA	↑ 19.10	— 0.11	↑ 21.88	NA	↑ 26.50	↓ -2.66	↑ 5.54	NA	↓ -24.14	— -0.04	↑ 2.54	NA	↓ -19.72
32	MRI-CGCM3	NA	NA	NA	NA	NA	NA	NA	NA	↓ -9.53	↓ -11.89	↓ -12.48	↓ -22.91	— 0.01	↑ 3.18	↓ -3.37	↓ -8.77
33	NorESM1-M	↑ 2.45	↓ -32.92	↑ 6.33	↑ 11.39	— 0.02	↓ -36.28	↑ 7.99	↑ 13.90	↑ 6.50	↑ 2.49	↑ 11.20	↑ 10.72	— 0.07	— 0.31	↑ 6.74	↑ 4.94
34	NorESM1-ME	— 0.62	↑ 6.06	↑ 6.84	↑ 67.28	— 0.03	↑ 10.12	↑ 10.59	↑ 84.99	↑ 1.16	↑ 9.52	↑ 7.52	↑ 2.63	— 0.08	↑ 14.06	↑ 3.06	↑ 5.77

Table 9c. Future percent change in net primary production and total runoff.

% Change		Surface Runoff								Soil Moisture							
#	MODEL NAME	North				South				North				South			
		RCP 2.6	RCP 4.5	RCP 6.0	RCP 8.5	RCP 2.6	RCP 4.5	RCP 6.0	RCP 8.5	RCP 2.6	RCP 4.5	RCP 6.0	RCP 8.5	RCP 2.6	RCP 4.5	RCP 6.0	RCP 8.5
1	ACCESS1-0	NA	↓ -2.52	NA	↓ -8.64	NA	↑ 5.35	NA	↑ 17.76	NA	↓ -3.66	NA	↓ -5.53	NA	↓ -2.37	NA	↓ -2.09
2	ACCESS1-3	NA	↑ 39.94	NA	↑ 64.71	NA	↑ 50.81	NA	↑ 95.42	NA	↓ -5.00	NA	↓ -8.67	NA	↓ -3.25	NA	↓ -5.40
3	bcc-csm1-1	↑ 7.90	↑ 4.51	↑ 5.75	↑ 9.15	— 0.08	↑ 5.52	↑ 2.10	↑ 6.73	— -0.01	— -0.27	— -0.26	— -0.35	— 0.00	— -0.16	— -0.26	— -0.21
4	bcc-csm1-1-m	↑ 1.28	— 0.21	↓ -4.62	↓ -10.25	— 0.01	— 0.61	— 0.08	↑ 2.67	— -0.36	— -0.41	— -0.59	— -0.84	— 0.00	— -0.31	— -0.37	— -0.38
5	BNU-ESM	↓ -11.59	↓ -10.40	NA	↓ -1.95	— -0.03	— 0.77	NA	↑ 9.12	↓ -1.32	↓ -1.13	NA	— -0.65	— -0.01	— -0.37	NA	— -0.19
6	CanESM2	↑ 2901.88	↑ 4292.09	NA	↑ ######	Inf	Inf	NA	Inf	↓ -2.35	↓ -4.18	NA	↓ -5.46	— -0.03	↓ -4.67	NA	↓ -6.16
7	CCSM4	— -0.88	↓ -1.19	↑ 2.55	↓ -2.09	— 0.01	↑ 3.87	↑ 9.06	↑ 10.52	— -0.48	— -0.74	— -0.10	— -0.65	— 0.00	— 0.08	↑ 1.17	↑ 2.41
8	CESM1-BGC	NA	— -0.74	NA	↓ -5.72	NA	↑ 1.46	NA	↑ 5.64	NA	— -0.76	NA	— -0.98	NA	— -0.38	NA	↑ 1.46
9	CESM1-CAM5	NA	NA	NA	↓ -22.00	NA	NA	NA	↑ 1.70	NA	NA	NA	↑ #####	NA	NA	NA	↑ #####
10	CMCC-CM	NA	NA	NA	NA	NA	NA	NA	NA	NA	↓ -3.66	NA	↓ -8.22	NA	↓ -4.03	NA	↓ -6.46
11	CMCC-CMS	NA	NA	NA	NA	NA	NA	NA	NA	NA	↓ -3.17	NA	↓ -8.80	NA	↓ -3.01	NA	↓ -5.42
12	CNRM-CM5	↑ 5.28	↓ -2.38	NA	↓ -10.11	— -0.10	↓ -9.35	NA	↓ -7.83	NA	Inf	NA	NA	NA	Inf	NA	NA
13	CSIRO-Mk3-6-0	↑ 132.54	↑ 133.91	↑ 144.38	↑ 84.80	↑ 3.58	↑ 245.48	↑ 222.61	↑ 446.53	— 0.89	— -0.89	— -0.08	— -0.70	— 0.01	— -0.24	— 0.03	— 0.33
14	FGOALS-g2	↑ 7.80	↑ 15.67	NA	↑ 30.15	— 0.13	↑ 14.37	NA	↑ 30.03	— 0.26	— 0.43	NA	— 0.78	— 0.00	— 0.22	NA	— 0.44
15	GFDL-CM3	↓ -5.17	— -0.01	↑ 2.86	— -0.59	— -0.19	↓ -20.90	↓ -21.82	↓ -30.54	↓ -1.05	↓ -1.12	— -0.72	↓ -1.63	— -0.03	↓ -3.01	↓ -3.00	↓ -5.06
16	GFDL-ESM2G	↑ 7.25	↑ 5.28	↑ 15.85	↑ 35.99	— -0.06	↓ -4.76	↓ -4.70	↑ 1.74	— 0.36	— 0.27	↑ 1.37	↑ 2.22	— -0.01	— -0.13	— -0.40	— -0.30
17	GFDL-ESM2M	NA	↑ 10.42	↑ 21.15	↑ 21.02	NA	↑ 2.08	↑ 10.12	— -0.98	NA	— 0.55	— 0.95	— 0.94	NA	— 0.43	— 0.33	— -0.69
18	GISS-E2-H	NA	NA	NA	NA	NA	NA	NA	NA	NA	NA	NA	NA	NA	NA	NA	NA
19	GISS-E2-R	↑ 1.75	— 0.99	↑ 6.73	↑ 11.23	— -0.01	↓ -1.78	↑ 1.03	↑ 3.26	↓ -1.20	↓ -4.07	↓ -3.38	↓ -4.61	— -0.02	↓ -6.10	↓ -6.09	↓ -8.26
20	HadGEM2-AO	↓ -10.64	↓ -3.53	↓ -8.55	↓ -13.58	— -0.16	↑ 1.64	↑ 2.21	↓ -1.02	NA	NA	NA	NA	NA	NA	NA	NA
21	HadGEM2-CC	NA	NA	NA	NA	NA	NA	NA	NA	NA	NA	NA	NA	NA	NA	NA	NA
22	HadGEM2-ES	NA	NA	NA	NA	NA	NA	NA	NA	NA	NA	NA	NA	NA	NA	NA	NA
23	inmcm4	NA	↑ 2.79	NA	↑ 6.14	NA	↓ -3.96	NA	↑ 3.29	NA	— 0.55	NA	↓ -1.69	NA	↓ -5.50	NA	↓ -5.73
24	IPSL-CM5A-LR	↓ -2.95	↑ 17.97	↑ 14.53	↑ 27.23	— 0.01	↑ 17.93	↑ 20.20	↑ 25.81	↓ -5.37	↑ 3.21	— 0.33	↑ 2.08	— -0.08	↓ -2.23	↓ -7.44	↓ -7.91
25	IPSL-CM5A-MR	↑ 30.99	↑ 48.69	↑ 60.78	↑ 55.32	— 0.14	↑ 15.95	↑ 19.26	↑ 20.45	↑ 6.52	↑ 8.97	↑ 11.92	↑ 7.98	— 0.02	— -0.92	↑ 2.23	↓ -4.28
26	IPSL-CM5B-LR	NA	↓ -9.18	NA	↓ -19.73	NA	↓ -8.78	NA	↓ -9.81	NA	↓ -7.53	NA	↓ -9.95	NA	↓ -10.44	NA	↓ -17.92
27	MIROC-ESM	↑ 1.57	↑ 5.35	↑ 5.25	↑ 10.92	— -0.06	↓ -6.56	↓ -8.50	↓ -13.63	↓ -7.78	↓ -10.30	↓ -8.63	↓ -9.33	— -0.10	↓ -16.01	↓ -14.13	↓ -17.01
28	MIROC-ESM-CHEM	↑ 8.97	↑ 7.09	↑ 9.98	↑ 12.96	— -0.05	↓ -6.85	↓ -7.14	↓ -14.57	↓ -9.77	↓ -10.15	↓ -9.00	↓ -10.83	— -0.11	↓ -14.64	↓ -13.64	↓ -17.42
29	MIROC5	↑ 4.18	↑ 5.15	↑ 12.04	↑ 12.10	— 0.06	↑ 9.68	↑ 11.58	↑ 16.74	↓ -2.01	↓ -3.10	↓ -2.35	↓ -4.55	— -0.03	↓ -4.05	↓ -4.44	↓ -6.41
30	MPI-ESM-LR	— 0.02	↓ -1.79	NA	↓ -18.28	— -0.08	— -0.81	NA	↓ -19.17	↓ -3.03	↓ -4.45	NA	↓ -9.75	— -0.01	— -0.97	NA	↓ -4.88
31	MPI-ESM-MR	— -0.33	↑ 9.87	NA	↓ -19.67	— -0.03	↑ 5.71	NA	↓ -16.98	↓ -3.27	↓ -3.27	NA	↓ -9.15	— -0.01	↓ -1.18	NA	↓ -5.40
32	MRI-CGCM3	↑ 61.96	↑ 141.06	↑ 167.20	↑ 370.73	↑ 0.73	↑ 156.29	↑ 171.64	↑ 385.54	↓ -3.04	↓ -4.59	↓ -5.20	↓ -11.02	— -0.05	↓ -2.97	↓ -5.16	↓ -9.65
33	NorESM1-M	↑ 3.25	— 0.57	↑ 5.53	↑ 5.88	— 0.03	↓ -1.12	↑ 3.63	↑ 3.82	— -0.30	↓ -1.25	— -0.66	— -0.76	— 0.00	— -0.41	— 0.69	↑ 1.99
34	NorESM1-ME	— 0.23	↑ 5.37	↑ 3.72	— 0.70	— 0.06	↑ 10.16	↑ 1.96	↑ 5.87	— -0.49	— -0.57	— -0.51	↓ -1.34	— 0.00	— 0.99	— 0.30	↑ 1.92

Table 9d. Future percent change in surface runoff and soil moisture content.

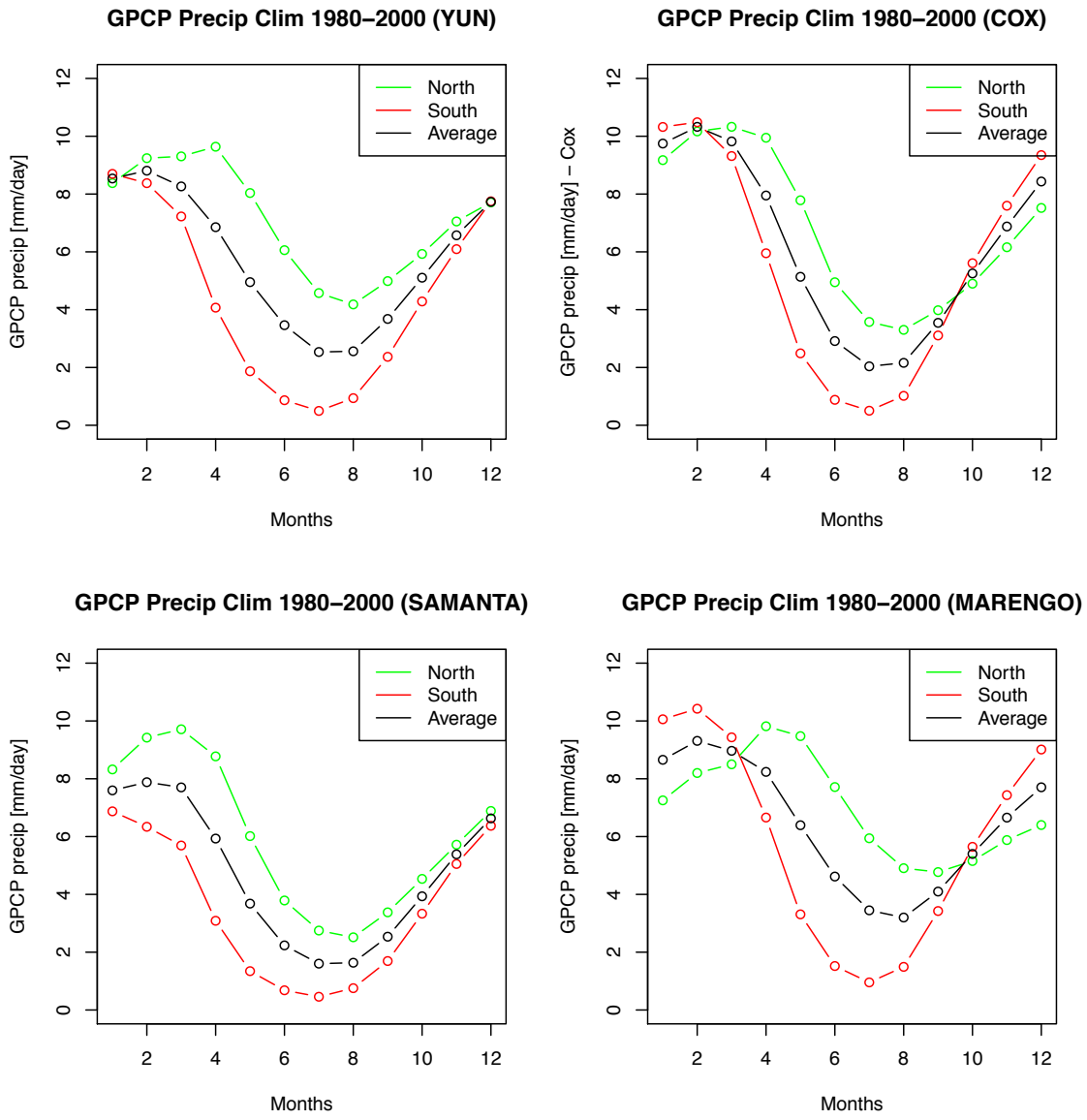

Figure 1. Precipitation climatology for different grid box definitions for 1980-2000.

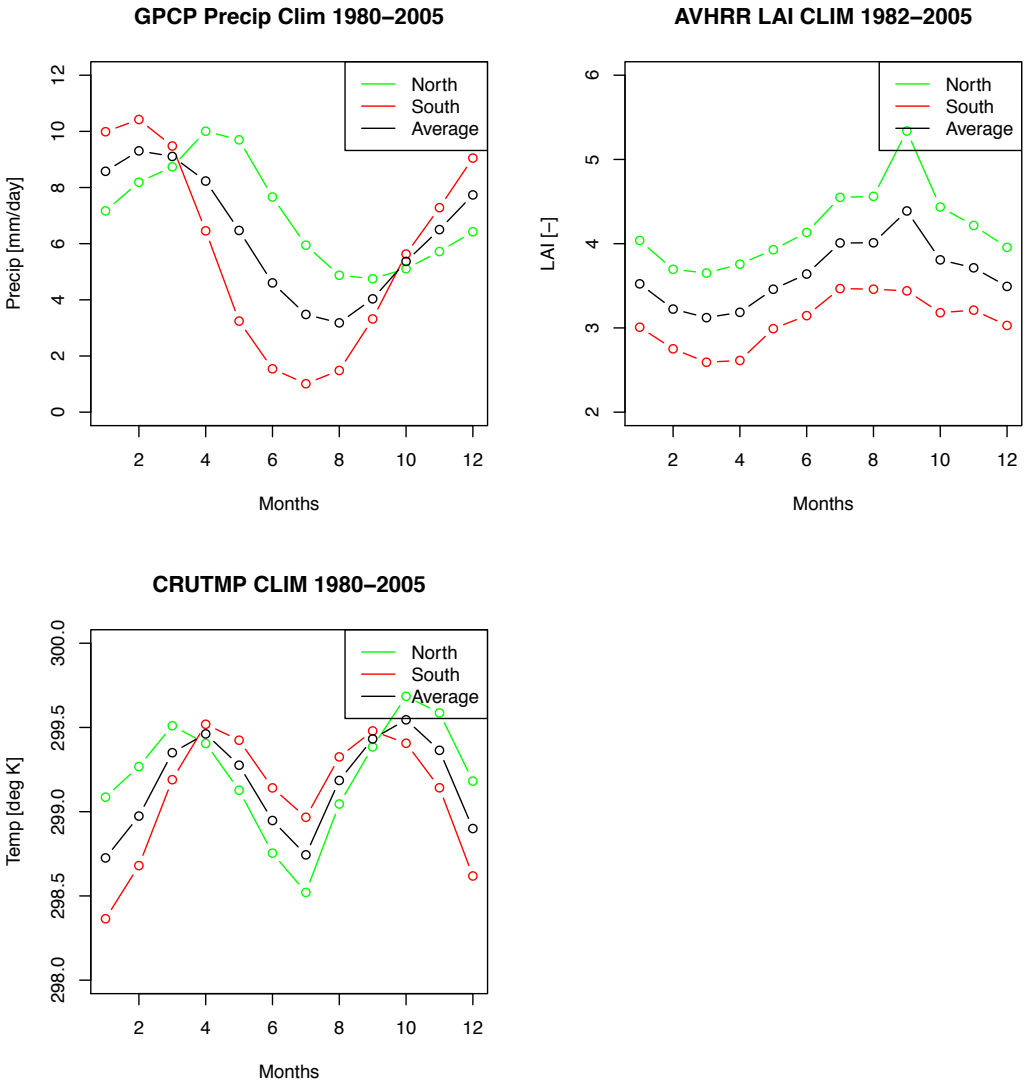

Figure 2a. Climatological seasonal and annual means of observed precipitation, temperature, and leaf index (1980-2005).

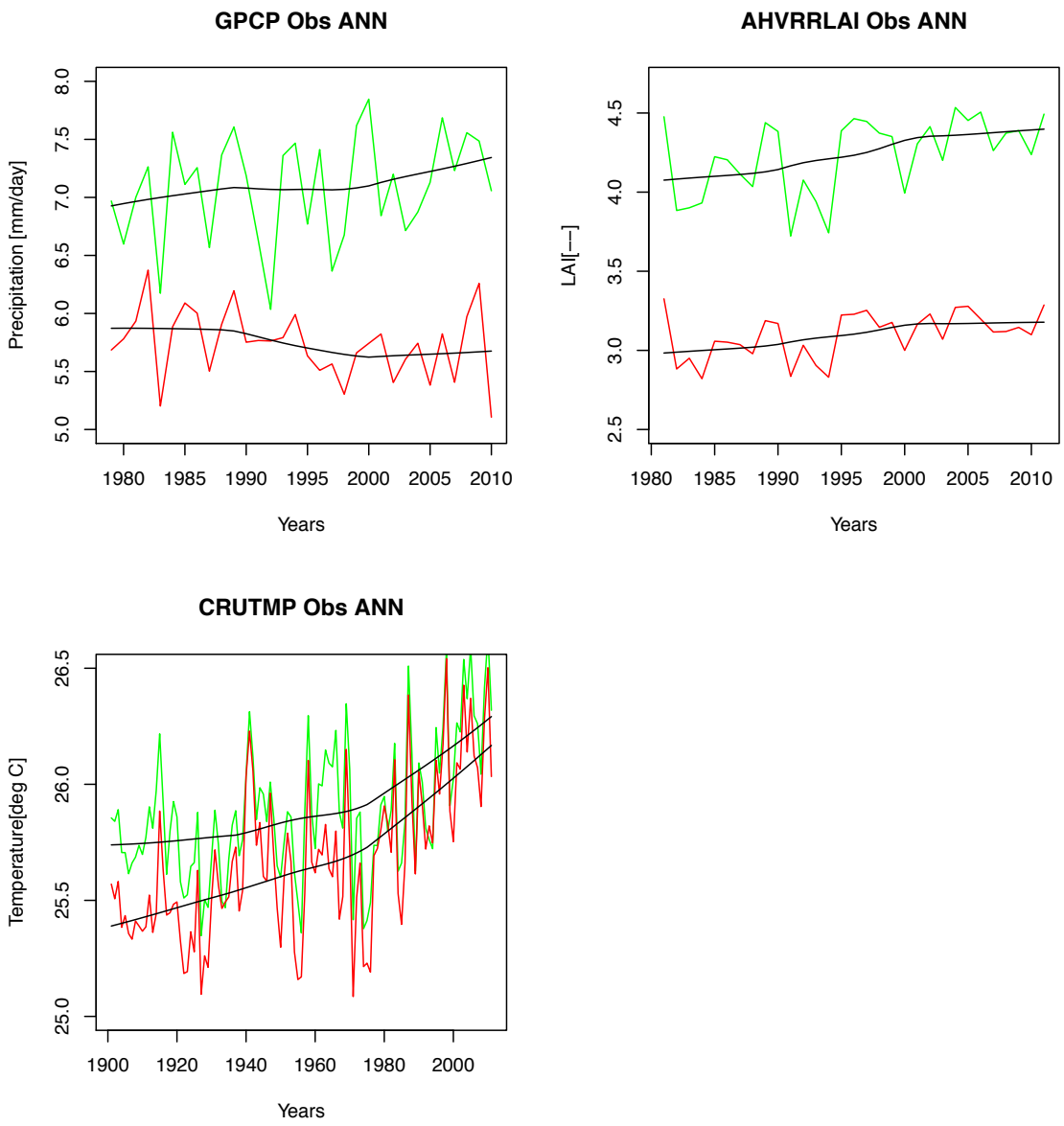

Figure 2b. Interannual time series and seasonal climatology plots of observed precipitation, temperature, and LAI in north (green) and south (red) Amazon.

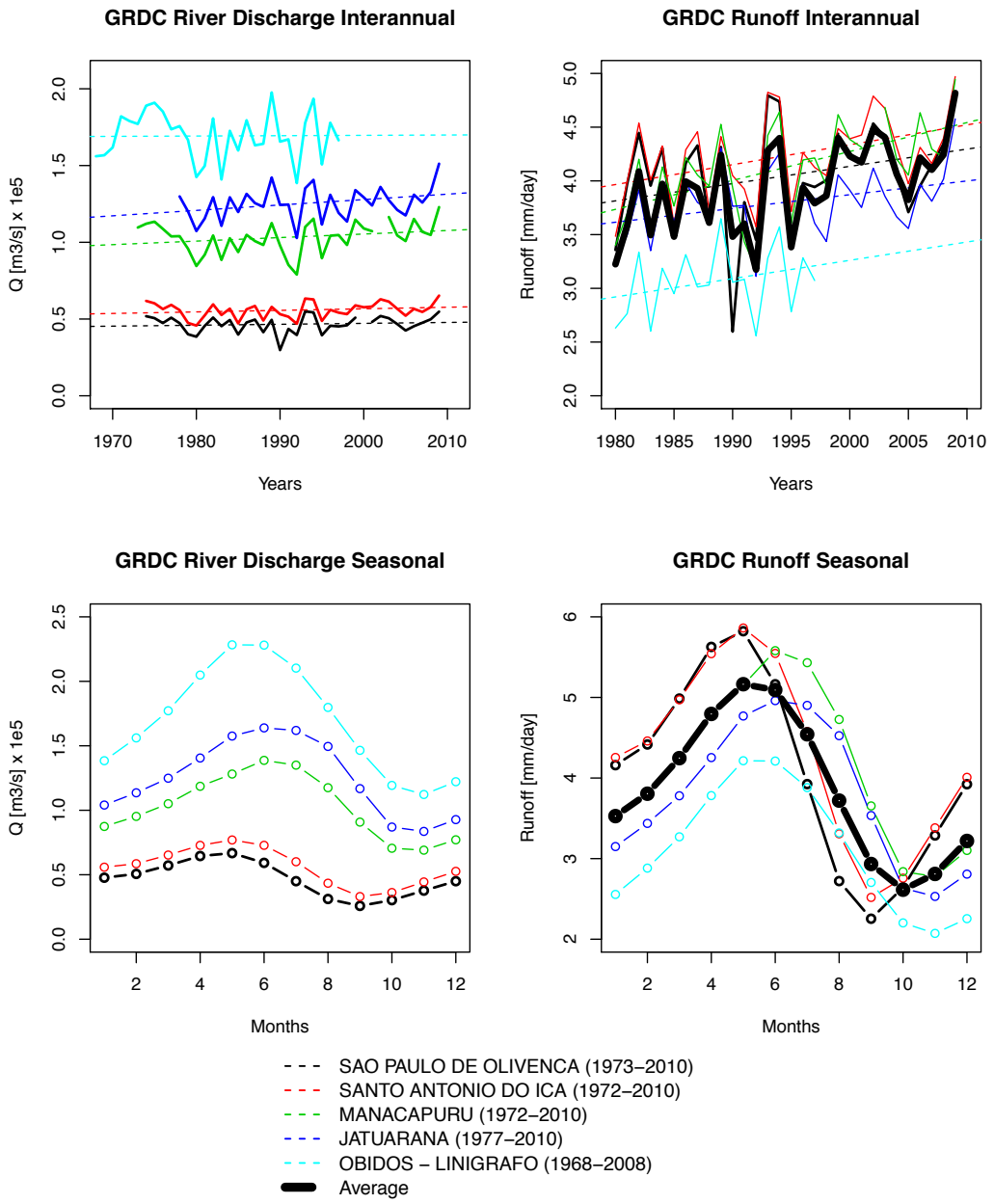

Figure 3. Interannual time series and seasonal climatology plots of GRDC river discharge and runoff.

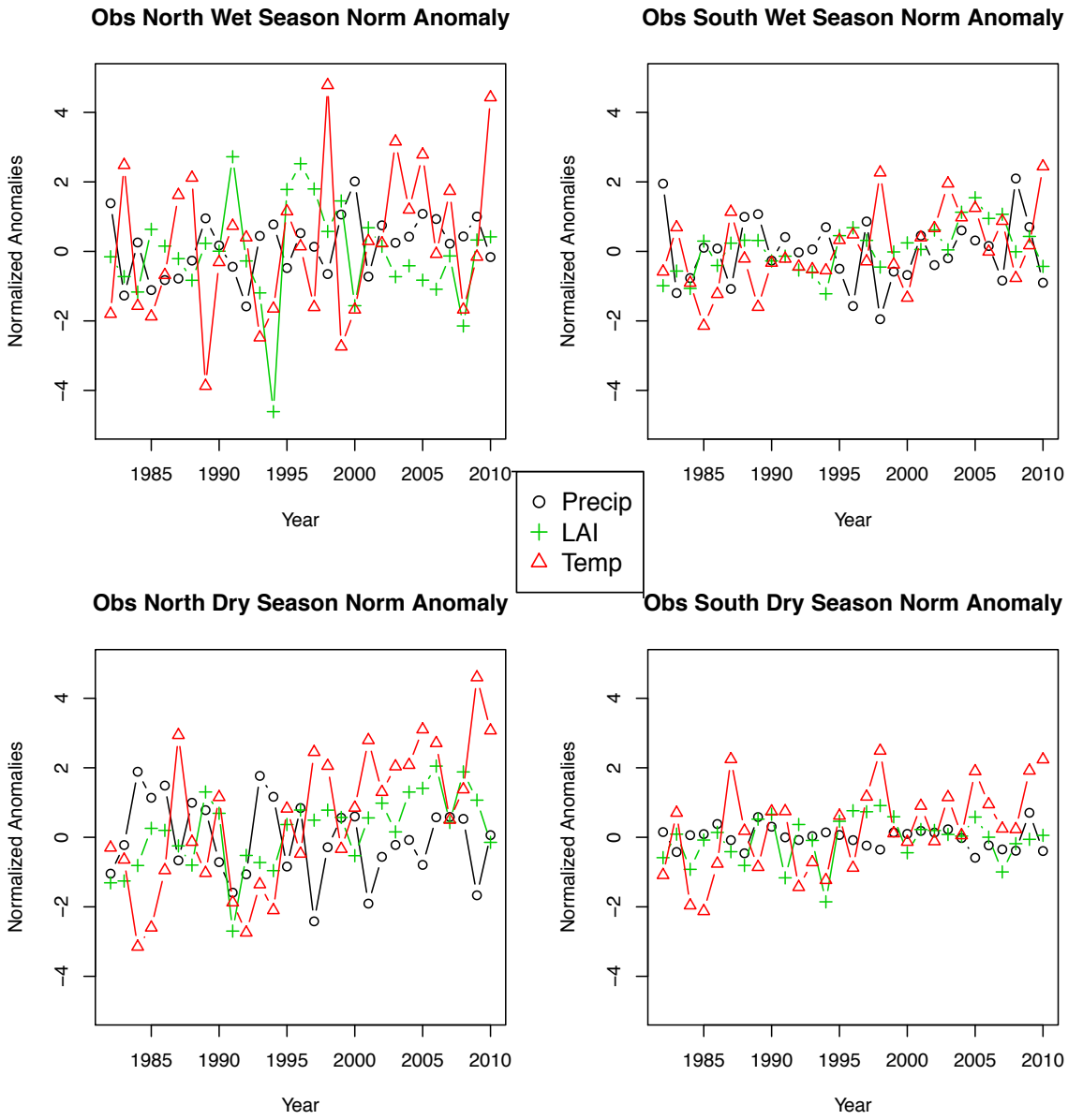

Figure 4a. North and South wet and dry seasonal normalized anomalies from 2000-2011 (observed data).

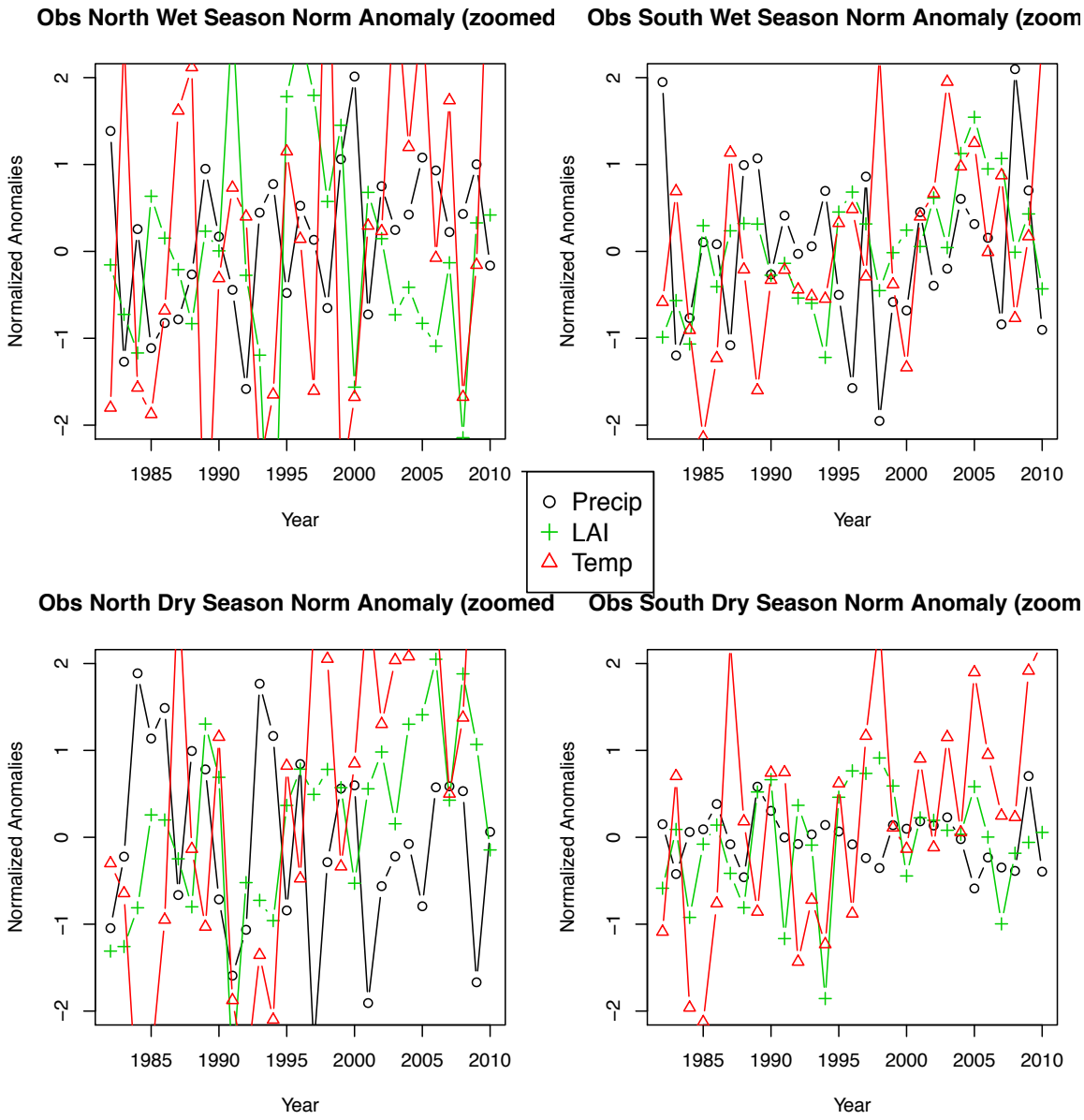

Figure 4b. North and South wet and dry seasonal normalized anomalies from 2000-2011 (observed data), zoomed in.

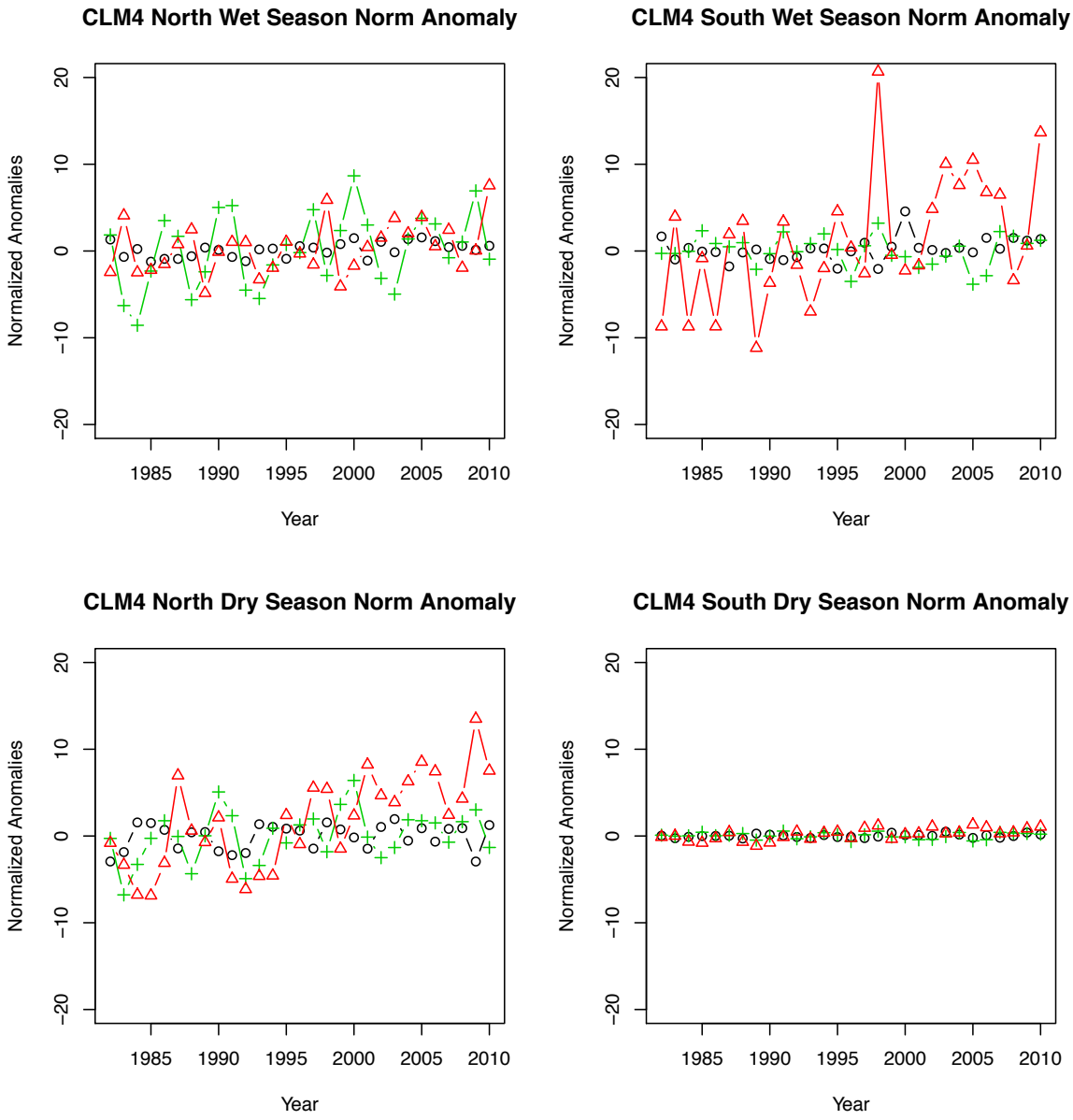

Figure 5a. North and South wet and dry seasonal normalized anomalies from 2000-2011 (CLM4 model).

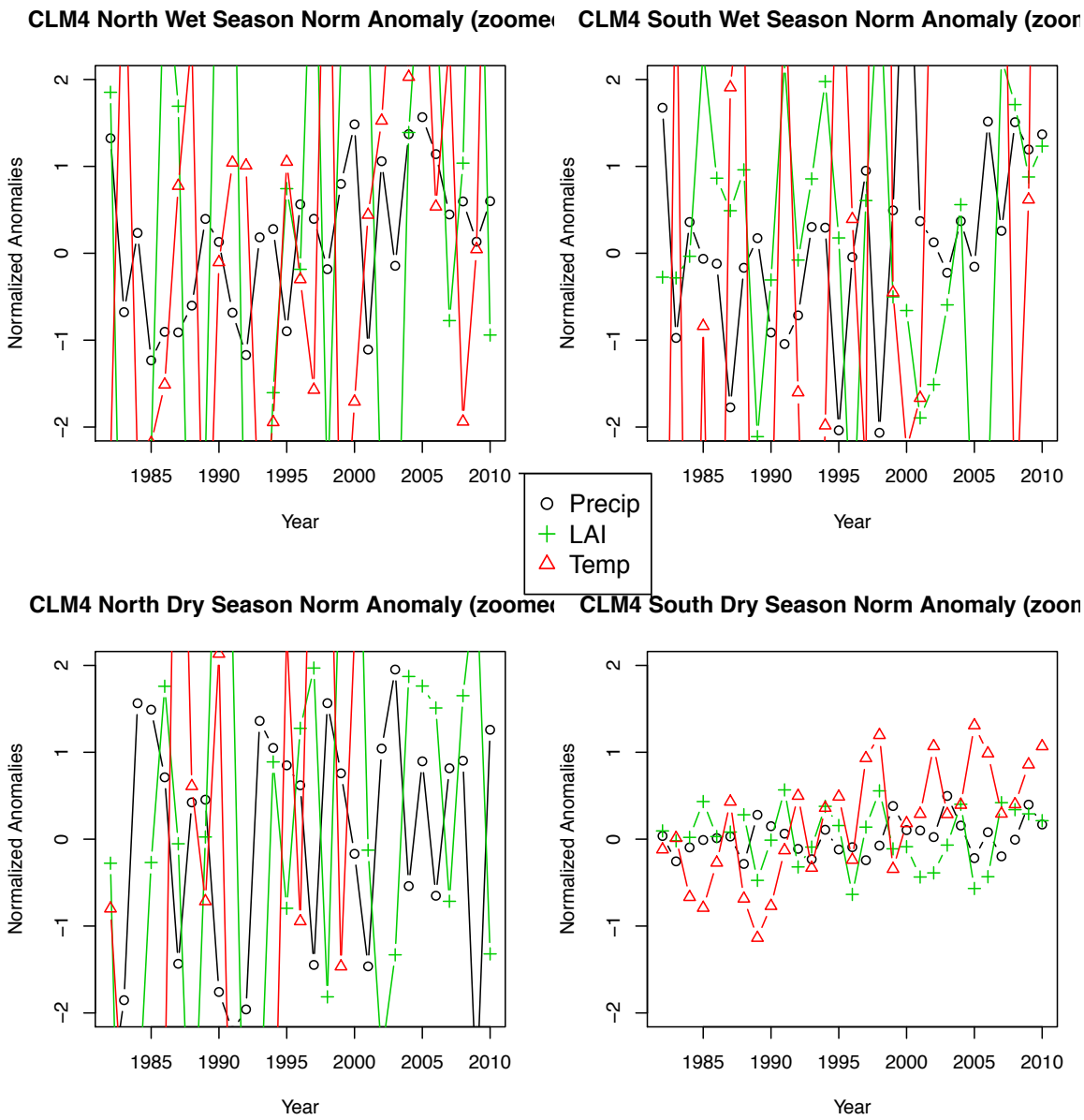

Figure 5b. North and South wet and dry seasonal normalized anomalies from 2000-2011 (CLM4 model), zoomed in.

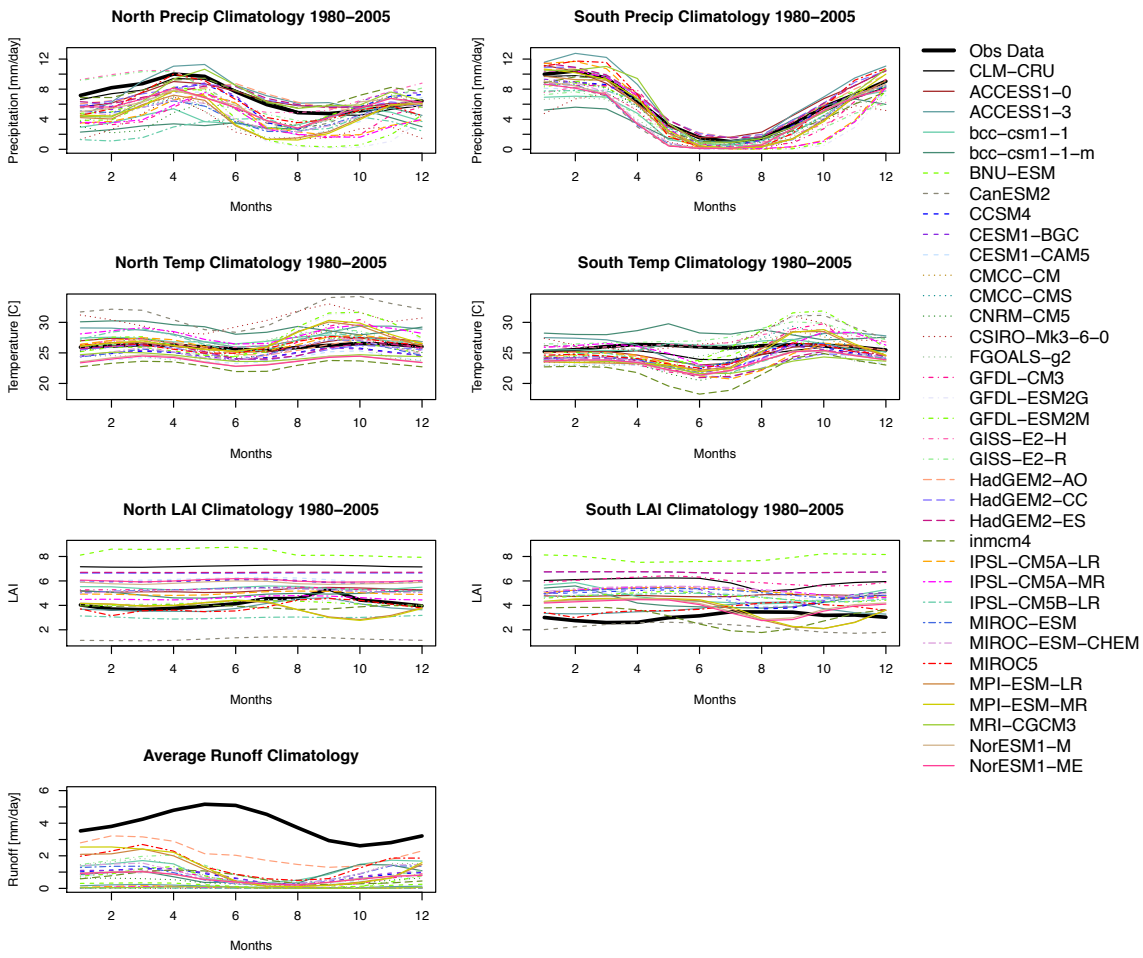

Figure 6. Seasonal cycles of models and observed data were compared by taking annual averages of each month over the years 1980-2005.

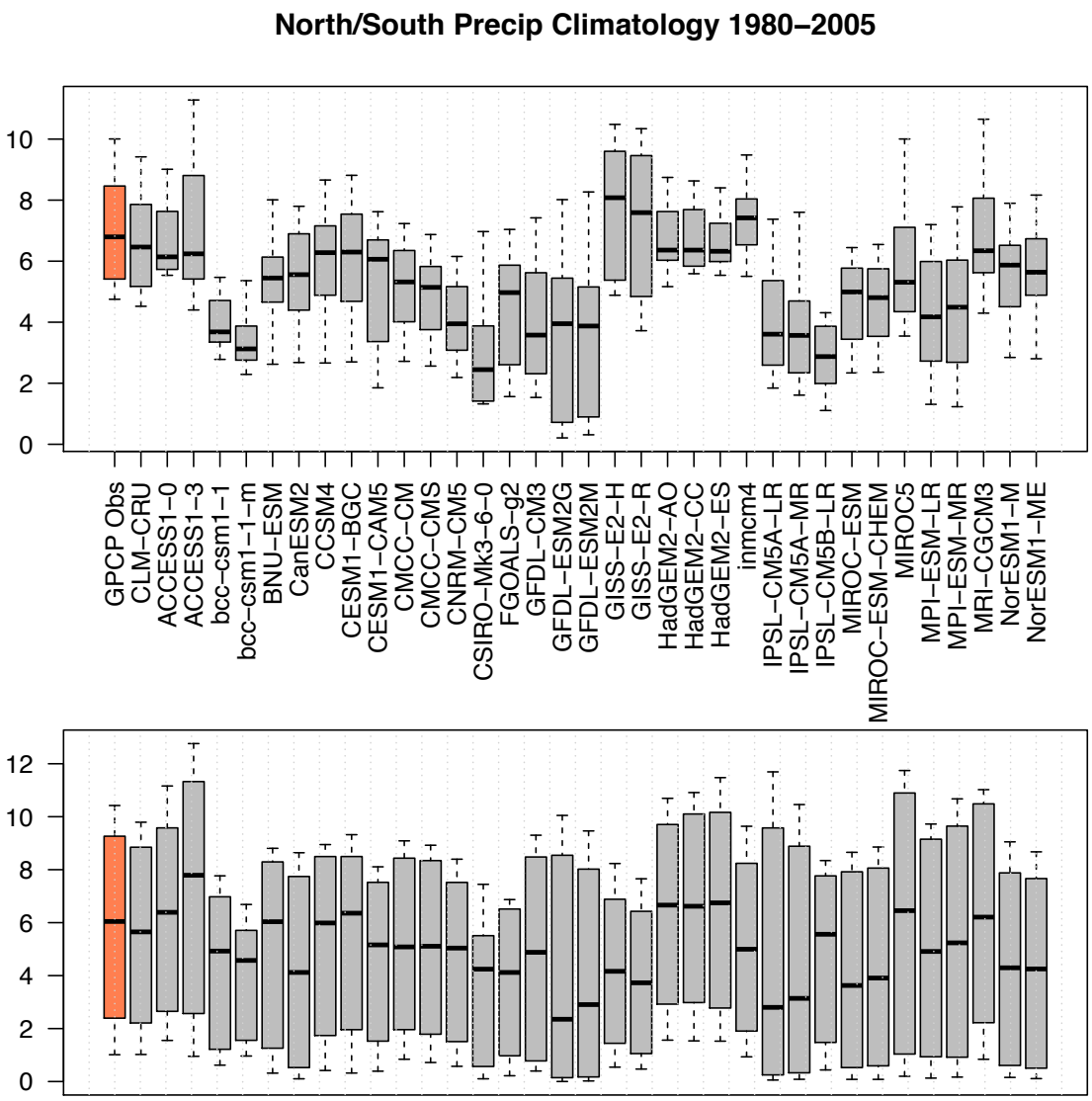

Figure 7a. Current climatology boxplots for North/South precipitation.

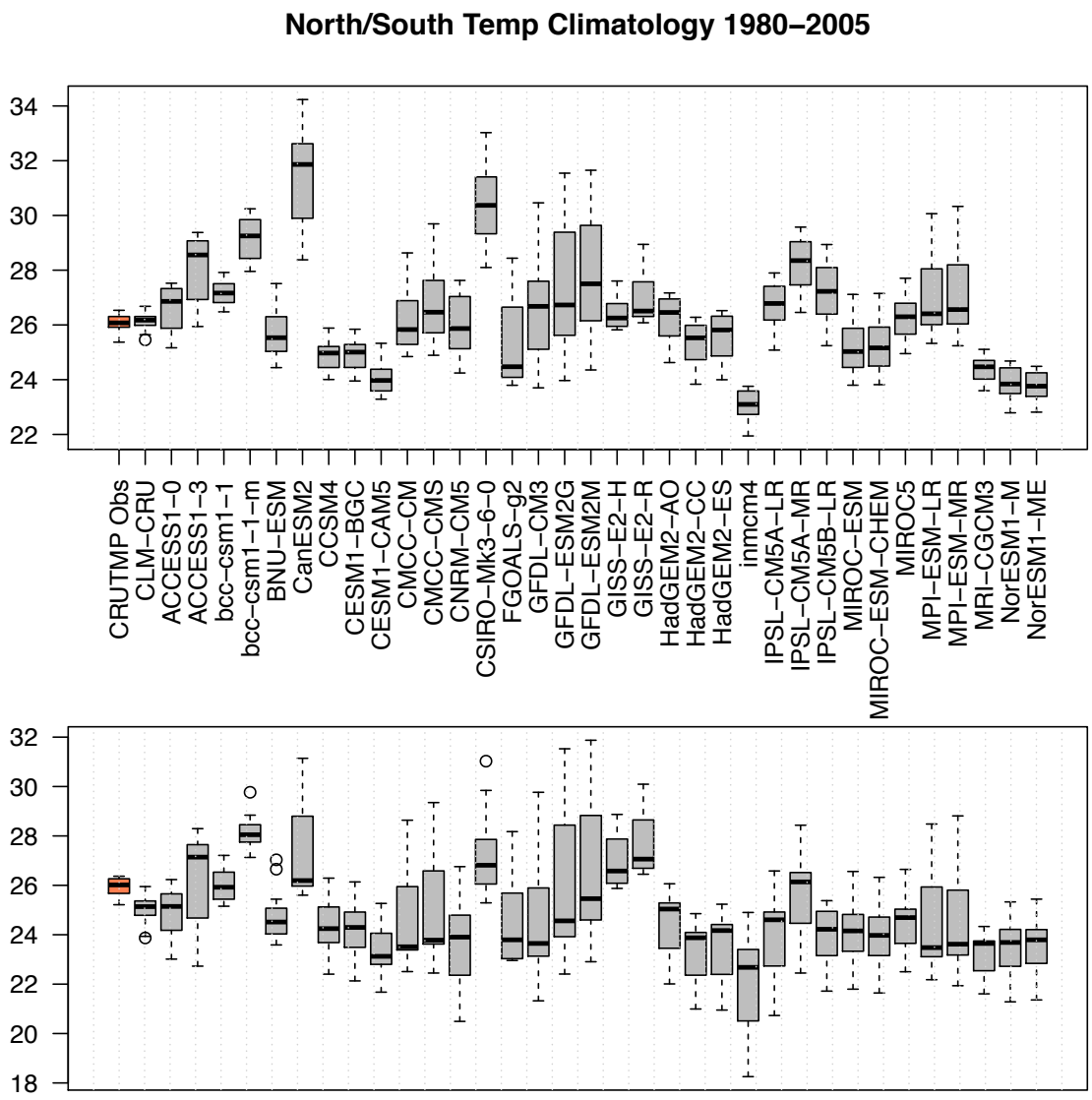

Figure 7b. Current climatology boxplots for North/South temperature.

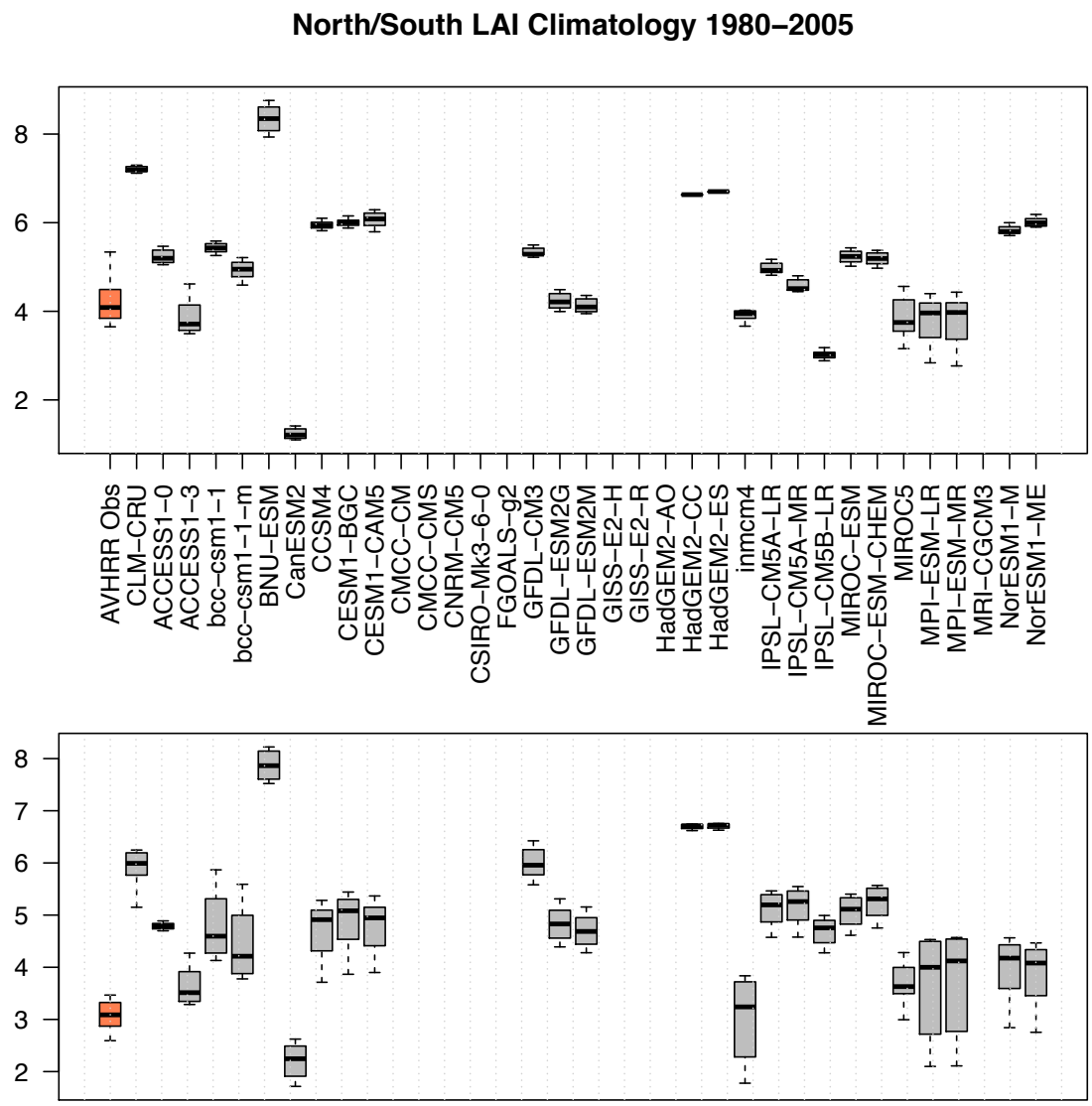

Figure 7c. Current climatology boxplots for North/South leaf area index.

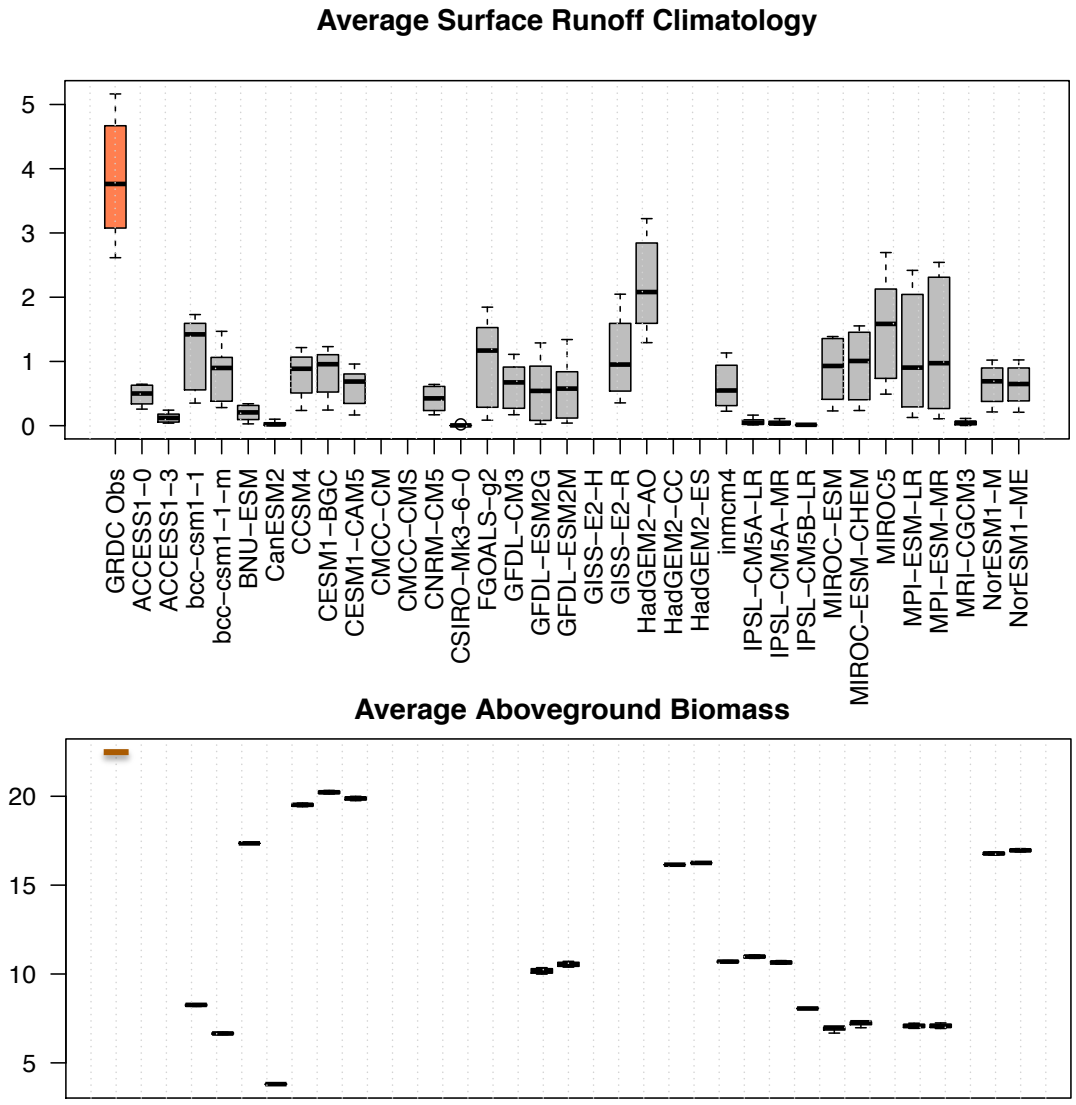

Figure 7d. Current climatology boxplots for Amazon runoff and average of aboveground biomass. Note that CLM4 run is not included for these two variables and that aboveground biomass is only mean from 1990-2000, with no seasonal distribution available.

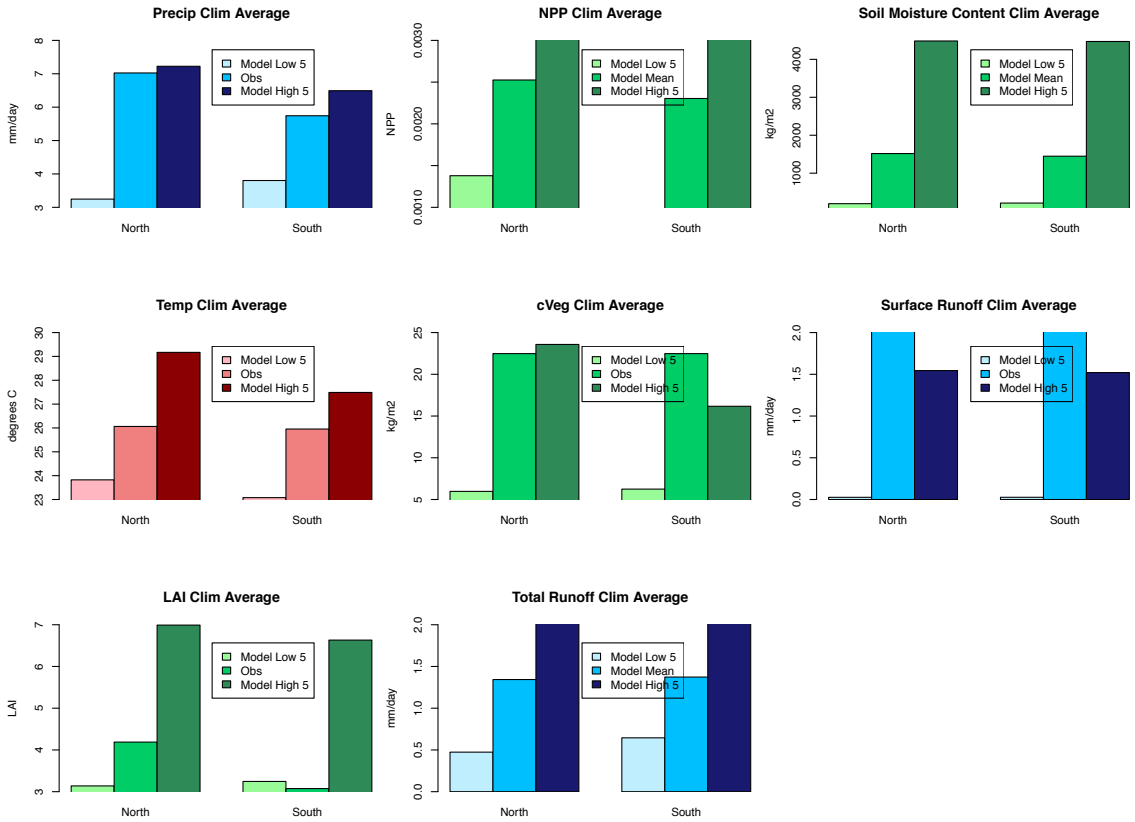

Figure 8. Bar plots of model 5 highs and 5 lows compared with observed data for current climate. Note that NPP, Total Runoff, and Soil Moisture are compared against models' mean due to lack of observed data.

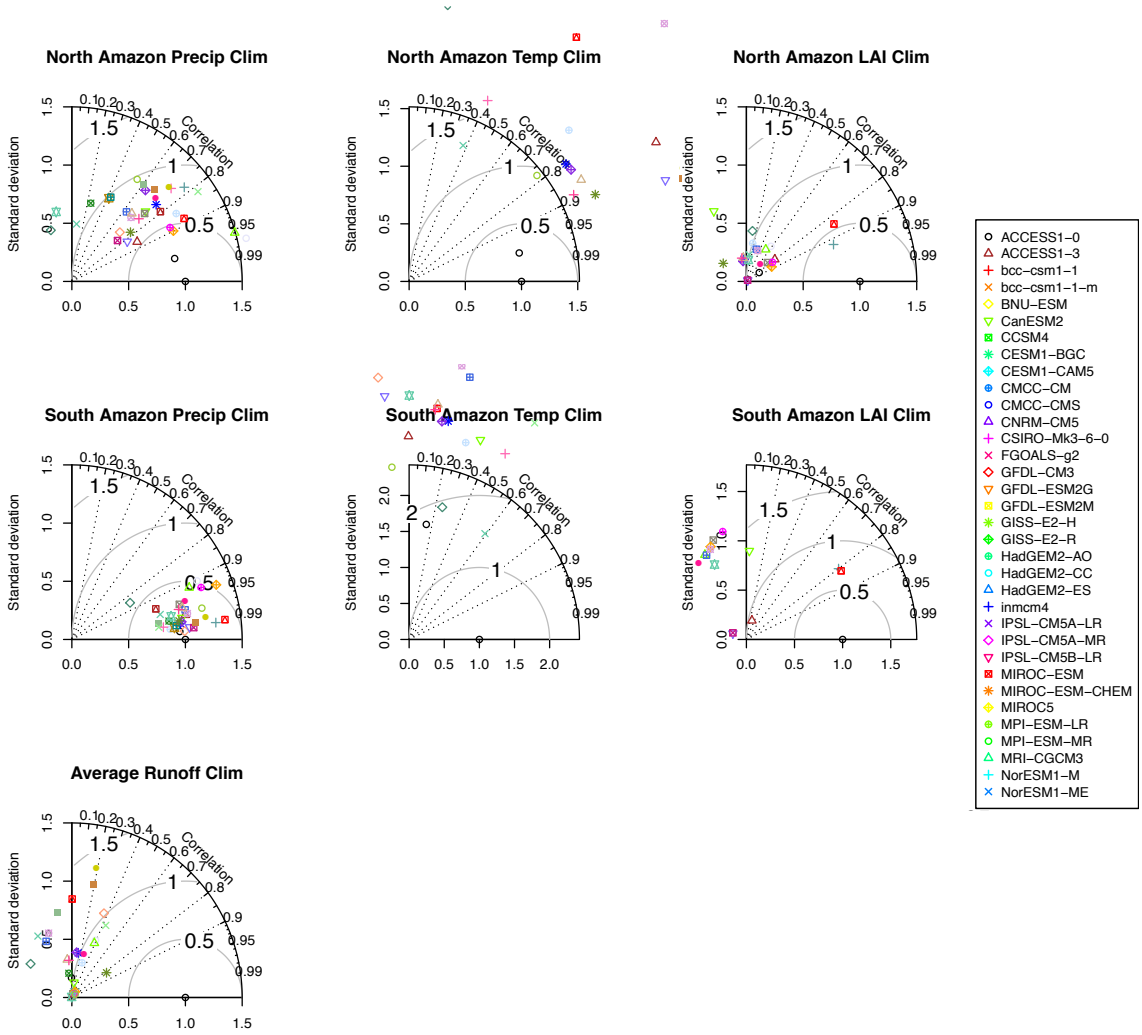

Figure 9. The correlation of the models to the observed data in the form of Taylor diagrams, which is essentially a graphic representation of Tables 6-7. Taylor diagrams are strong visualization tools that can show how closely model outputs match the observed data. The similarity, or "good fit", between two datasets is quantified by the correlation coefficient, which is the centered root-mean-square difference, and the amplitude of variations (represented by their standard deviations). For example, most models fall within +/- 0.5 mm/day in standard deviation and between 0.5 and 1 mm/day in RMS error for precipitation in North Amazon.

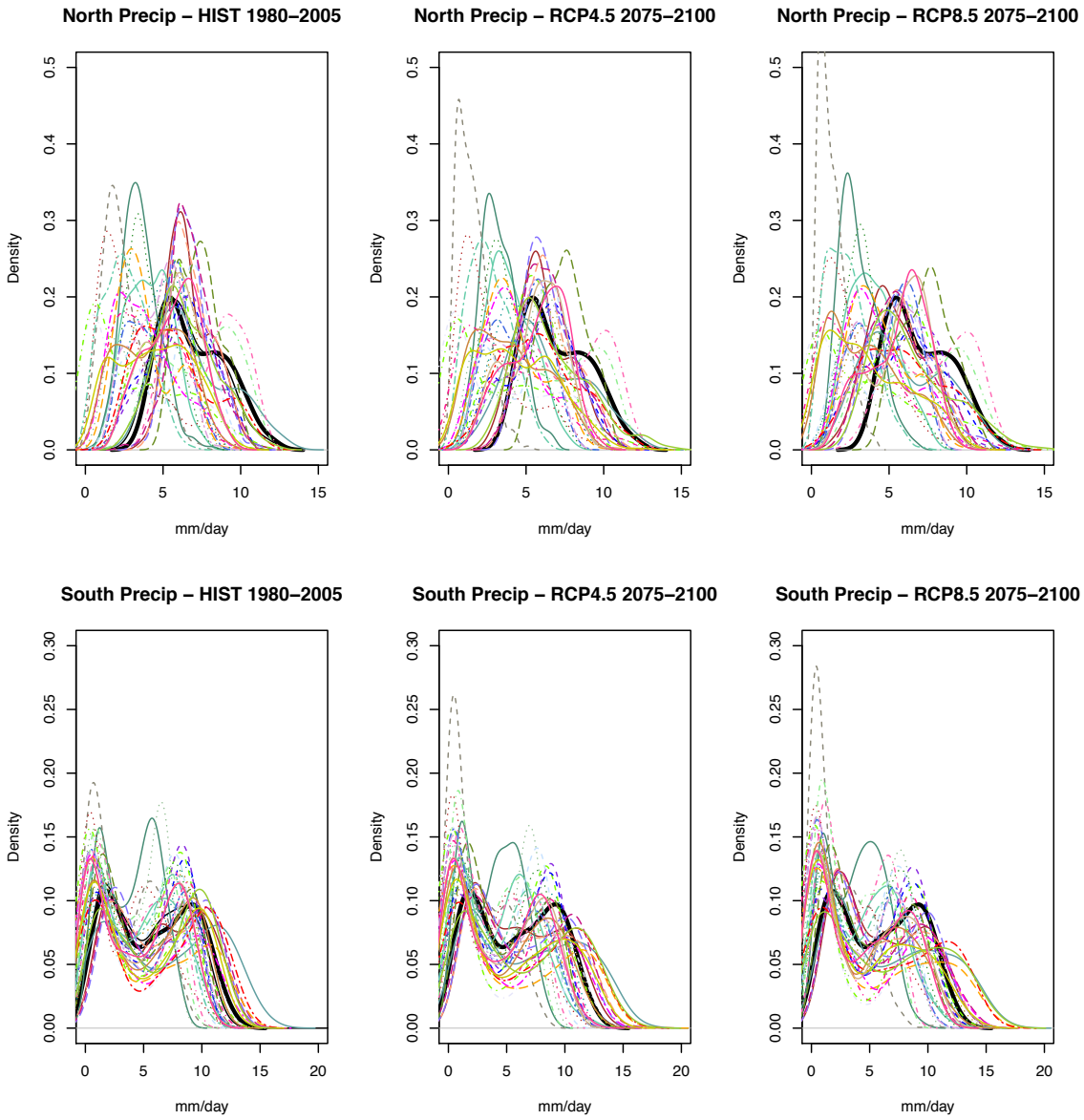

Figure 10a. Precipitation PDFs for CMIP5 historical run (1980-2005) and RCP scenarios (2075-2100). Bold black is observed data. Figures 10a-d shows the probability density function curves (PDF) for each observed variables in comparison to RCP 4.5 and RCP 8.5 future climate scenarios in the models. The observations are shown in each for ease of seeing changes, although we expect that changes may occur in the future.

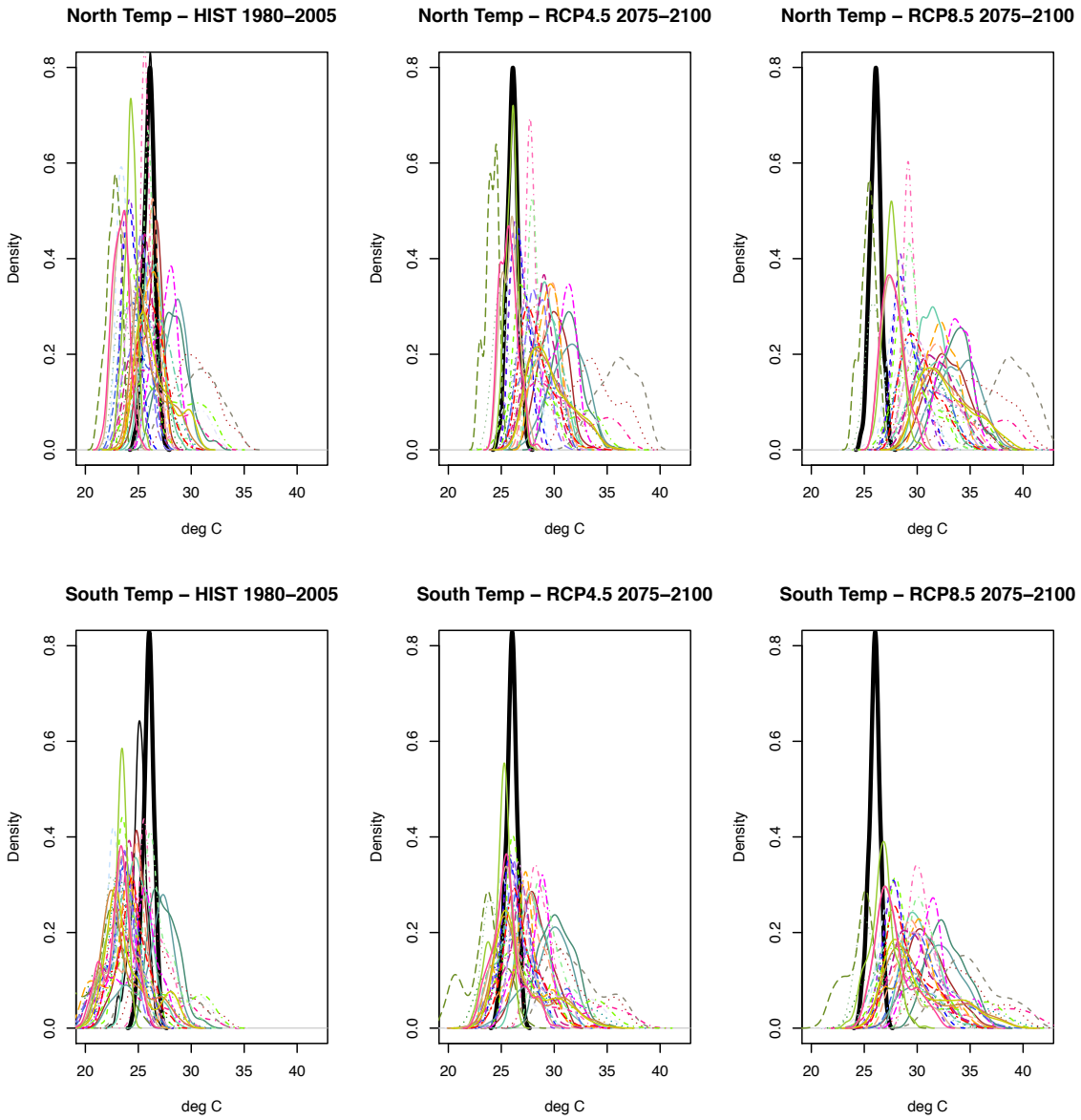

Figure 10b. Temperature PDFs for CMIP5 historical run (1980-2005) and RCP scenarios (2075-2100). Bold black is observed data.

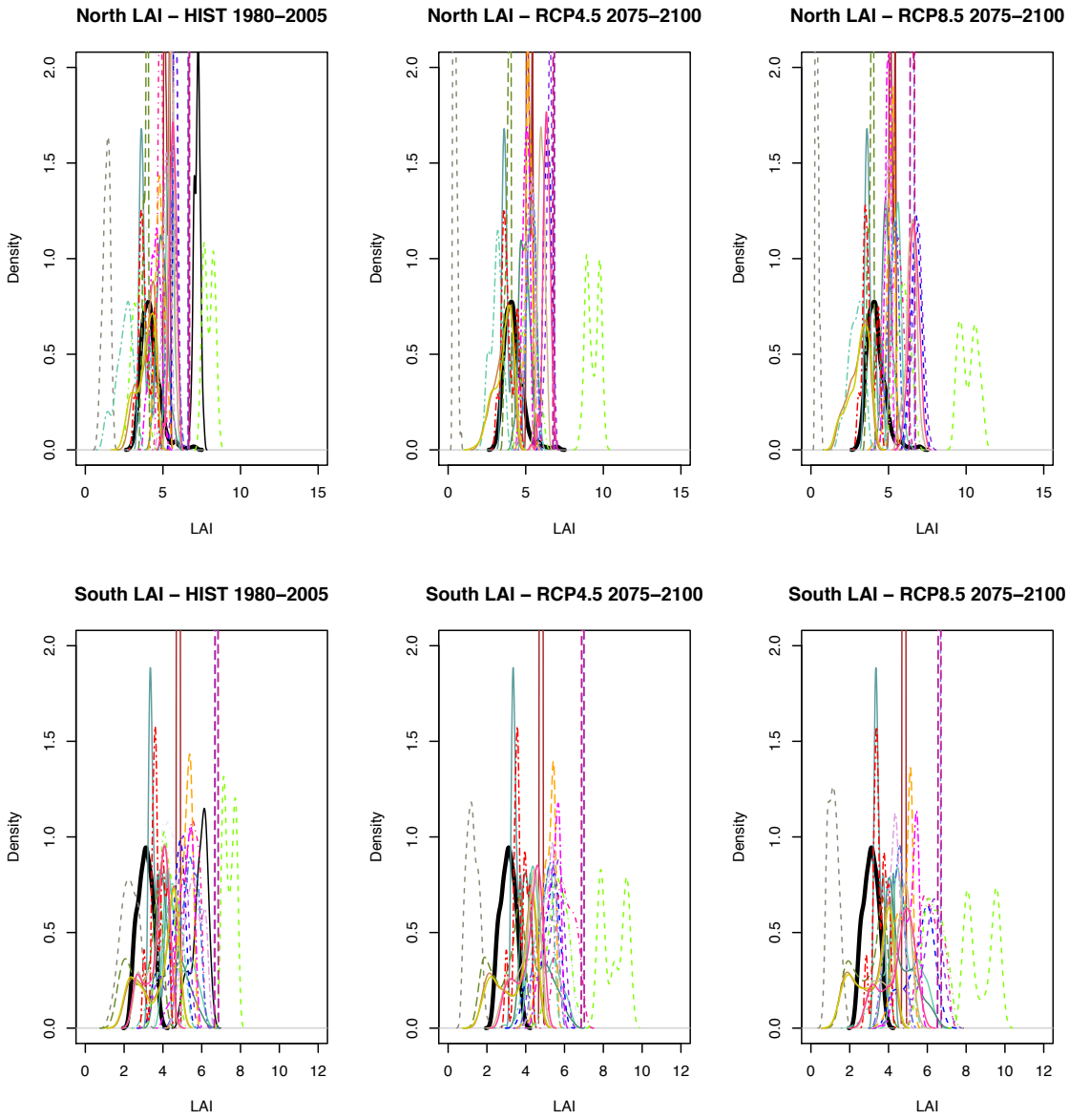

Figure 10c. Leaf Area Index PDFs for CMIP5 historical run (1980-2005) and RCP scenarios (2075-2100). Bold black is observed data.

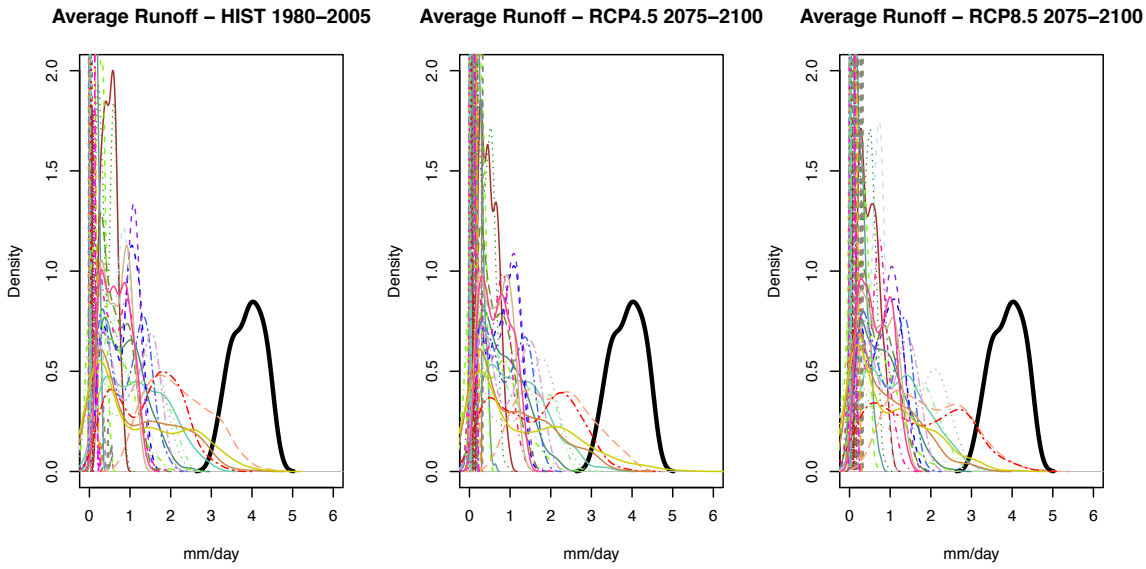

Figure 10d. Surface runoff PDFs for CMIP5 historical run (1980-2005) and RCP scenarios (2075-2100). Bold black is observed data.

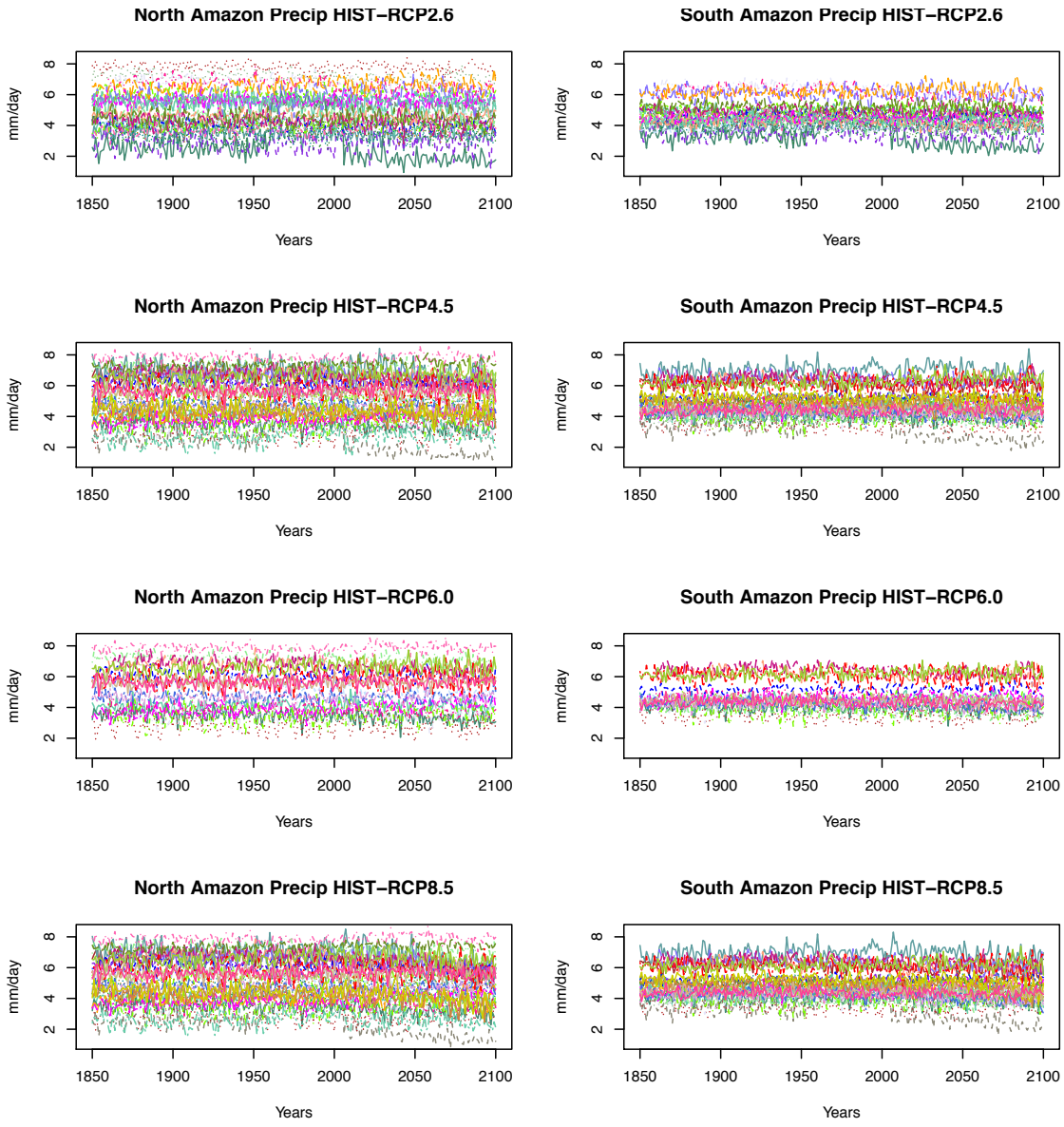

Figure 11a. Precipitation time series (HIST+RCP runs) of CMIP5 model outputs from 1850-2100 in different RCPs from present day climatology.

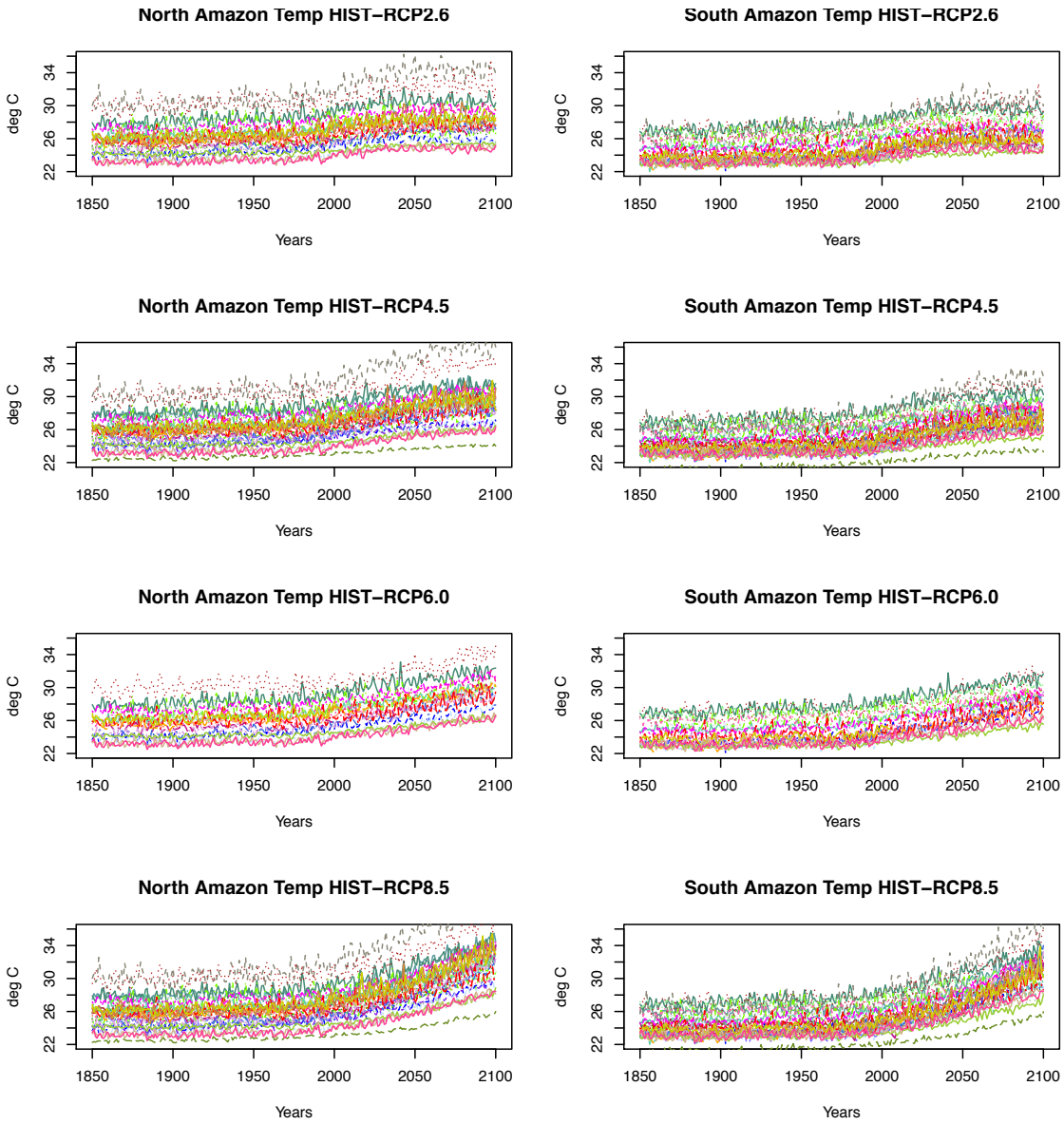

Figure 11b. Temperature time series (HIST+RCP runs) of CMIP5 model outputs from 1850-2100 in different RCPs from present day climatology.

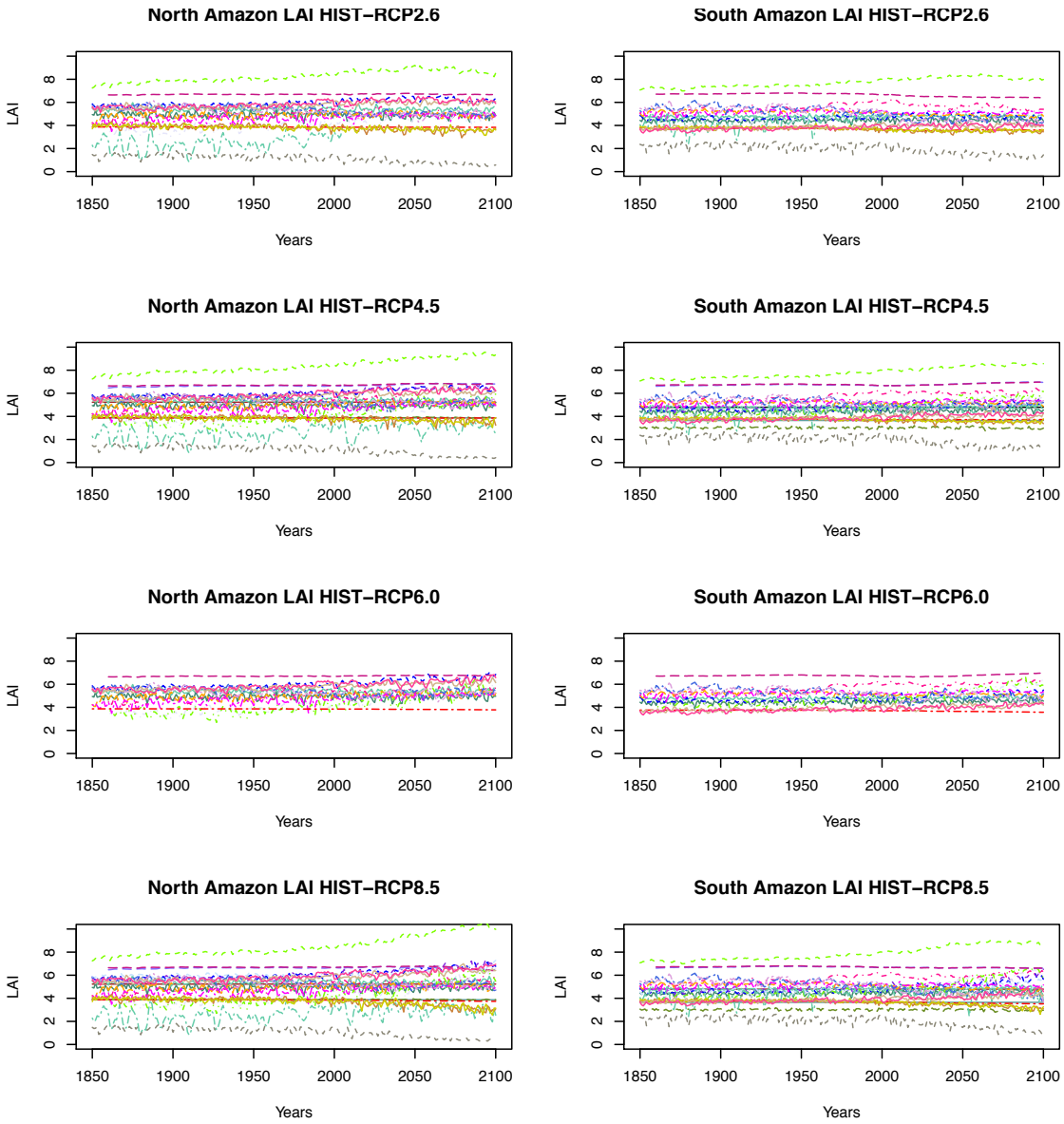

Figure 11c. Leaf Area Index time series (HIST+RCP runs) of CMIP5 model outputs from 1850-2100 in different RCPs from present day climatology.

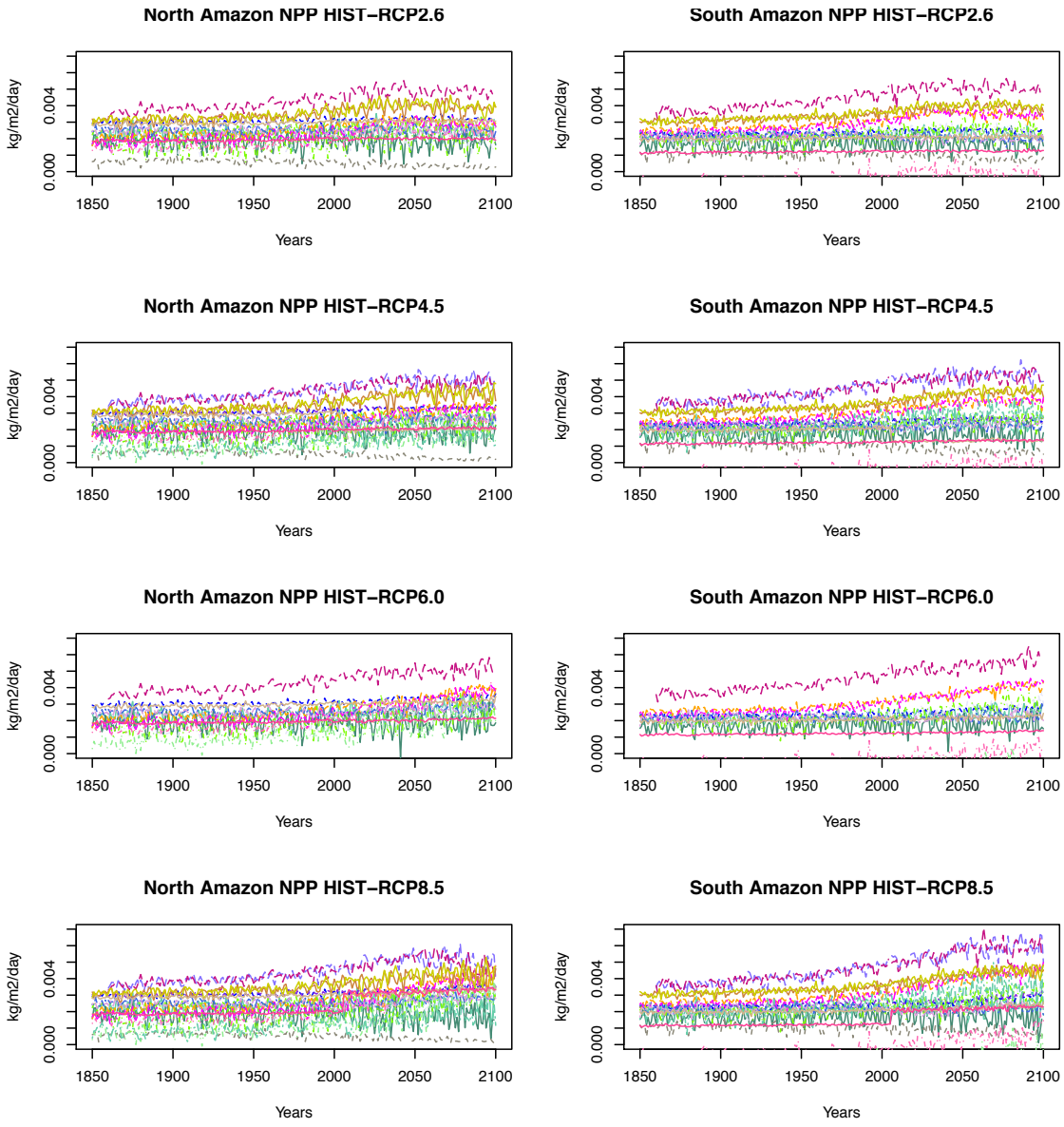

Figure 11d. Net primary production time series (HIST+RCP runs) of CMIP5 model outputs from 1850-2100 in different RCPs from present day climatology.

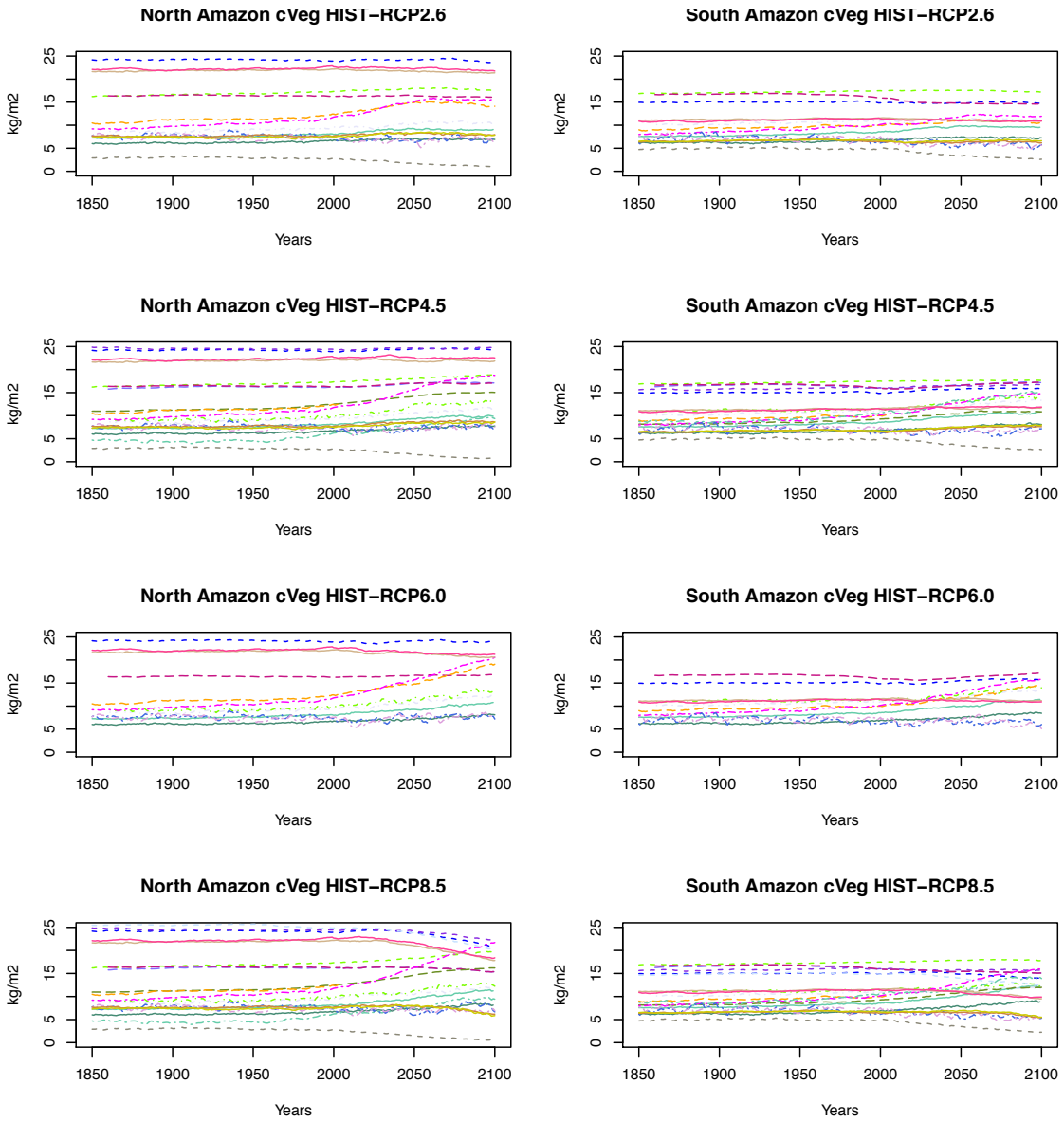

Figure 11e. Carbon in vegetation time series (HIST+RCP runs) of CMIP5 model outputs from 1850-2100 in different RCPs from present day climatology.

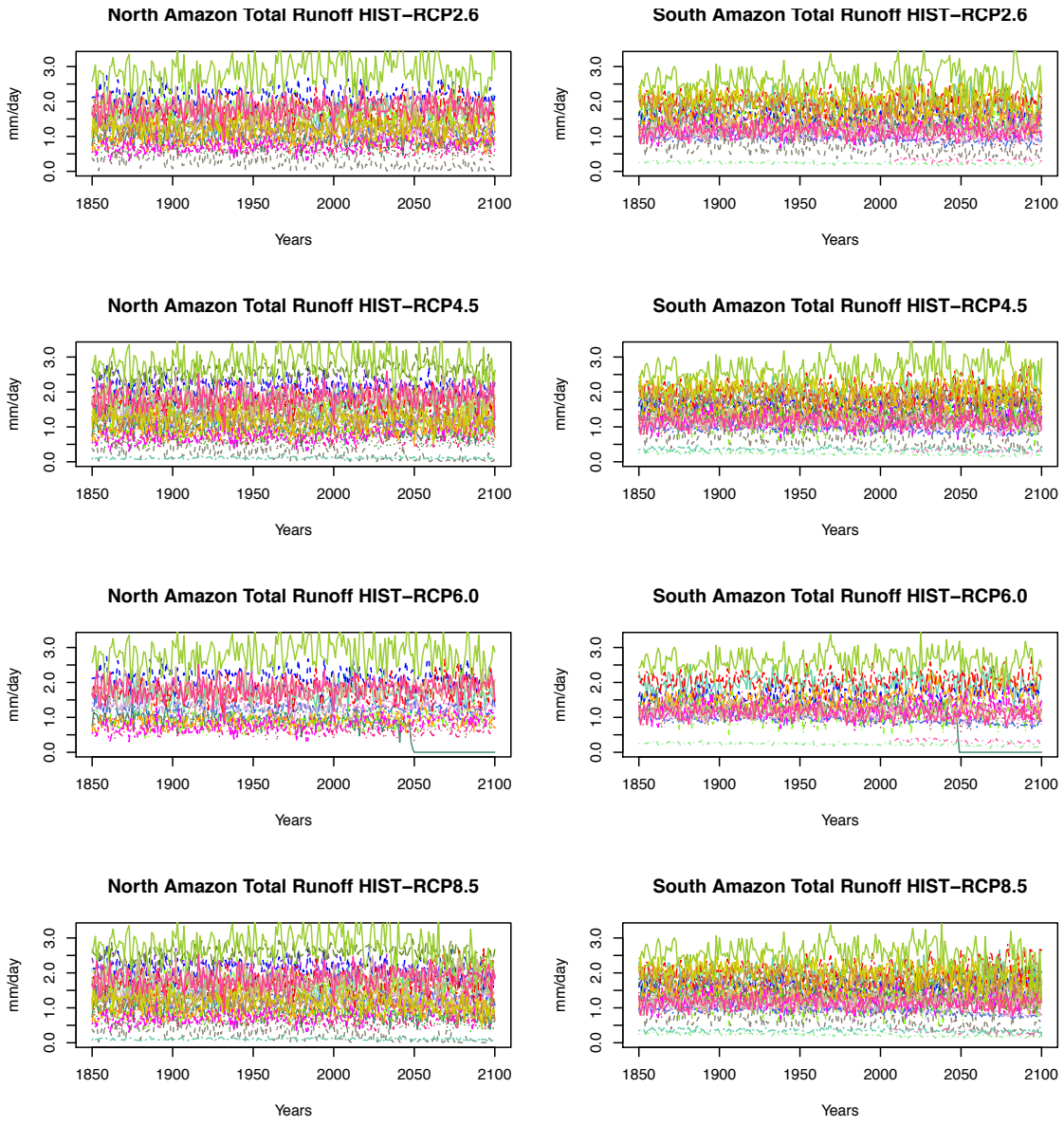

Figure 11f. Total Runoff time series (HIST+RCP runs) of CMIP5 model outputs from 1850-2100 in different RCPs from present day climatology.

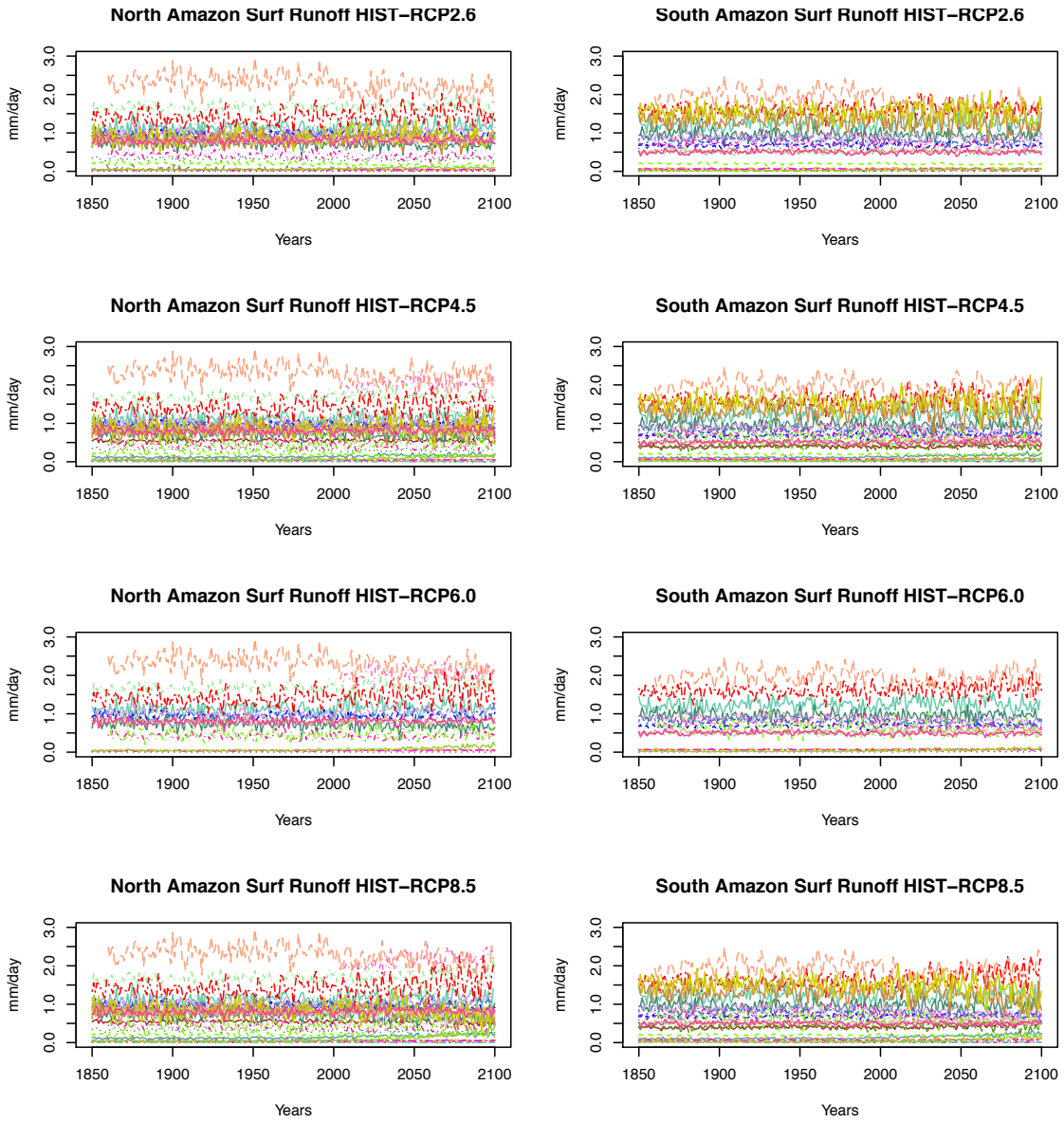

Figure 11g. Surface runoff time series (HIST+RCP runs) of CMIP5 model outputs from 1850-2100 in different RCPs from present day climatology.

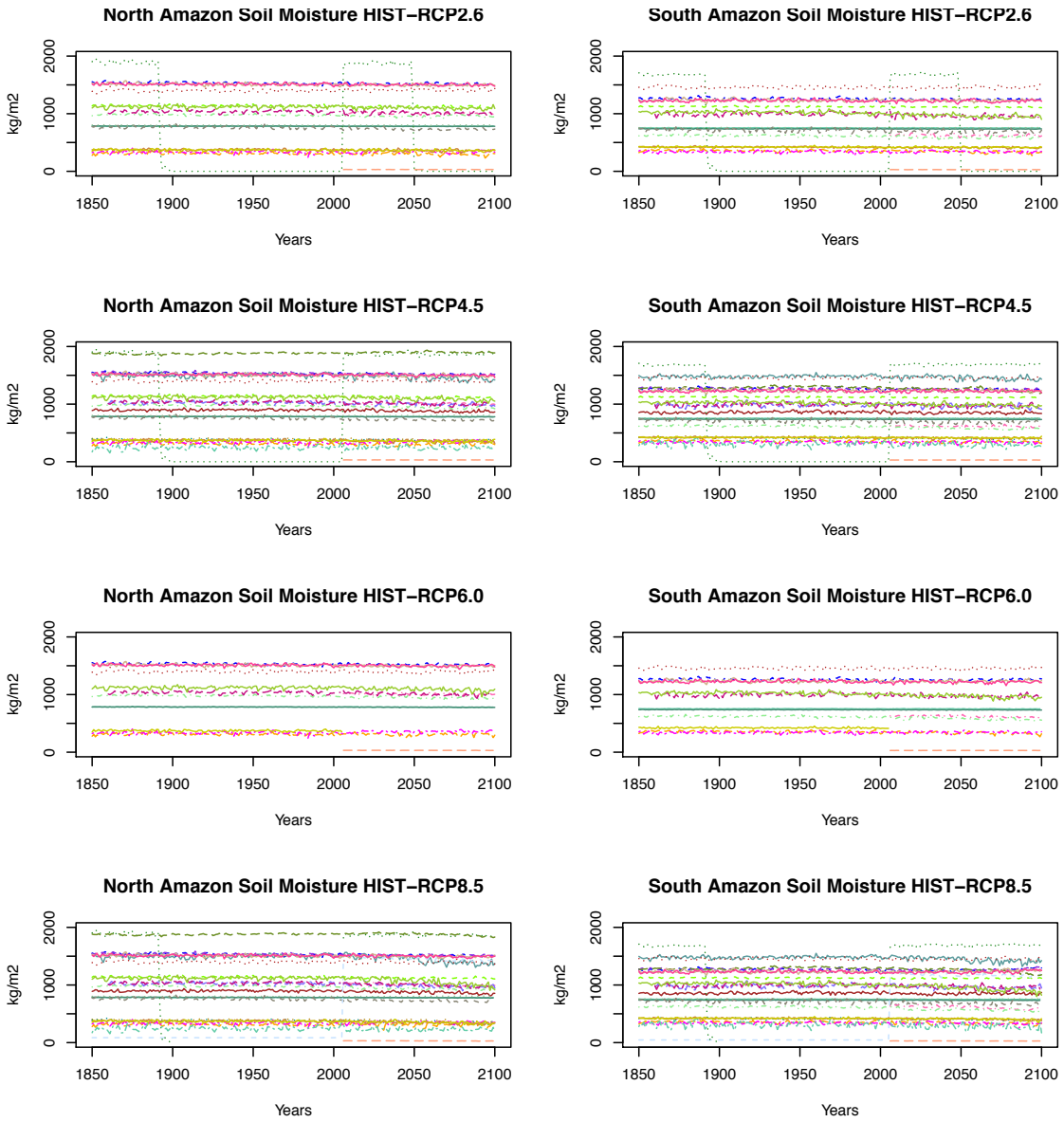

Figure 11h. Soil Moisture Content time series (HIST+RCP runs) of CMIP5 model outputs from 1850-2100 in different RCPs from present day climatology.

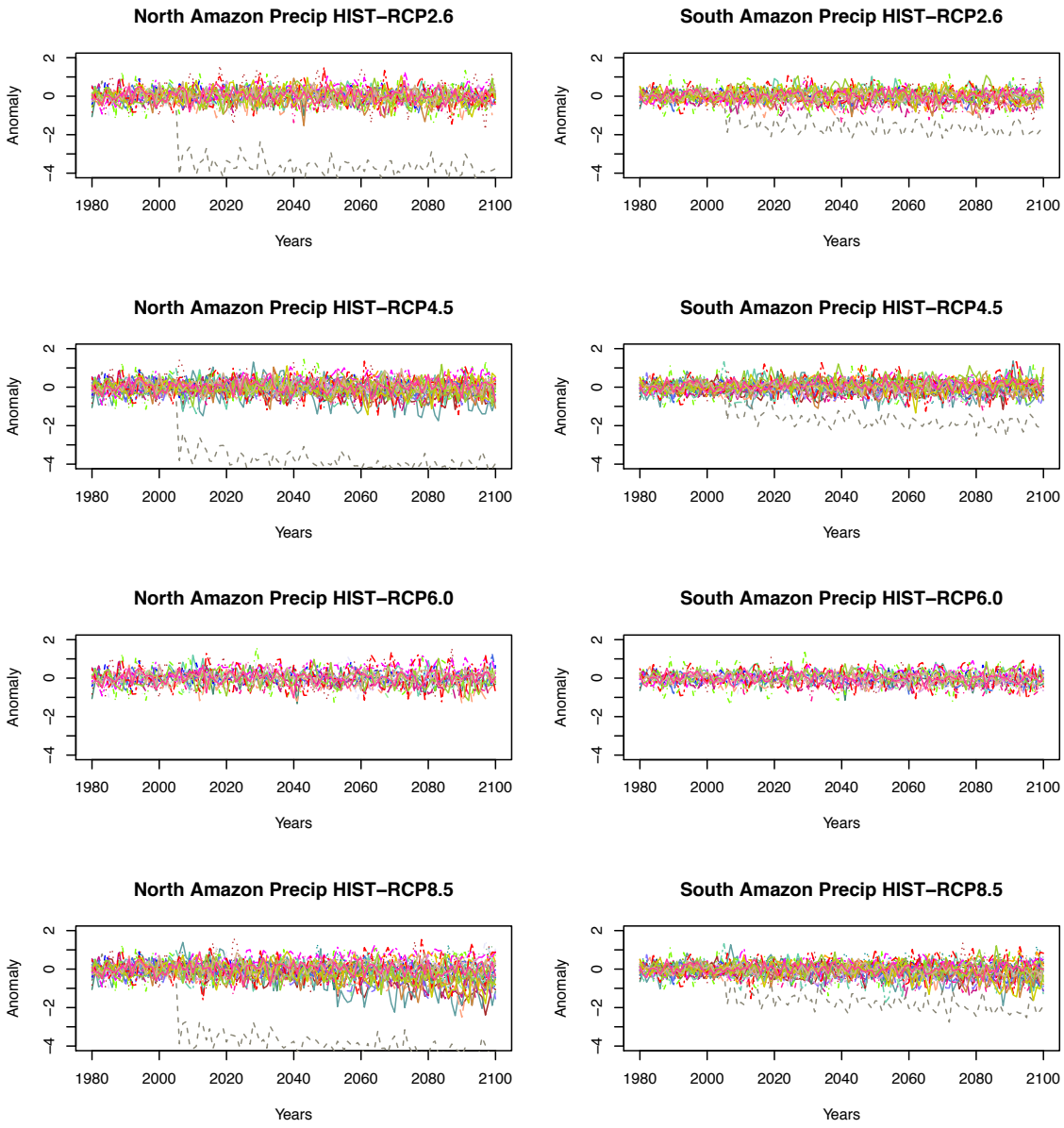

Figure 12a. Precipitation anomalies (from present day climatology) of CMIP5 model outputs in different RCPs.

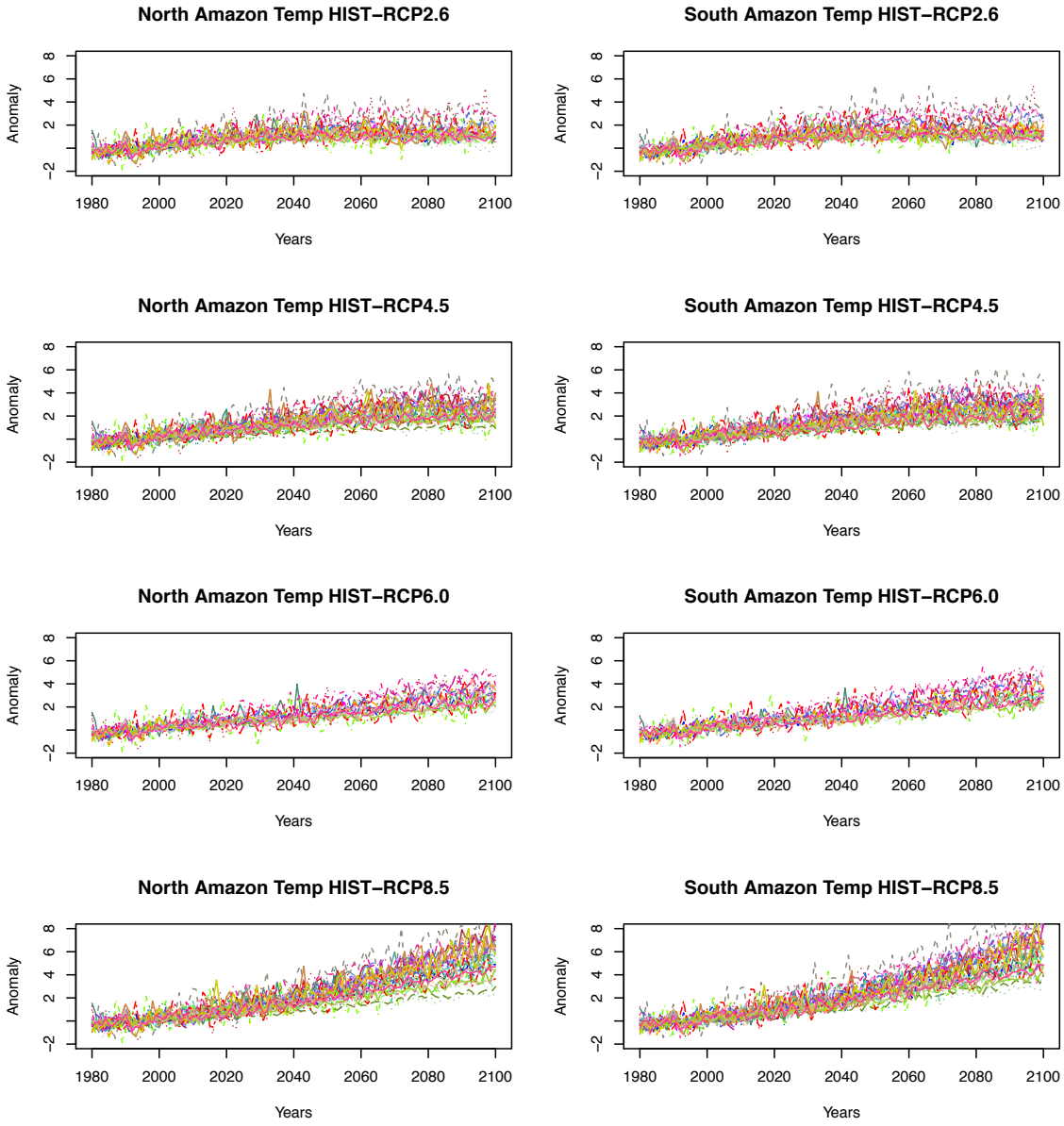

Figure 12b. Temperature CMIP5 anomalies (from present day climatology) of CMIP5 model outputs in different RCPs.

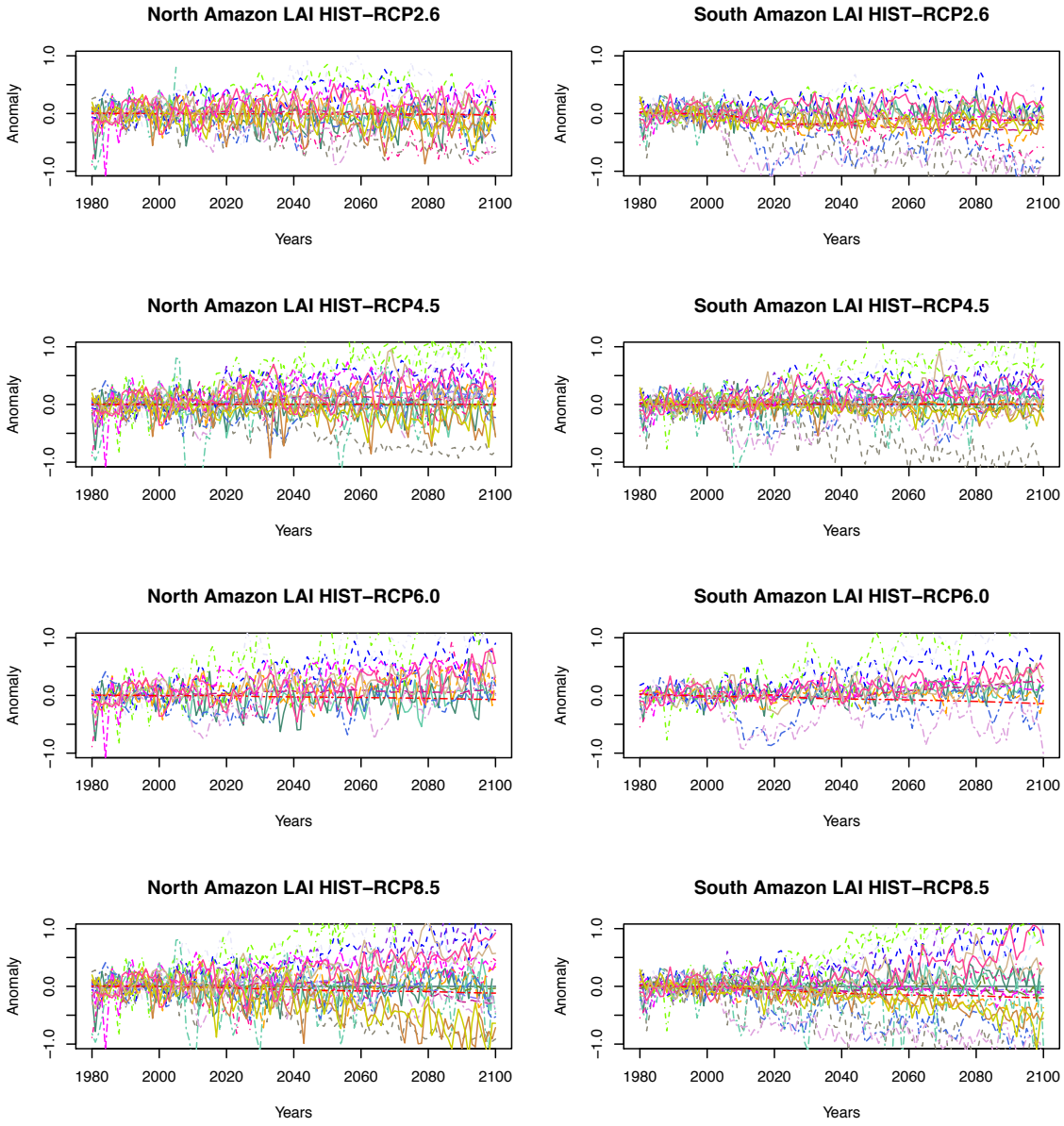

Figure 12c. Leaf Area Index CMIP5 anomalies (from present day climatology) of CMIP5 model outputs in different RCPs.

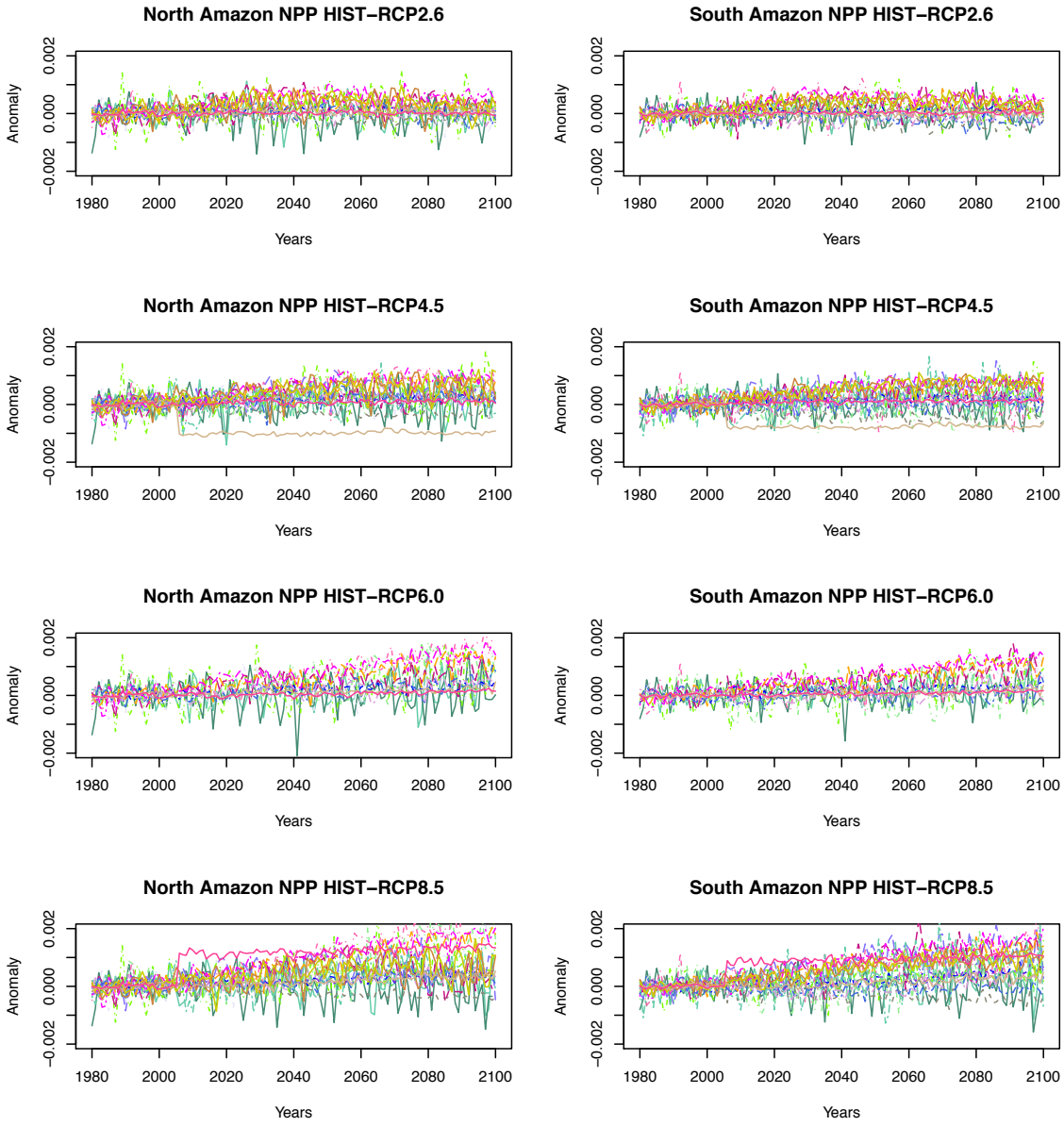

Figure 12d. Net primary production CMIP5 anomalies (from present day climatology) of CMIP5 model outputs in different RCPs.

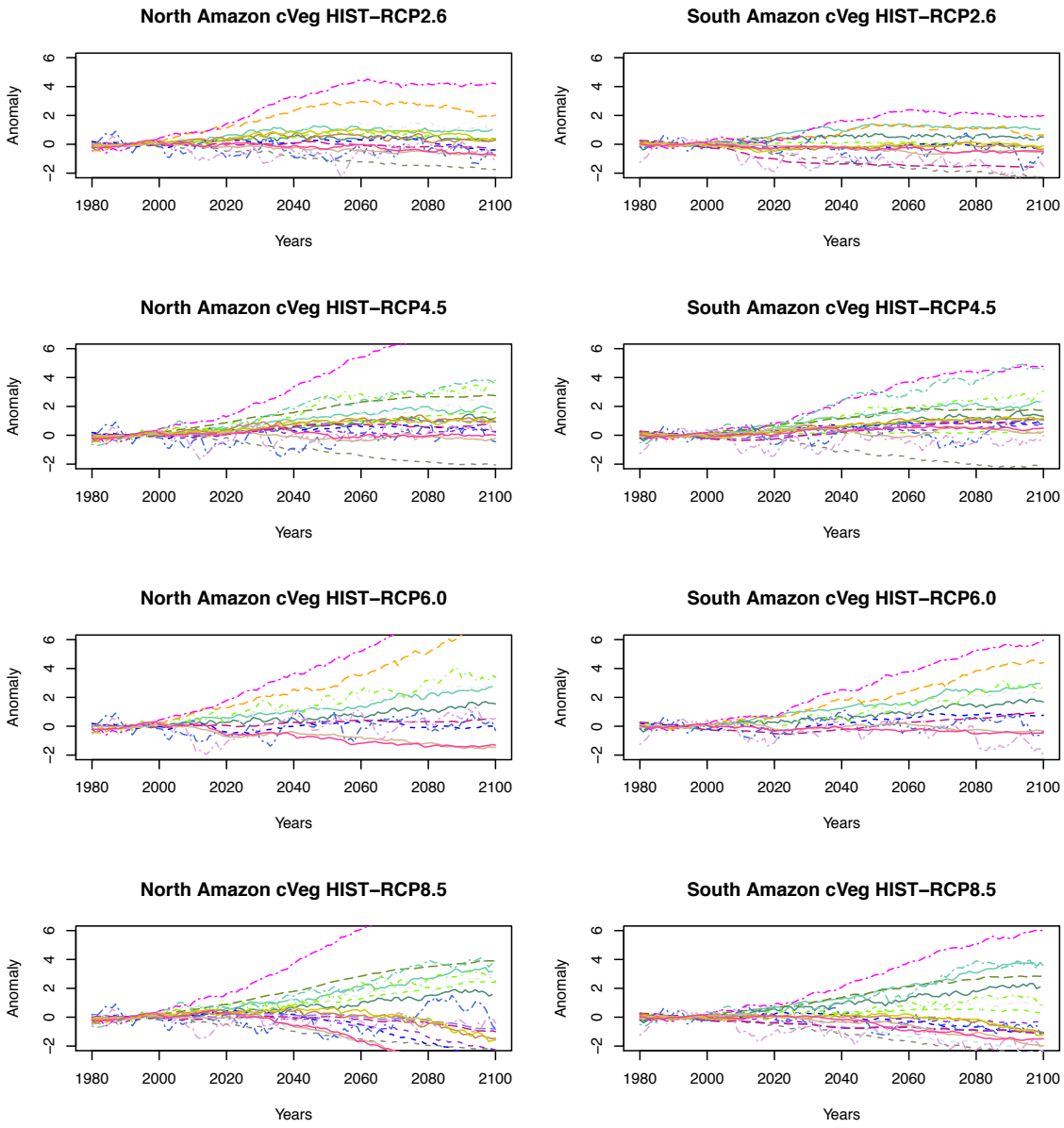

Figure 12e. Carbon in vegetation CMIP5 anomalies (from present day climatology) of CMIP5 model outputs in different RCPs.

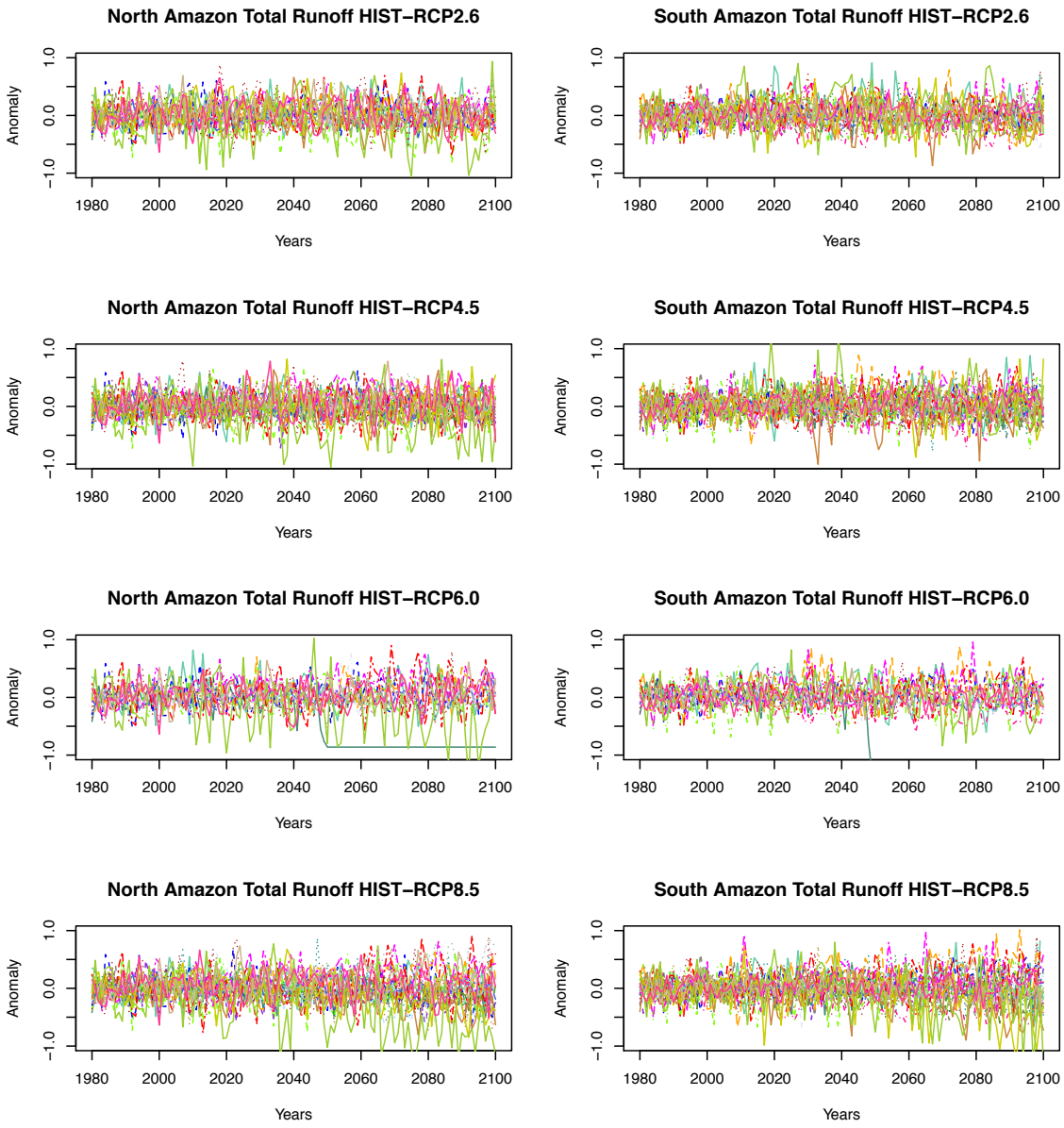

Figure 12f. Total runoff CMIP5 anomalies (from present day climatology) of CMIP5 model outputs in different RCPs.

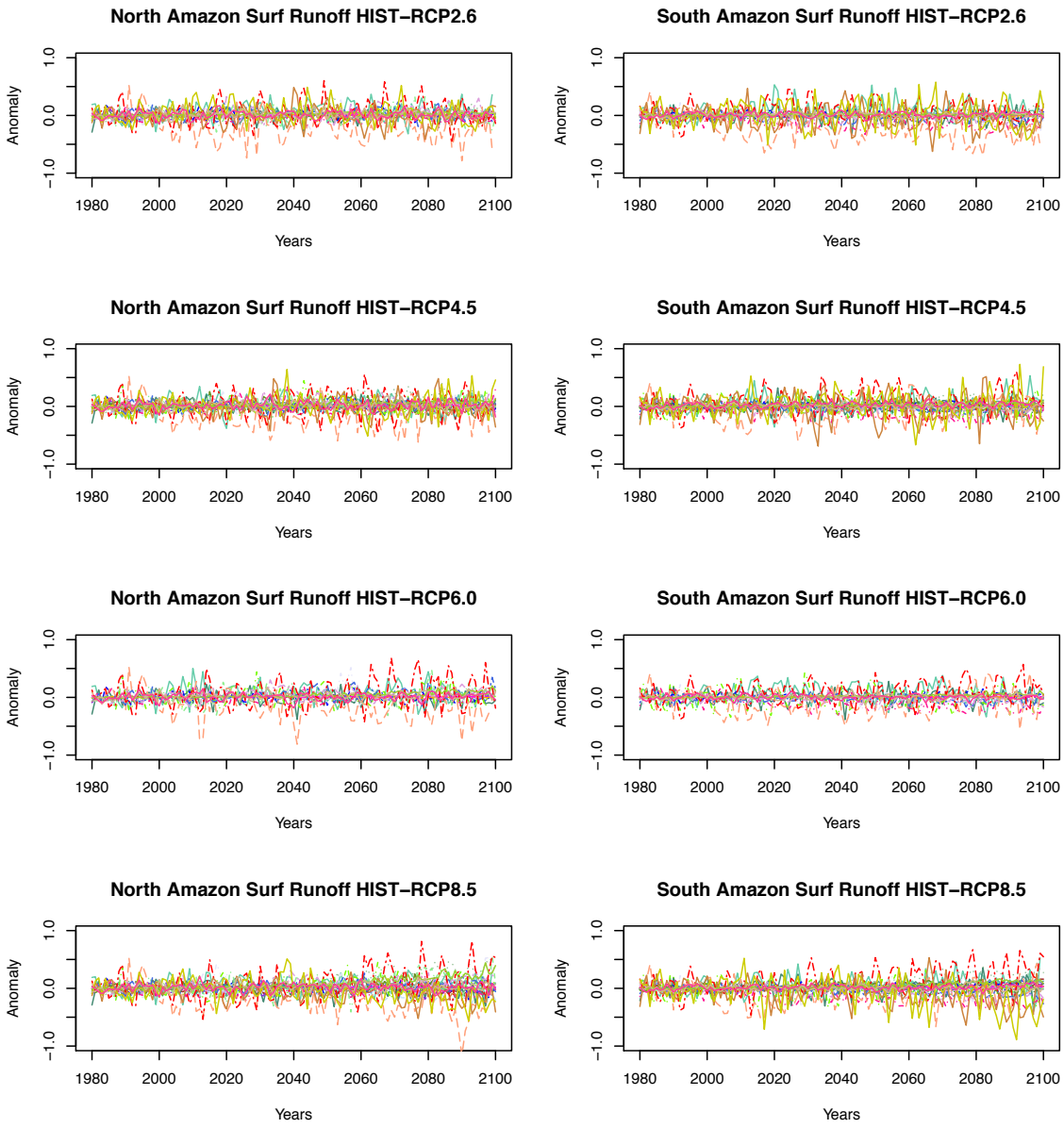

Figure 12g. Surface runoff CMIP5 anomalies (from present day climatology) of CMIP5 model outputs in different RCPs.

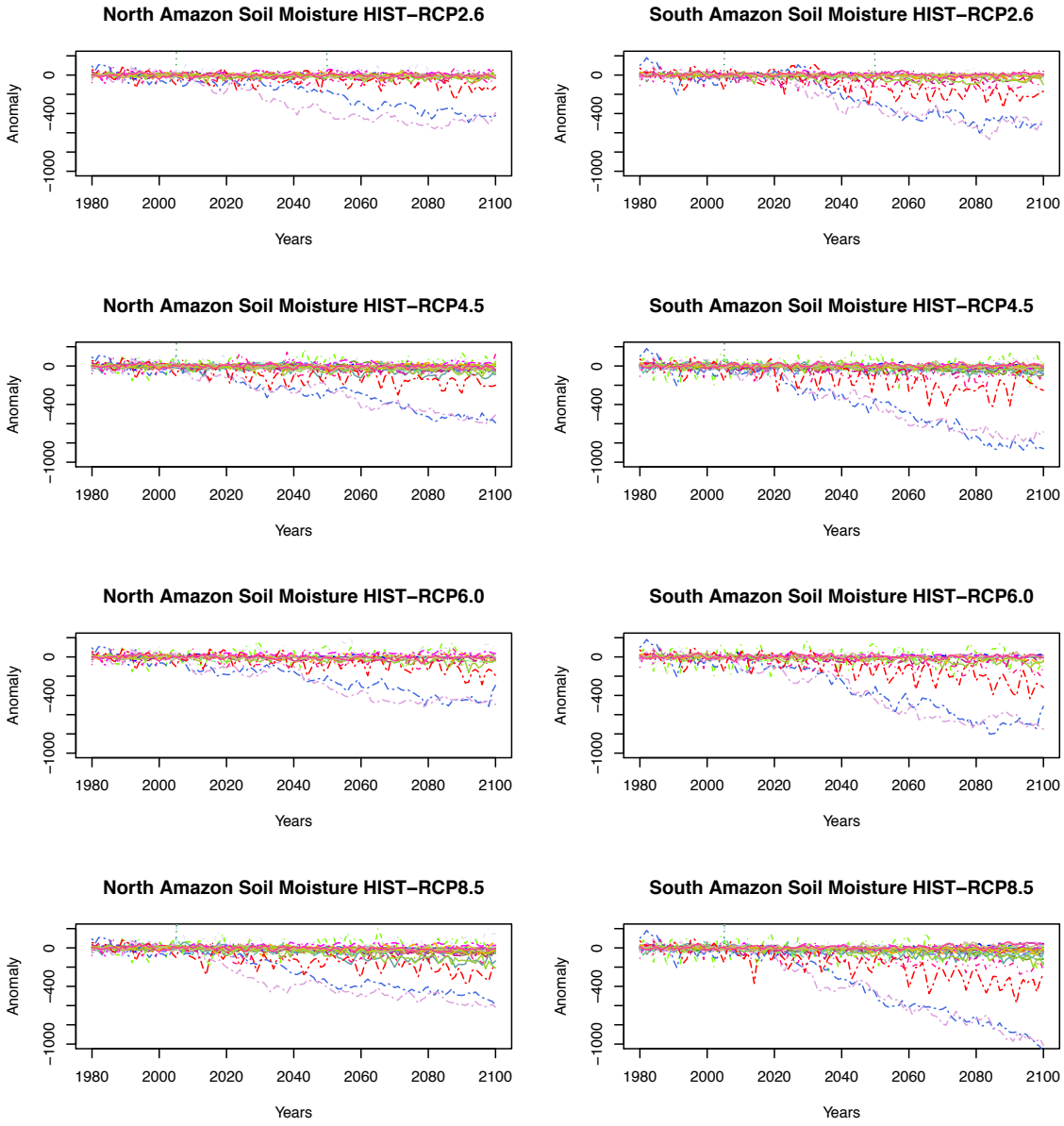

Figure 12h. Soil moisture content CMIP5 anomalies (from present day climatology) of CMIP5 model outputs in different RCPs.

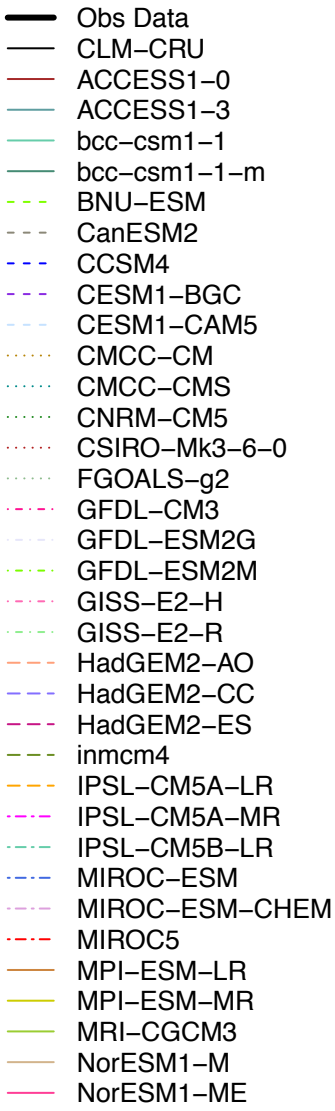

Figure 13. Legend for all line plot figures 10-12

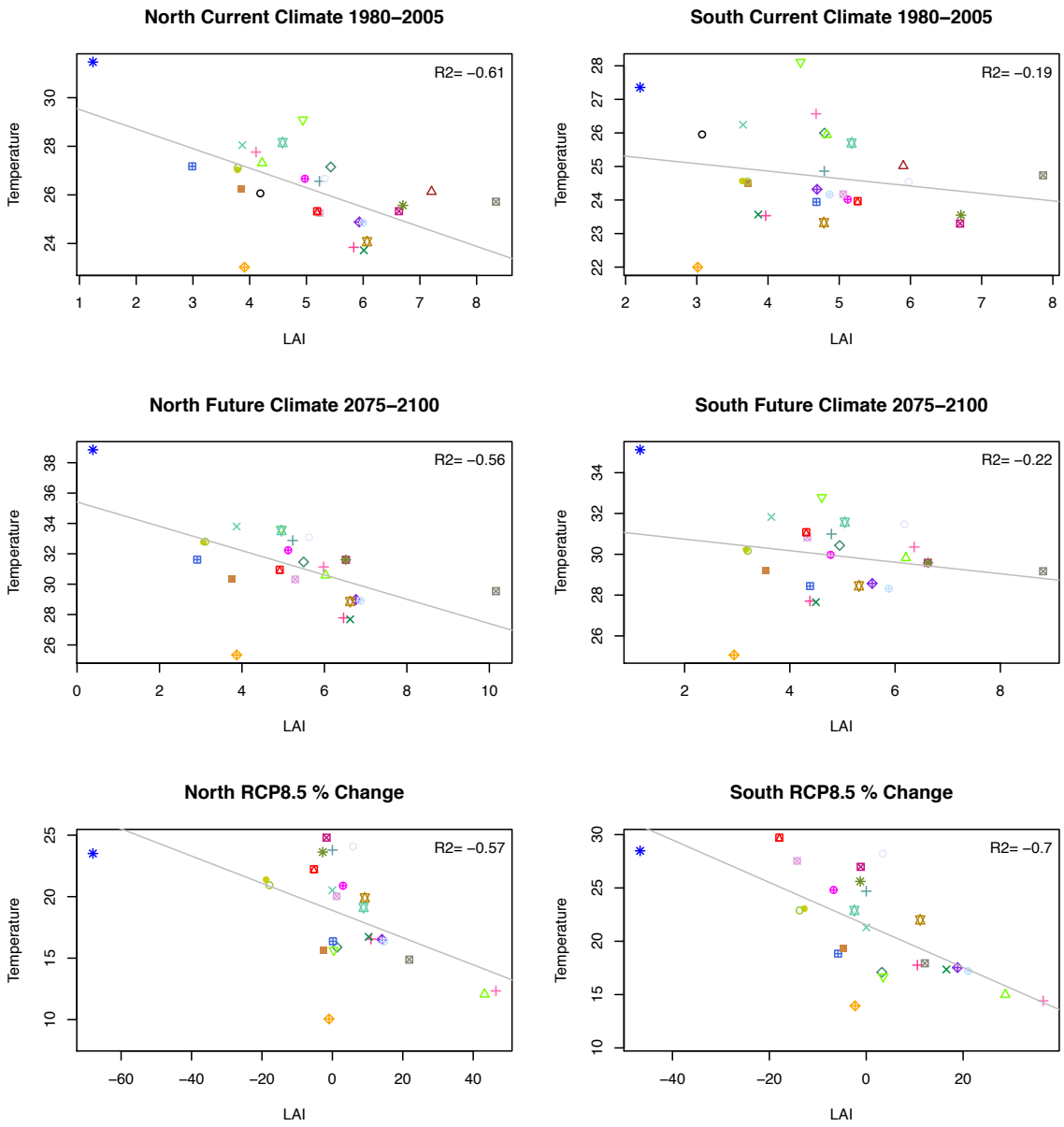

Figure 14a. Correlation plot between temperature and LAI for current climate, future climate, and % change.

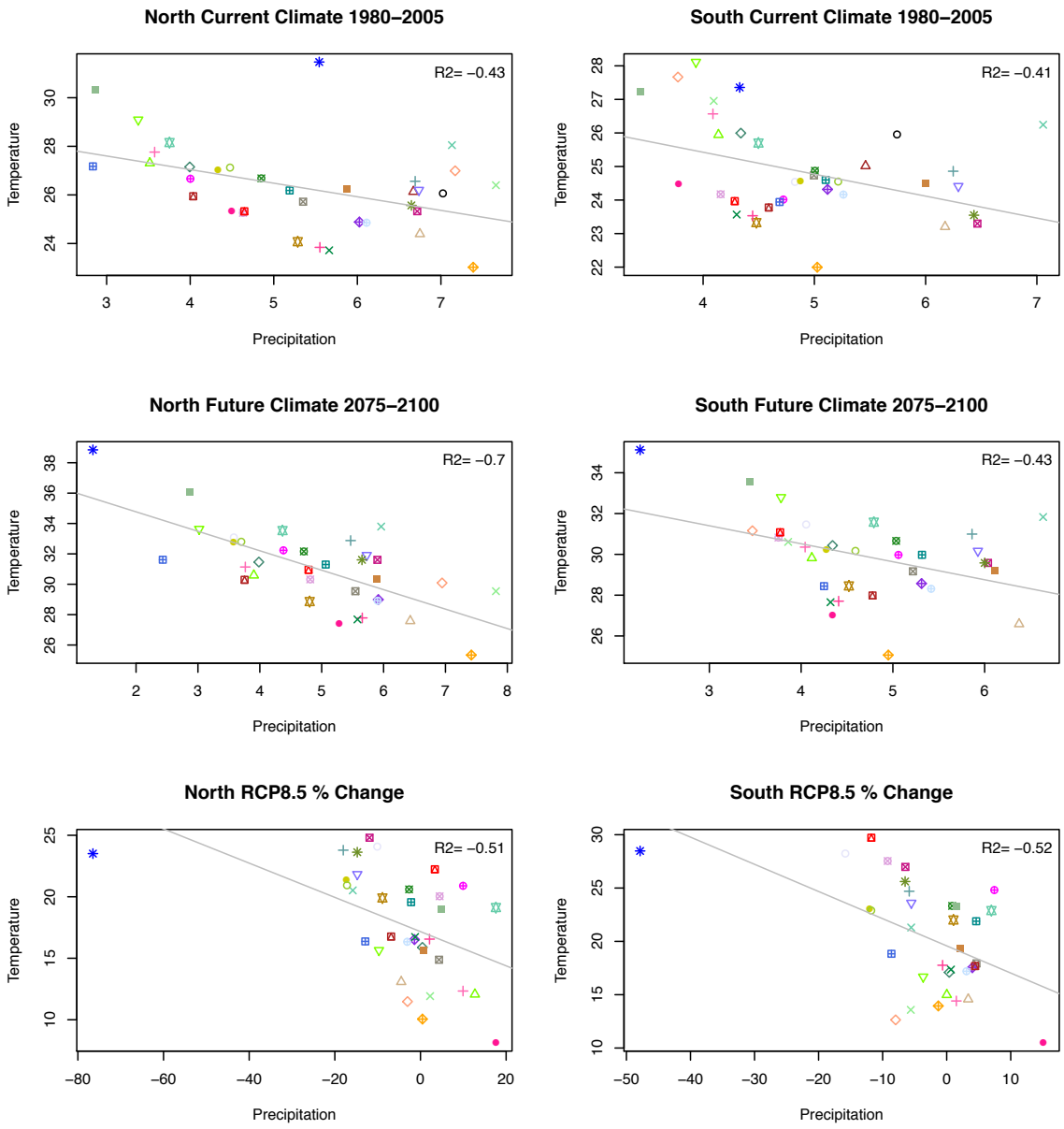

Figure 14b. Correlation plot between temperature and precipitation for current climate, future climate, and % change.

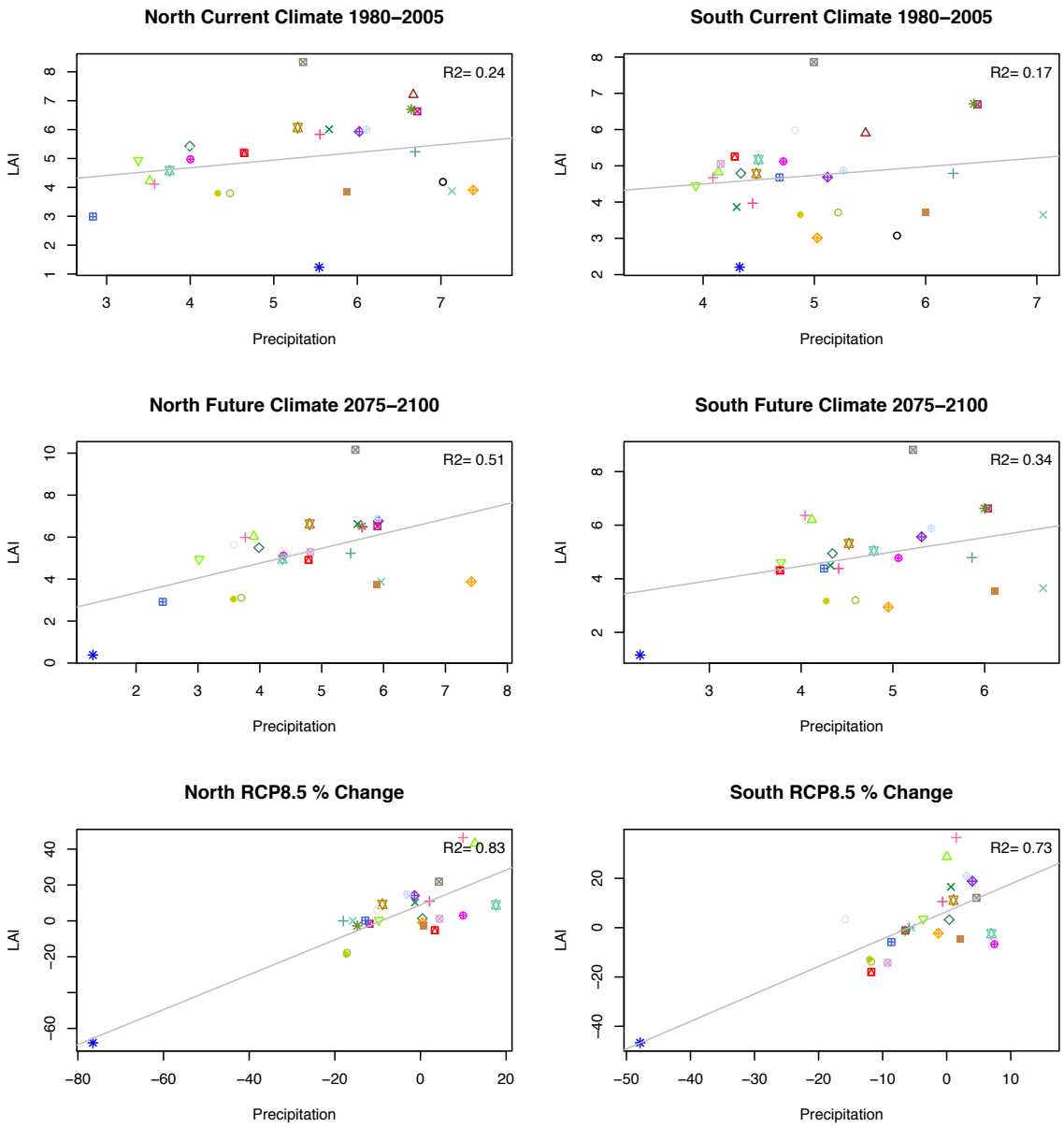

Figure 14c. Correlation plot between LAI and precipitation for current climate, future climate, and % change.

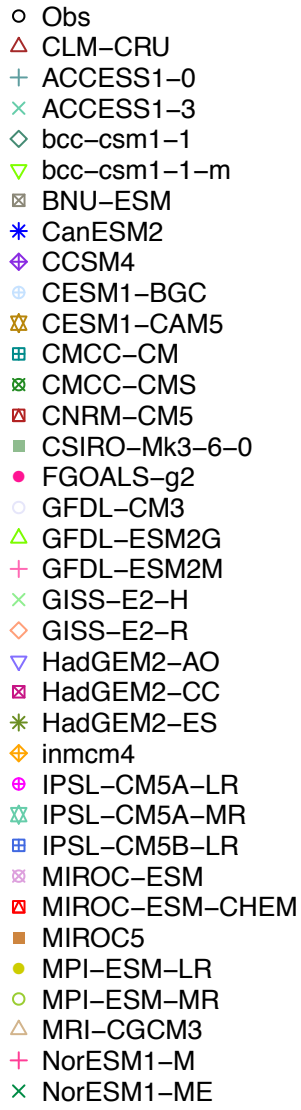

Figure 14d. Legend for figures14a-c correlation current climate correlation plots

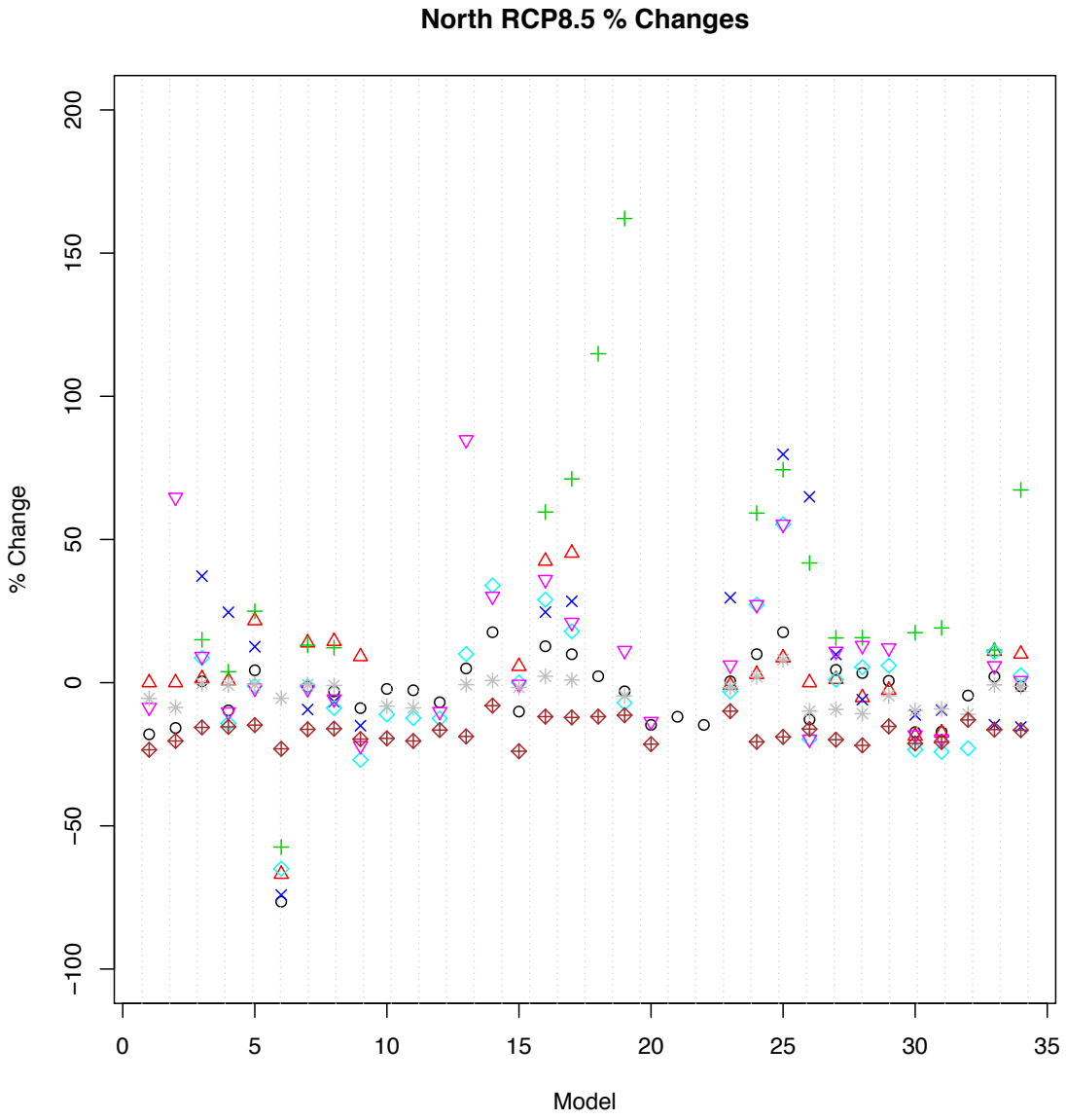

Figure 15a. RCP 8.5 % change in all variables for North Amazon. Note: Temperature percent changes are negative.

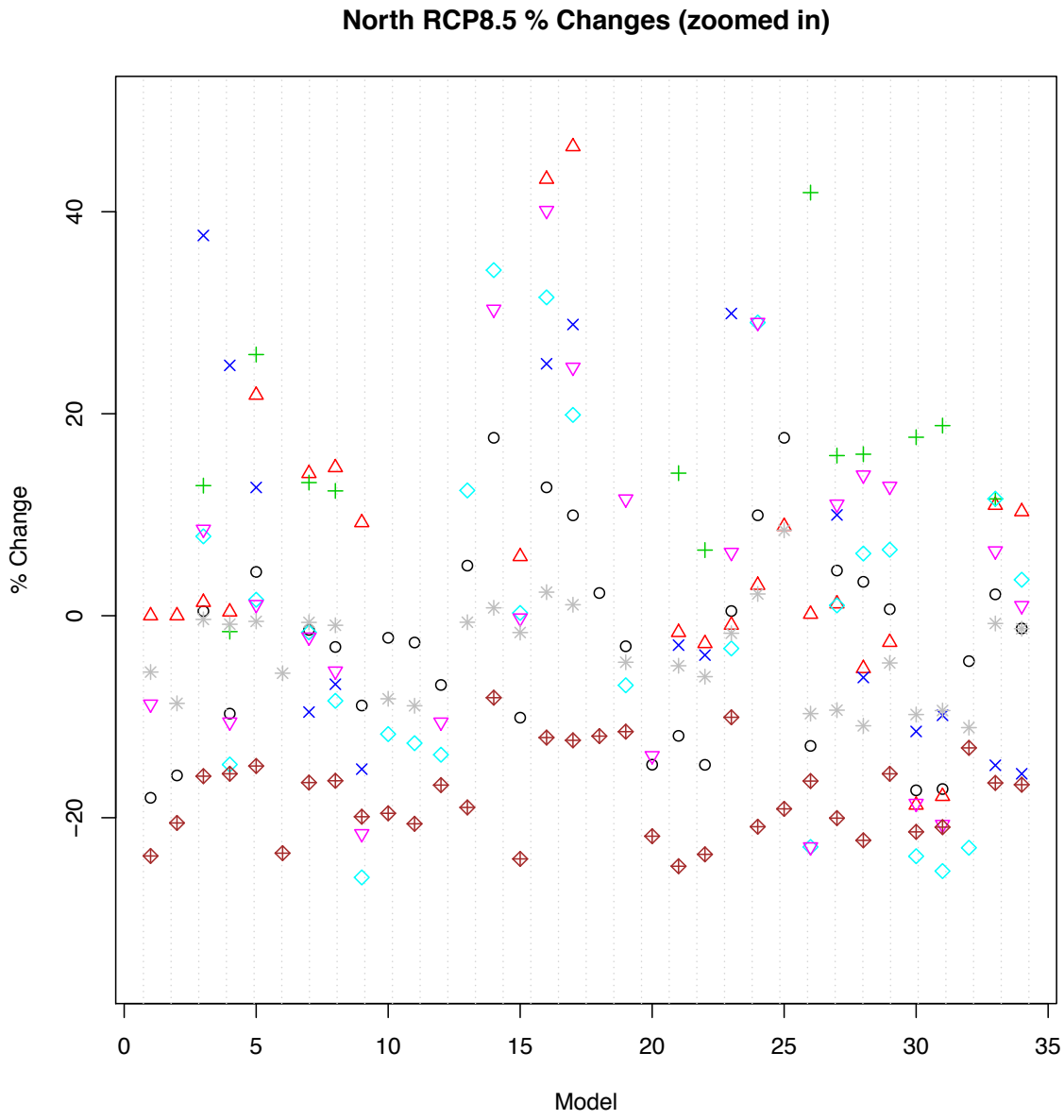

Figure 15b. RCP 8.5 % change in all variables for North Amazon (zoomed in)

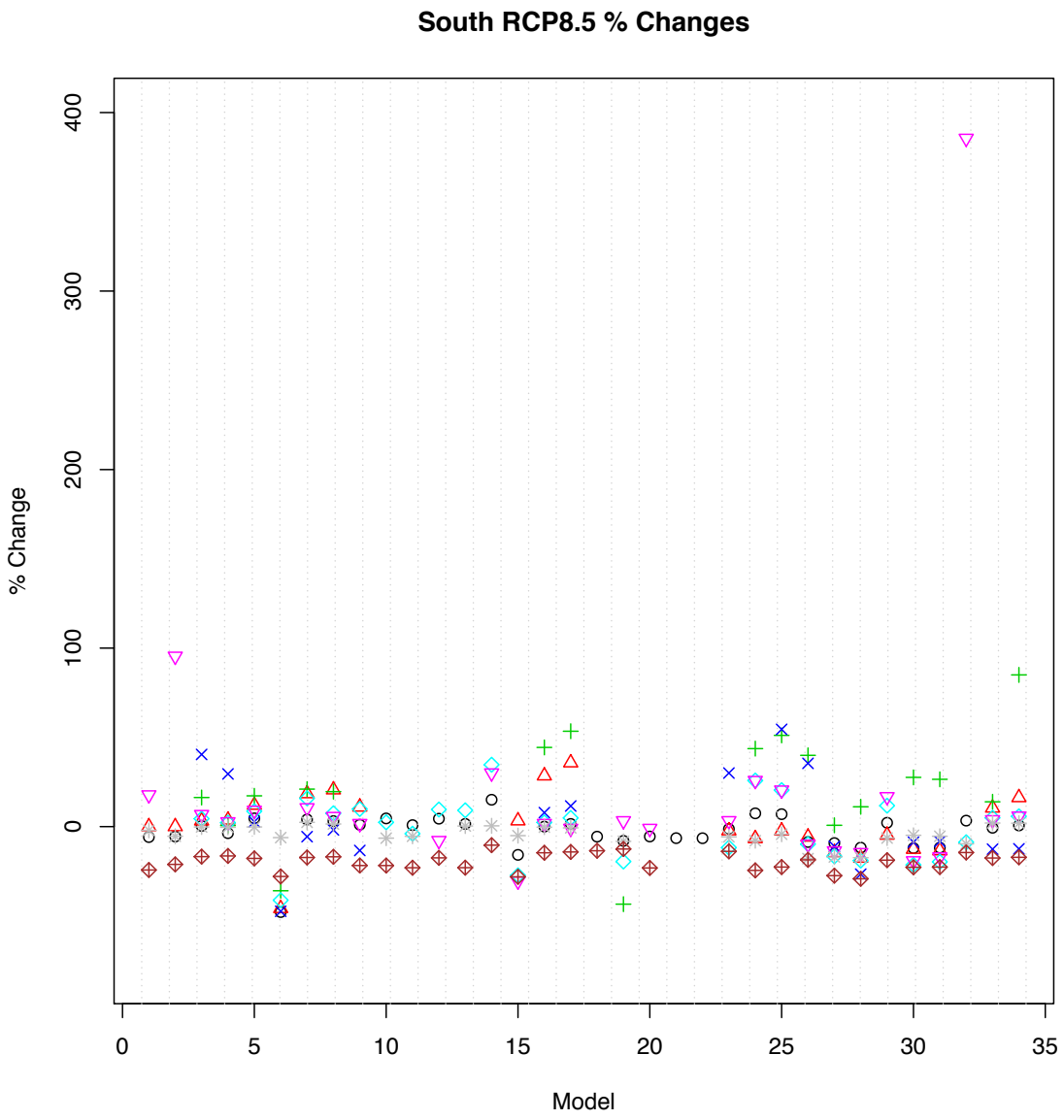

Figure 16a. RCP 8.5 % change in all variables for South Amazon. Note: Temperature percent changes are negative.

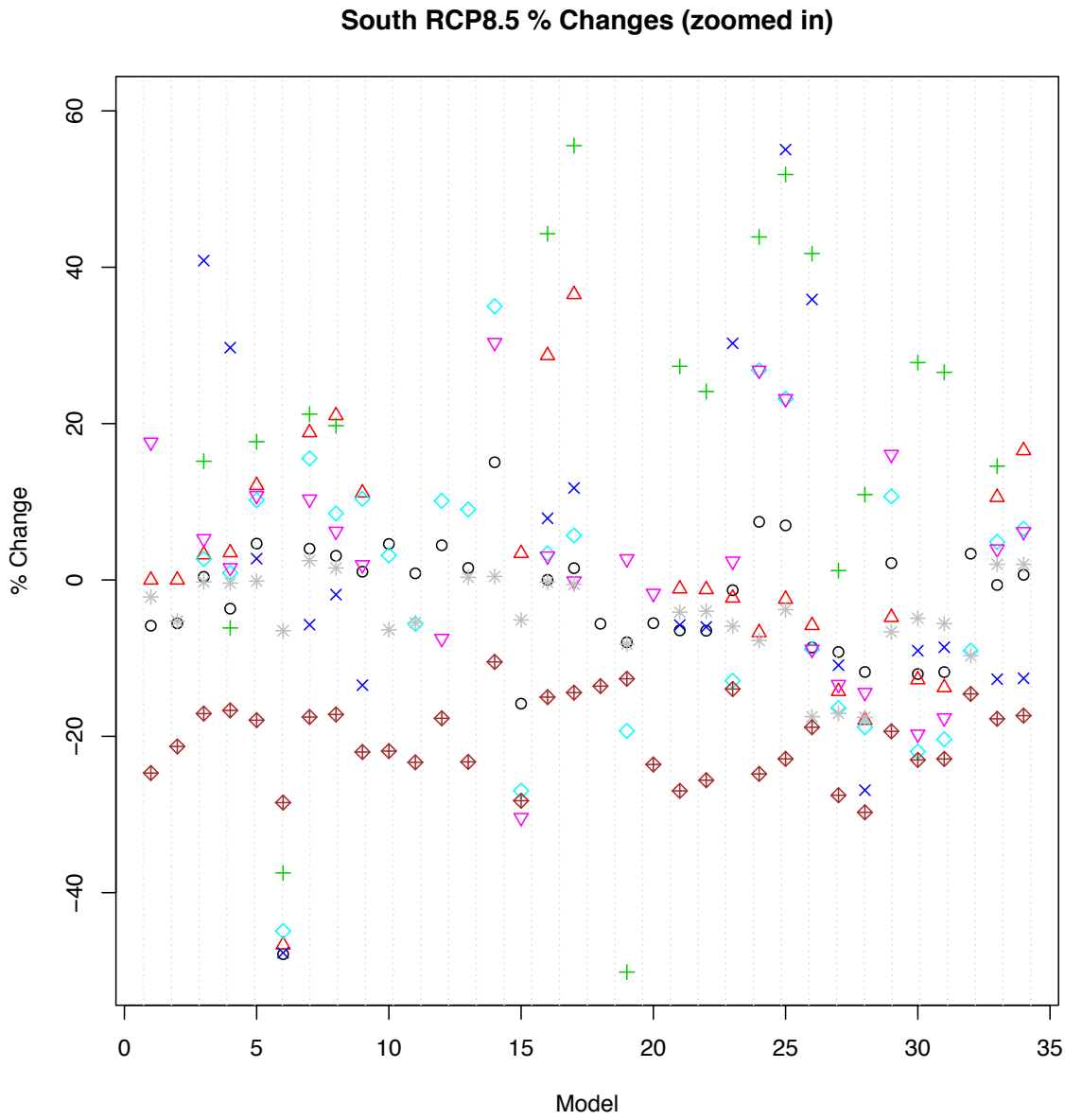

Figure 16b. RCP 8.5 % change in all variables for South Amazon (zoomed in)

- Precip
- LAI
- NPP
- cVeg
- Total Runoff
- Surface Runoff
- Soil Moisture
- Temperature

Figure 17. Legend Key for figures 15 and 16

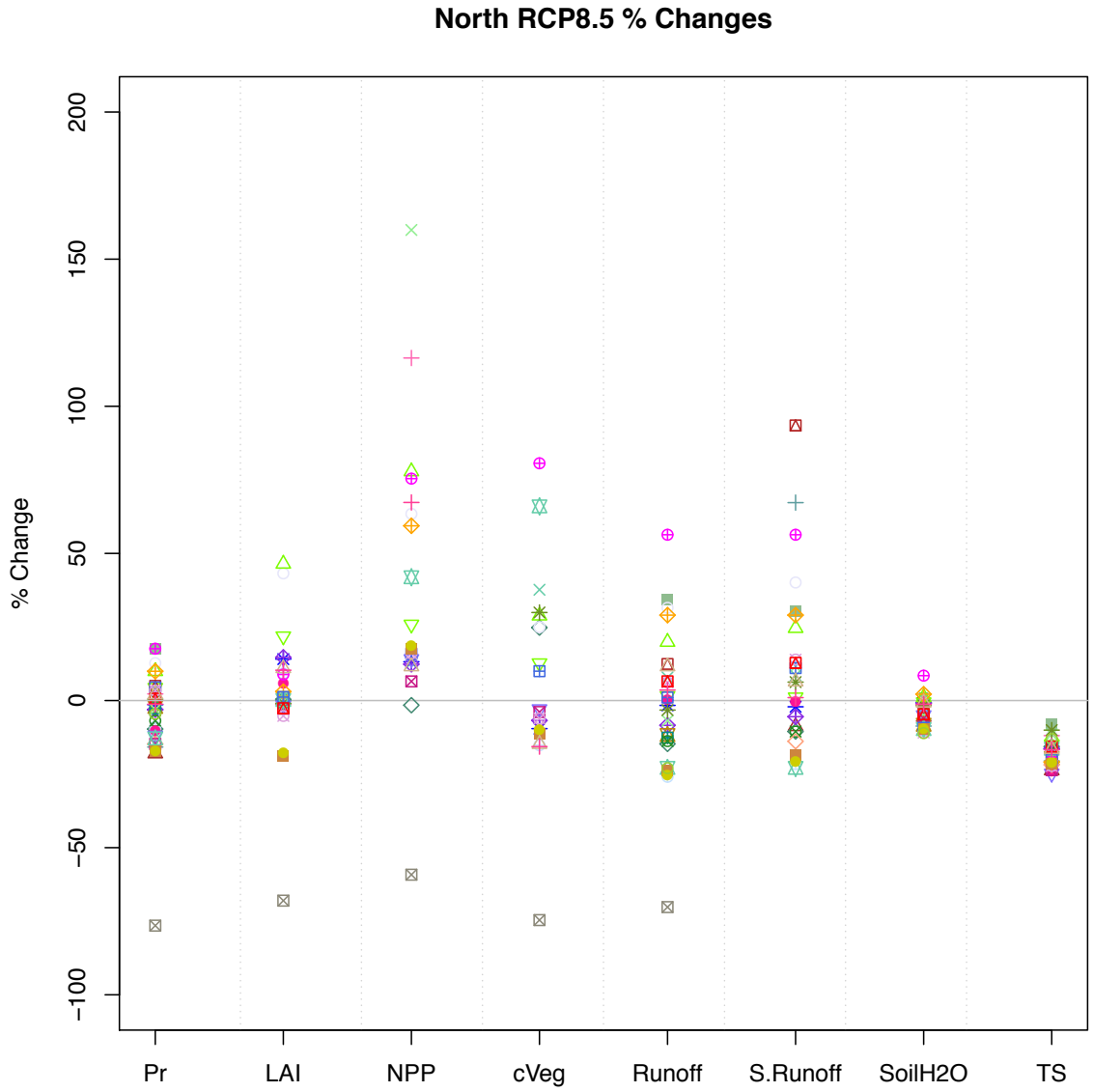

Figure 18a. North Amazon % Change for RCP8.5 of all variables

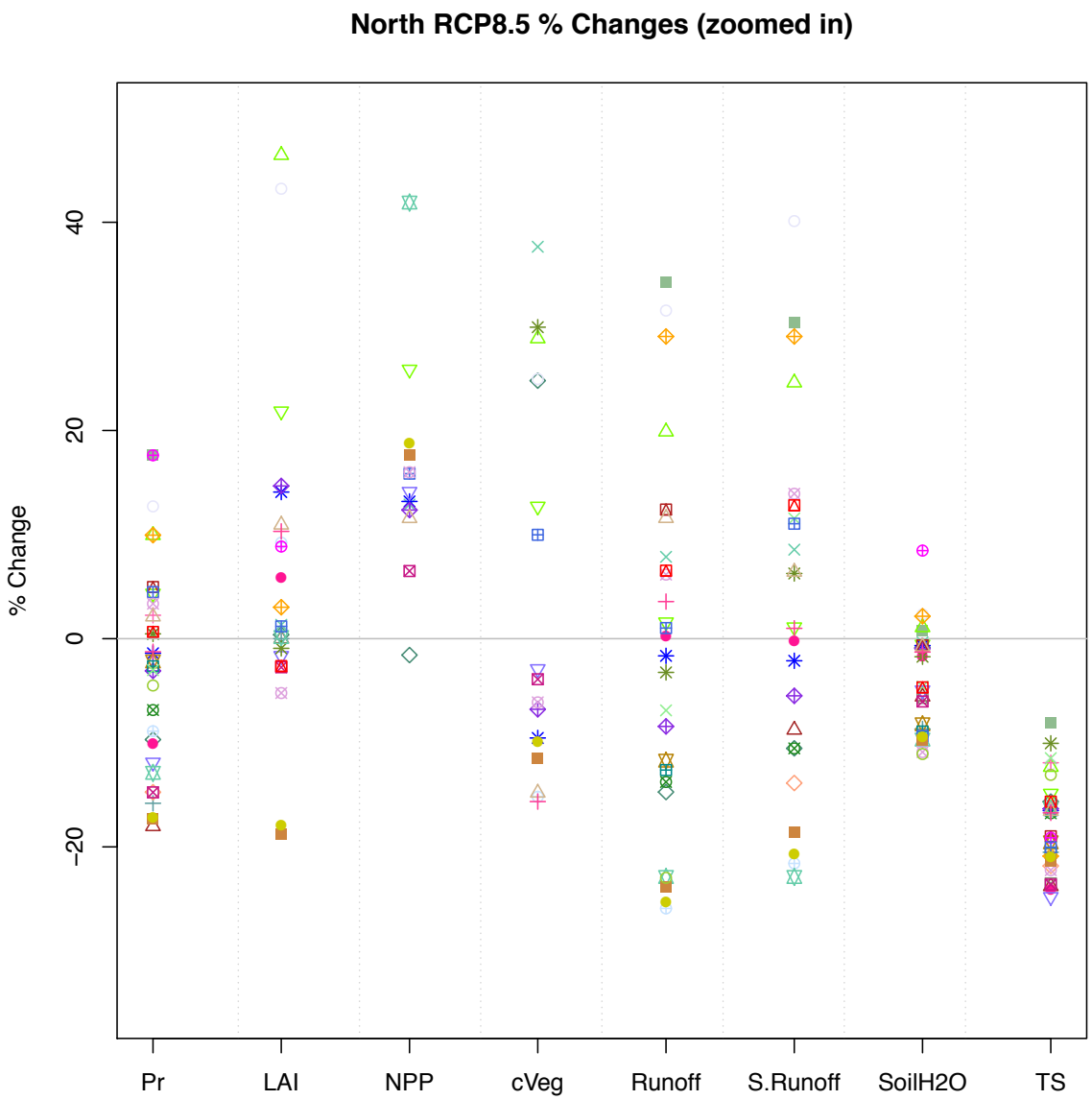

Figure 18b. North Amazon % Change for RCP 8.5 of all variables (zoomed in)

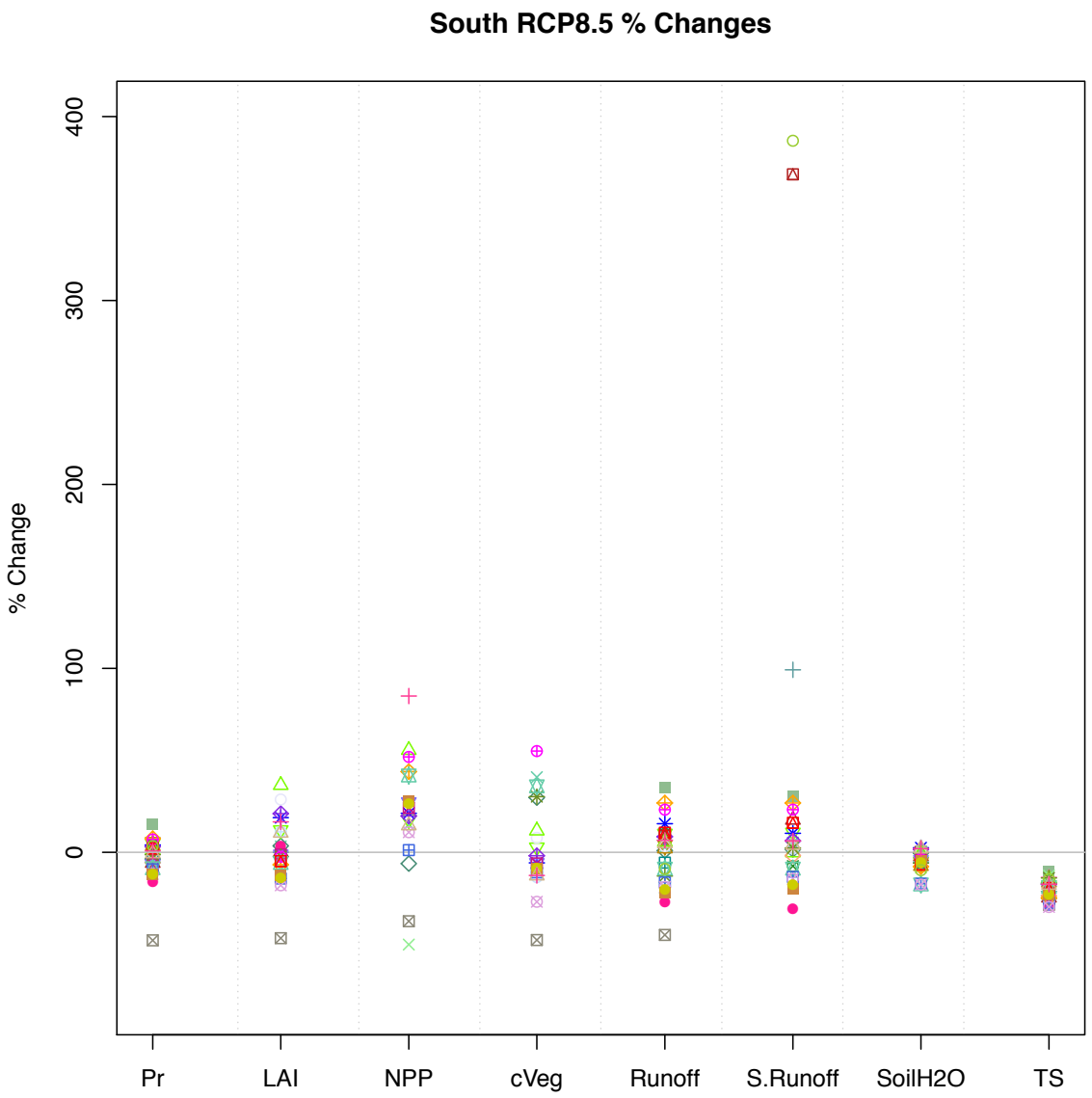

Figure 19a. South Amazon % Change for RCP8.5 of all variables

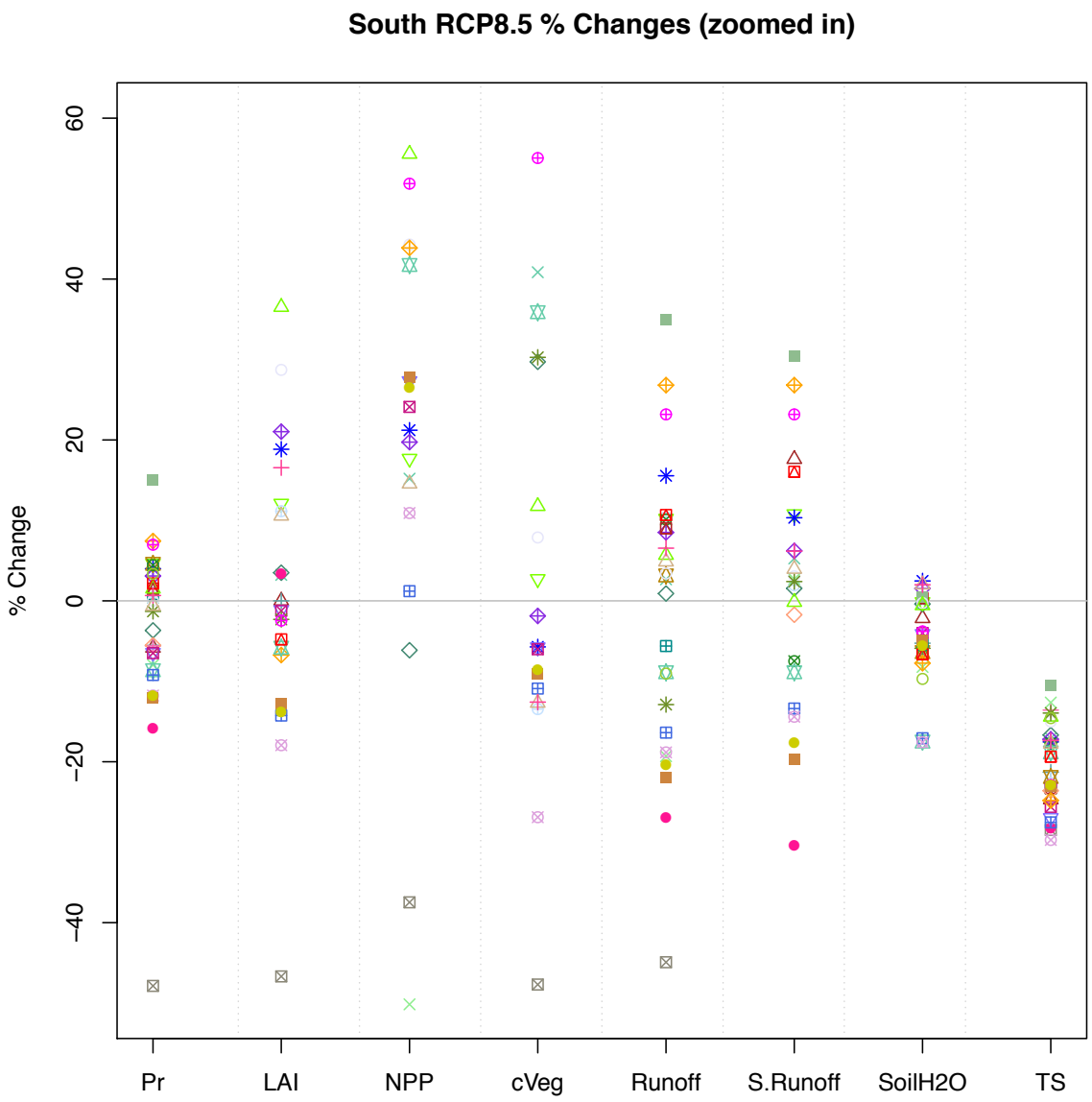

Figure 19b. South Amazon % Change for RCP8.5 of all variables (zoomed in)

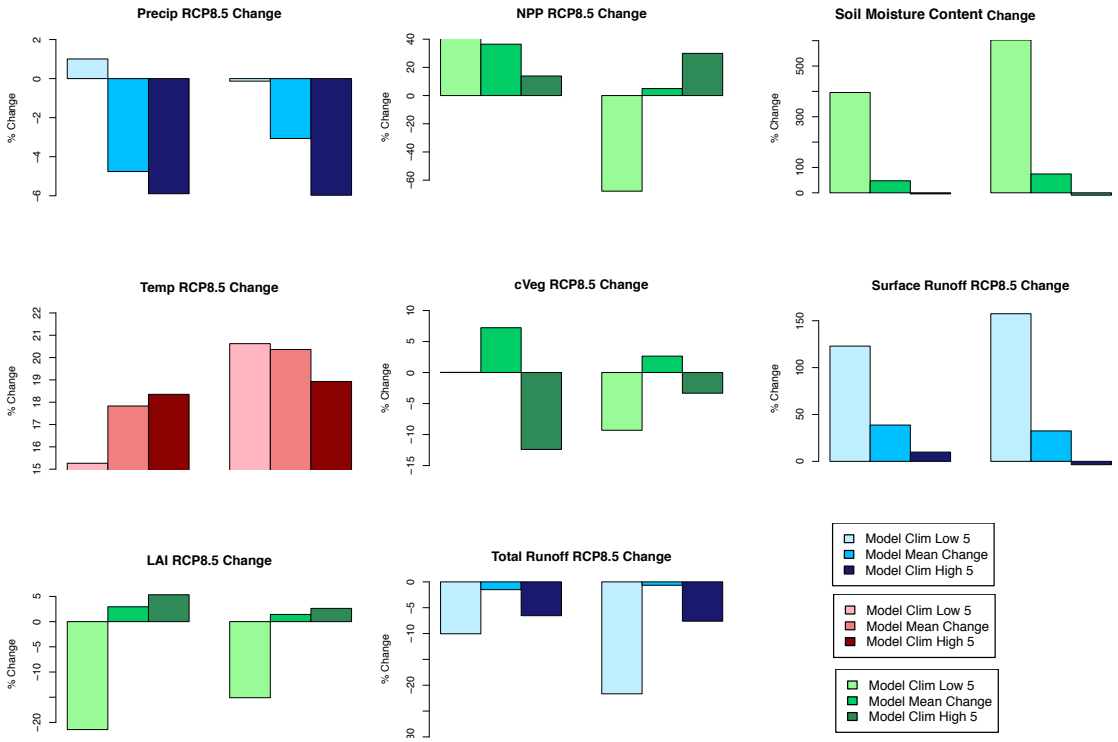

Figure 20. Bar plots of model 5 highs and 5 lows (same models from current climate) for future climate (RCP 8.5 scenario). This compares to Figure 8b to determine how the high 5 models and the low 5 models change for future climate scenario.

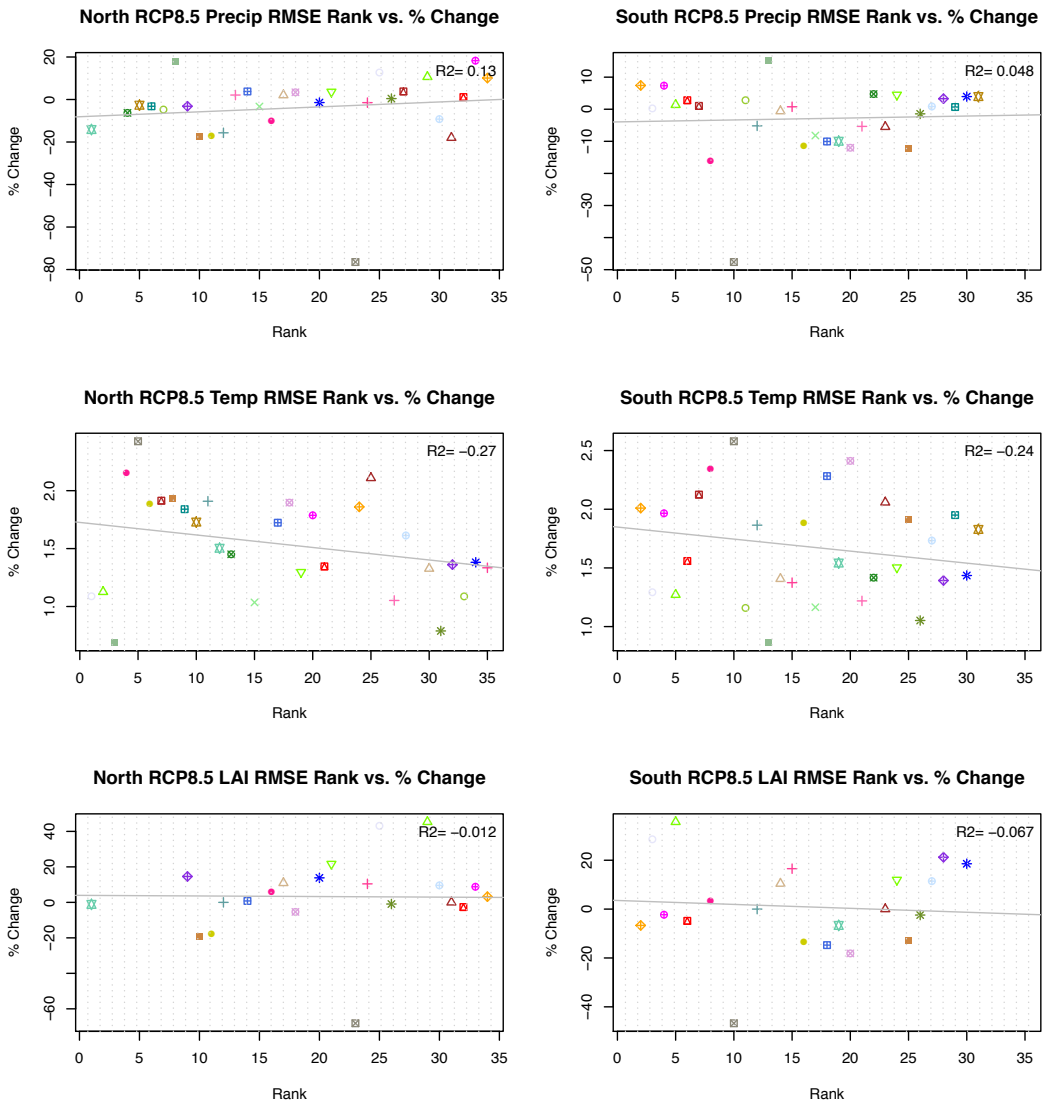

Figure 21. Correlation between RMSE based skill ranking (poor→perfect) and % change in future climate.

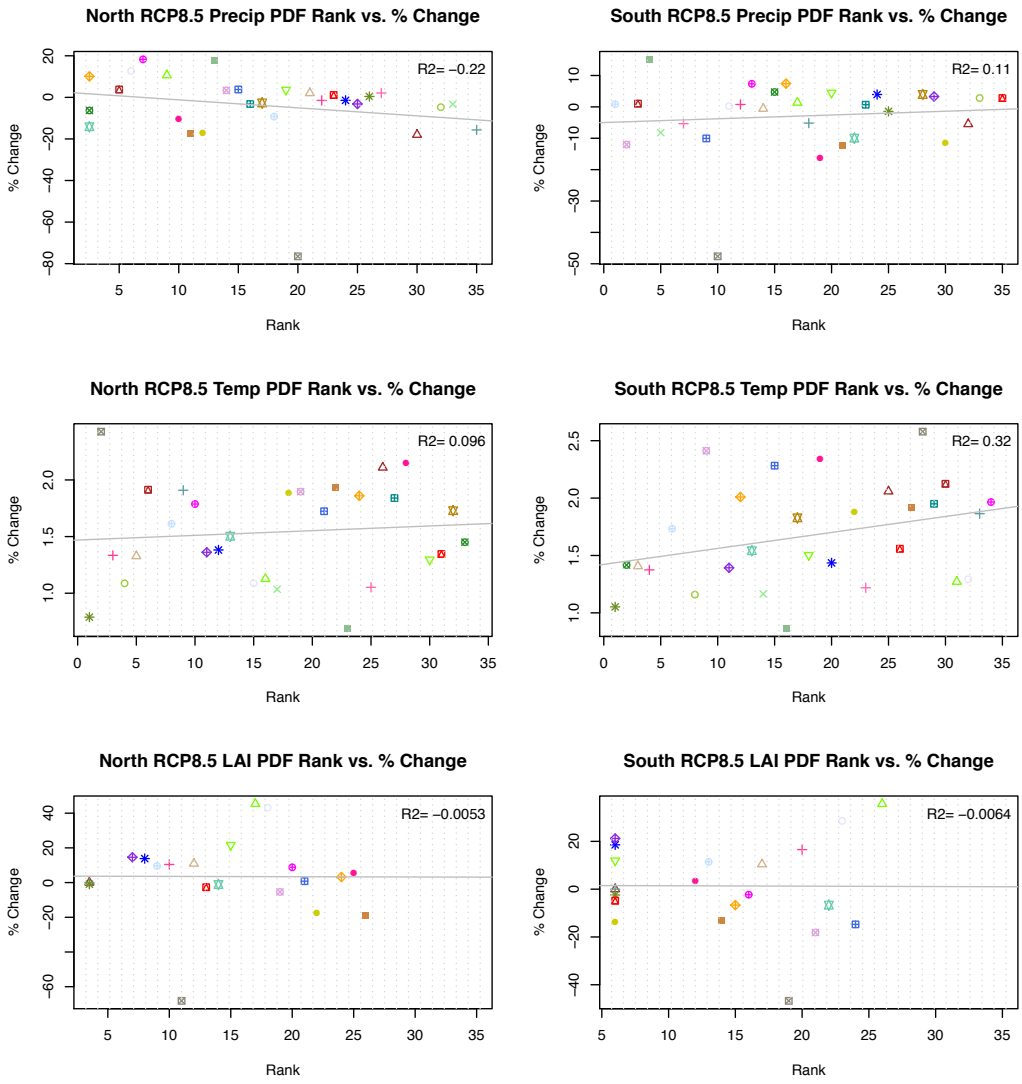

Figure 22. Correlation between PDF based skill ranking (poor → perfect) and % change in future climate.

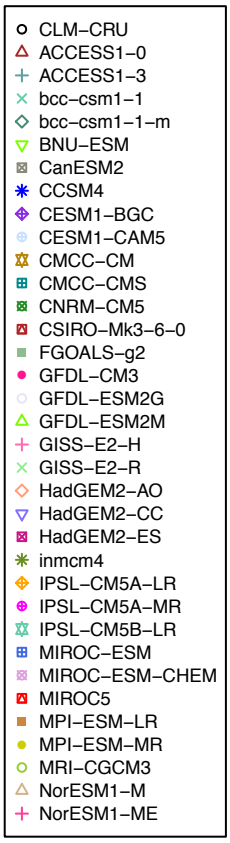

Figure 23. Legend for % change plots figures 18-21

REFERENCES

Allan, Richard P., and Brian J. Soden (2008), Atmospheric Warming and the Amplification of Precipitation Extremes, *Science,* Vol 321, 5895, pp. 1481-1484, doi:10.1126/science.1160787.

Anav, A., P. Friedlingstein, M. Kidston, L. Bopp, P. Ciais, P. Cox, C. Jones, M. Jung, R. Myneni, and Z. Zhu (2013), Evaluating the land and ocean components of the global carbon cycle in the CMIP5 Earth System Models, *J. Climate,* doi:10.1175/JCLI-D-12-00417.1, in press.

Asner, Gregory P., D. Nepstad, G. Cardinot, and D. Ray (2004), Drought stress and carbon uptake in an Amazon forest measured with spaceborne imaging spectroscopy, *PNAS, vol. 101, no. 16,* 6039-6044, doi:10.1073/pnas.0400168101.

Brando, Paulo M., S. J. Goetz, A. Baccini, D. C. Nepstad, P.S.A. Beck, and M.C. Christman (2010), Seasonal and interannual variability of climate and vegetation indices across the Amazon, *PNAS,* doi:10.1073/pnas.0908741107.

Cook, Kerry H., and Edward K. Vizy (2007), Effects of 21st Century Climate Change on the Amazon Rainforest, *Journal of Climate.*

Costa, M. (1999), Trends in the hydrologic cycle of the amazon basin, *Journal of Geophysical Research*, *104*(12), 14,189 -14,198.

Cox, P.M, R.A. Betts, C.D. Jones, S.A. Spall, and I.J. Totterdell (2000), Acceleration of global warming due to carbon-cycle feedbacks in a coupled climate model, *Nature,* 408, 184–187.

Cox, P.M., R.A. Betts, M. Collins, P.P. Harris, C. Huntingford, and C.D. Jones (2004), Amazonian forest dieback under climate-carbon cycle projections for the 21st century, *Theoretical and Applied Climatology, 78,* 137-156.

Cox, P.M., P.P. Harris, C. Huntingford, R.A. Betts, M. Collins, D. Chris, T. Jupp, J.A. Marengo, C. Nobre (2008), Increasing risk of Amazonian drought due to decreasing aerosol pollution, *Nature,* 453, 212-215, doi:10.1038/nature06960.

Davidson, Eric A., D. C. Nepstad, F. Y. Ishida, and P. M Brando (2008), Effects of an experimental drought and recovery on soil emissions of carbon dioxide, methane, nitrous oxide, and nitric oxide in a moist tropical forest, *Global Change Biology,* 14, 2582-2590, doi: 10.111/j.1365-2486.2008.01694.x.

Del Grosso, Stephen, W. Parton, T. Stohlgren, D. Zheng, D. Bachelet, S. Prince, K. Hibbary, and R. Olson (2011), Global Potential Net Primary Production Predicted from Vegetation Class, Precipitation, and Temperature, *Ecology, 89, pp. 2117-2126.*

Espinoza, Jhan Carlo, J Rochail, J. L. Guyot, C. Junquas, G. Drapeau, J.M. Martinez, W. Santini, P. Vauchel, W. Lavado, J. Ordoñez, and R. Espinoza (2012), From drought to flooding:

understanding the abrupt 2010-11 hydrological annual cycle in the Amazonas River and tributaries, *Environ. Res. Lett. 7,* doi:10.1088/1748-9326/7/2/024008

Errasti, I., A. Ezcurra, J. Sáenz, and G. Ibarra-Berastegi (2011), Validation of IPCC AR4 models over the Iberian Peninsula, *Theor. Appl. Climatol., 103:61-79,* DOI: 10.1007/s00704-010-0282-y.

Field, C.B., M.K. Behrenfeld, J.T. Randerson, and P. Falkowski (1998), Primary production of the biosphere: Integrating terrestrial and oceanic components, *Science,* 281(5374), 237-240,doi:10.1126/science.281.5374.237.

Figueroa, S. N., and C.A. Nobre (1990), Precipitation distribution over central and western tropical South America, *Climanálise, **6,*** 36-40.

Fu, R., M. Chen, W. Li, and R. E. Dickinson (2001), How do tropical sea surface temperatures influence the seasonal distribution of precipitation in the equatorial Amazon?, *J. Climate, 14,* 4003-4026.

Fung, Inez Y., S. C. Doney, K. Lindsay, and J. John (2005), Evolution of carbon sinks in a changing climate, *PNAS, 12,* 11201-11206, doi:10.1073/pnas.0504949102.

Galford, Gillian L., J.M. Melillo, D.W. Kicklighter, J.F., Mustard, T. W. Cronin, C. E. P. Cerri, and C.C. Cerri (2011), Historical carbon emissions and uptake from the agricultural frontier of the Brazilian Amazon, *Ecological Applications,* 21(3), pp. 750-763.

Gleckler, P.J., K.E. Taylor, and C. Doutriaux (2008), Performance metrics for climate models, *J. Geophys. Res., 113,* D06104, doi:10.1029/2007JD008972.

John, V.O., R.P. Allan, B.J. Soden (2009), How robust are observed and simulated precipitation responses to tropical ocean warming?, *Geophys. Res. Let.,* 36, L14702.

Kousky, V.E., M.T. Kagano, and I.F.A. Cavalcanti (1984), A review of the Southern Oscillation: Oceanic-atmospheric circulation changes and related rainfall anomalies, *Tellus, **36A,*** 490-504.

Houghton, R.A., J.I. House, J. Pongratz, G.R. van der Werf, R.S. DeFries, M.C. Hansen, C. Le Quéré, and N. Ramankutty (2012), Carbon emissions from land use and land-cover change, *Biogeosciences,* 9, 5125-5142, doi:10.5194/bg-9-5125-2012.

Huntington, Thomas G. (2006), Evidence for intensification of the global water cycle: Review and synthesis, *Journal of Hydrology,* 316, pp 83-95, doi:10.1016/j.jhydrol.2005.07.003.

Huntingford, Chris, R.A. Fisher, L. Mercado, B.B.B. Booth, S. Sitch, P. P. Harris, P. M. Cox, C. D. Jones, R. A. Betts, Y. Malhi, G. R. Harris, M. Collins, and P. Moorcroft (2008), Towards quantifying uncertainty in predictions of Amazon 'dieback', *Phil. Trans. R. Soc. B,* doi:10.1098/rstb.2007.0028.

Li, Wenhong, and Rong Fu (2004), Transition of the Large-Scale Atmosphere and Land Surface

Conditions from the Dry to the Wet Seasons over Amazonia as Diagnosed by the ECMWF Re-Analysis, *Journal of Climate, 17*, pp. 2637-2651.

Li, Wenhong, R. Fu, and R.E. Dickinson (2006), Rainfall and its seasonality over the Amazon in the 21st century as assessed by the coupled models for IPCC AR4, *Journal of Geophysical Research, 111,* D02111, doi:10.1029/2005JD006355.

Liebmann, Brant and José A. Marengo (2001), Interannual Variability of the Rainy Season and Rainfall in the Brazilian Amazon Basin, *Journal of Climate,* 14, 4308-4318.

Lewis, Simon L., P. M. Brando, O.L. Phillips, G.M.R. van der Heijden, and D. Nepstad (2011), The 2010 Amazon Drought, *Science, Vol 331,* doi:10.1126/science.1200807.

Malhi, Yadviner, J.T. Roberts, R. A. Betts, T.J. Killeen, W. Li, and C. A. Nobre (2008), Climate Change, Deforestation, and the Fate of the Amazon, *Science, Vol. 319.*

Marengo, J.A. (1992), Interannual variability of surface climate in the Amazon Basin, *Int. J. Climatol., 12,* 853-863.

Marengo, J.A., J. Tomasella, L.M. Alves, W.R. Soares, and D.A. Rodriguez (2011), The drought of 2010 in the context of historical droughts in the Amazon region, *Geophysical Research Letters, Vol. 38,* LI 270, doi:10.1029/2011GL047436.

Maxino, C.C., B.J. McAvaney, A.J. Pitman, and S. E. Perkins (2008), Ranking the AR4 climate models over the Murray Darling Basin using simulated maximum temperature, minimum temperature and precipitation, *Int. J. Climatol.,* 28, 1097-1112.

Meir, P. D.B. Metcalfe, A.C.L. Costa, and R.A. Fisher (2008), The fate of assimilated carbon during drought: impacts on respiration in Amazon rainforests, *Phils. Trans. R. Soc. B,* 363, 1849-1855, doi: 10.1098/rstb.2007.0021.

Meir, P., P.M. Brando, D. Nepstad, S. Vasconcelos, A.C. L. Costa, E. Davidson, S. Almeida, R.A. Fisher, E.D. Sotta, D. Zarin, and G. Cardinot (2009), The Effects of Drought on Amazonian Rain Forests (2009), *Amazonia and Global Change, Geophysical Monograph Series 186,* 10.1029/2009GM00882.

Metcalfe, D.B., P. Meir, L.E.O.C. Aragão, R. Lobo-do-Value, D. Galbraith, R.A. Fisher, M.M. Chaves, J.P. Maroco, A.C.L. da Costa, S.S. de Almeida, A.P. Braga, P.H.L. Goncalves, J. de Athaydes, M. da Costa, T.T.B. Portela, A.A.R. de Oliveira, Y. Malhi, and M. Williams (2010), Shifts in plant respiration and carbon use efficiency at a large-scale drought experiment in the eastern Amazon, *New Phytologist,* 187, 608-621, doi:10.1111/j.1469-8137.2010.03319.x.

Myneni, Ranga B., W. Yang, R. R. Nemani, A. R. Huete, R. E. Dickinson, Y. Knyazikhin, K. Didan, R. Fu, R.I. Negrón Juárez, S.S. Saatchi, H. Hashimoto, K. Ichii, N.V. Shabanov, B. Tan, P. Ratana, J. L. Privette, J. T. Morisette, E. F. Vermote, D. P. Roy, R. E. Wolfe, M. A. Friedl, S. W. Running, P. Votava, N. El-Saleous, S. Devadiga, Y. Su, and V. V. Salomonson (2007), Large seasonal swings in leaf area of Amazon rainforests, *PNAS,*

104, 4820-4823,doi: 10.1073/pnas.0611338104.

Neelin (2008), Causes and impacts of the 2005 Amazon drought, *Environ. Res. Lett., 3,* 014002, 9 pp., doi:10.1088/1748-9326/3/1/014002.

Nepstad, Daniel, P. Lefebvre, U. Lopes Da Silva, J. Tomasella, P. Schlesinger, L. Solórzano, P. Moutinho, D. Ray, and J.G. Benito (2004), Amazon drought and its implications for forest flammability and tree growth: a basin-wide analysis, 10, 704-717, doi: 10.1111/j.1529-8817.2003.00772.x.

Poulter, Benjamin, L. Aragão, U. Heyder, M. Gumpenberger, J. Heinke, F. Langerwisch, A. Rammig, K. Thonicke, and W. Cramer (2010), *Global Change Biology,* 16, 2062-2075, doi:10.1111/j.1365-2485.2009.02064.x.

Poulter, Benjamin, F. Hattermann, E. Hawkins, S. Zaehles, S. Sitch, N. Restrepo-Coupe, U. Heyder, and W. Cramer (2010), *Global Change Biology,* 16, 2476-2495, doi:10.1111/j.1365-2486.2009.02157.x.

Rao, V.B., I. Cavalcanti, and K. Hada (1996), Annual variation of rainfall over Brazil and water vapor characteristics over South America, *J. Geophys. Res., 101,* 26 539-26, 551.

Richey, Jeffrey E., J.I. Hedges, A.H. Devol, P.D. Quay, R. Victoria, L. Martinelli, and B.R. Forsberg (1990), Biogeochemistry of Carbon in the Amazon River, *Limnology and Oceanography,* Vol 35, No. 2, pp 352-371.

Robock, Alan, K. Y. Vinnikov, G. Srinivasan, J.K. Smith, S. E. Hollinger, N.A. Speranskaya, S. Liu, and A. Namkhai (2000), The Global Soil Moisture Data Bank, *Bull. Amer. Meteorol. Soc.,* 81, 1281-1299.

Schwalm, C.R., C.A. Williams, and K. Schaefer (2011), Carbon consequences of global hydrologic change, 1948-2009, *Journal of Geophysical Research, Vol. 116,* G03042, doi:10.1029/2011JG001674.

Saatchi, S. S., R.A. Houghton, R. Alvala, J.V. Soares, and Y. Yu (2007), Distribution of aboveground live biomass in the Amazon basin, *Global Change Biology,* 1, 816-837, doi: 10.1111/j.1365-2486.2007.01323.x.

Saatchi, S.S., R.A. Houghton, D. Alves, B. Nelson. 2009. LBA-ECO LC-15 Amazon Basin Aboveground Live Biomass Distribution Map: 1990-2000. Data set. Available on-line [http://daac.ornl.gov] from Oak Ridge National Laboratory Distributed Active Archive Center, Oak Ridge, Tennessee, U.S.A., doi:10.3334/ORNLDAAC/908.

Saleska,S.R., K. Didan, A.R. Huete, and H.R. da Rocha (2007), Amazon Forests Green-Up During 2005 Drought, *Science*, 318, DOI: 10.1126/science.1146663.

Samanta, A., S. Ganuly, H. Hashimoto, S. Devadiga, E. Vermote, Y. Knyazikhin, R. R. Nemani, and R.B. Myneni (2010), Amazon forests did not green-up during the 2005 drought, *Geophysical Research Letters*, 37, L05401, doi:10.1029/2009GL042154.

Scherrer, S.C. (2011), Present-day interannual variability of surface climate in CMIP3 models and its relation to future warming, *Int. J. Climatol.,* 31 1518-1529.

Shi, Xiaoying, J. Mao, P.E. Thornton, F. M. Hoffman, and W.M. Post (2011), The impact of climate, CO_2, nitrogen deposition and land use change on simulated contemporary global river flow, *Geophysical Research Letters, 38, L08704,* doi:10.1029/2011GL046773.

Tomasella, Javier, L. S. Borma, J.A. Marengo, D.A. Rodriguez, L. A. Cuartas, C.A. Nobre, and M.C.R. Prado (2010), The droughts of 1996-1997 and 2004-2005 in Amazonia: hydrological response in the river main-stem, *Hydrological Processes,* DOI:10.1002/hyp.7889.

Toomey, Michael, D.A. Roberts, C. Still, M.L. Goulden, and J.P. McFadden (2011), Remotely sensed heat anomalies linked with Amazonian forest biomass declines, *Geophysical Research Letters,* Vol 38, L19704, doi:10.1029/2011GL049041.

Trenberth, K.E., A. Dai, R.M. Rasmussen, and D.B. Parsons (2003), The changing character of precipitation, *Bull Am Meteorol Soc,* 84, 1205-1217.

Verbeeck, Hands, P. Peylin, C. Bacour, D. Bonal, K. Steppe, and P. Ciais (2011), Seasonal patterns of CO_2 fluxes in Amazon forests: Fusion of eddy covariance data and the ORCHIDEE model, *Journal of Geophysical Research, Vol. 116,* doi:10.1029/2010JG001544.

van der Molen, M.K., A.J. Dolman, P. Ciais, T. Eglin, N. Gobron, B.E. Law, P. Meir, W. Peters, O.L. Phillips, M.Reichstein, T. Chen, S.C. Dekker, M. Doubkova, M.A. Friedl, M. Jung, B.J.J.M. van den Hurk, R.A.M. de Jeu, B. Kruijt, T. Ohta, K.T. Rebel, S. Plummer, S.I. Seneviratne, S. Sitch, A. J. Teuling, G. R. van der Werf, and G. Wang (2011), Drought and ecosystem carbon cycling, *Agricultural and Forest Meteorology,* 151, 765-773, doi: 10.1016/j.agrformet.2011.01.018.

Yoon, J-H. and N. Zeng (2010), An Atlantic influence on Amazon rainfall, *Clim Dyn*, 34:249-26, doi:10.1007/s00382-009-0551-6.

Zeng, Ning (1999), Seasonal cycle and interannual variability in the Amazon hydrologic cycle, *Journal of Geophysical Research, Vol. 104,* No. D8, pages 9097-9106.

Zeng, Ning, J.H. Yoon, J.A. Marengo, A. Subramaniam, C.A. Nobre, A. Mariotti, and J.D. Neelin (2008), Causes and impacts of the 2005 Amazon drought, *Environmental Research Letters,* 3, doi:10.1088/1748-9326/3/1/014002.

Zhu, Zaichun, J. Bi, Y. Pan, S. Ganguly, A. Anav, L. Xu, A. Samanta, S. Piao, R. R. Nemani, and R. B. Myneni (2013), Global Data Sets of Vegetation Leaf Area Index (LAI)3g and Fraction of Photosynthetically Active Radiation (FPAR)3g Derived from Global Inventory Modeling and Mapping Studies (GIMMS) Normalized Difference Vegetation Index (NDVI)3g for the Period 1981 to 2011, *Remote Sens.* 5(2), 927-948, doiL10.3390/rs5020927.